GEOMETRY AND ALGORITHMS FOR PART FIXTURING, GRASPING AND MANIPULATION WITH MODULAR FIXTURING ELEMENTS, A NEW RECONFIGURABLE GRIPPER AND MOBILE ROBOTS

Attawith Sudsang, Ph.D.
Department of Computer Science
University of Illinois at Urbana-Champaign, 1999
Jean Ponce, Advisor

This thesis addresses the problem of immobilizing and manipulating parts with devices that have a mixture of discrete and continuous degrees of freedom. Immobilizing an object requires calculating the device parameters that reduce the positions and orientations of the object compatible with the contact constraints to a single point of its configuration space. Likewise, manipulating an object requires identifying the regions of its configuration space where it is free to move under the contact constraints. The kinematic theory of second order mobility of rigid bodies is used, together with the new concept of Inescapable Configuration Space region, to devise efficient algorithms for planning immobilizing fixtures, grasps, in-hand manipulation sequences and obstacle avoidance manipulation plans for parts with known geometry. This approach is applied to three different mechanisms: a fixturing device assembled from standard modular elements, a novel reconfigurable gripper, and a team of mobile robots.

GEOMETRY AND ALGORITHMS FOR PART FIXTURING, GRASPING
AND MANIPULATION WITH MODULAR FIXTURING ELEMENTS,
A NEW RECONFIGURABLE GRIPPER AND MOBILE ROBOTS

BY

ATTAWITH SUDSANG

B.Eng., Chulalongkorn University, 1991
M.S., University of Illinois, 1994

THESIS

Submitted in partial fulfillment of the requirements
for the degree of Doctor of Philosophy in Computer Science
in the Graduate College of the
University of Illinois at Urbana-Champaign, 1999

Urbana, Illinois

ABSTRACT

This thesis addresses the problem of immobilizing and manipulating parts with devices that have a mixture of discrete and continuous degrees of freedom. Immobilizing an object requires calculating the device parameters that reduce the positions and orientations of the object compatible with the contact constraints to a single point of its configuration space. Likewise, manipulating an object requires identifying the regions of its configuration space where it is free to move under the contact constraints. The kinematic theory of second order mobility of rigid bodies is used, together with the new concept of Inescapable Configuration Space region, to devise efficient algorithms for planning immobilizing fixtures, grasps, in-hand manipulation sequences and obstacle avoidance manipulation plans for parts with known geometry. This approach is applied to three different mechanisms: a fixturing device assembled from standard modular elements, a novel reconfigurable gripper, and a team of mobile robots.

ACKNOWLEDGMENTS

TABLE OF CONTENTS

CHAPTER 1

INTRODUCTION

1.1 Problem Statement

This thesis addresses the problem of immobilizing and manipulating parts through a few contacts with devices that have a mixture of discrete and continuous degrees of freedom (Figure 1.1). Immobilizing an object requires calculating the device parameters that reduce the positions and orientations of a part compatible with the contact constraints to a single point of its configuration space [48]. Likewise, manipulating an object requires identifying the regions of its configuration space where it is free to move under the contact constraints. Assuming frictionless contacts, we propose to use Rimon's and Burdick's kinematic theory of second-order mobility of rigid bodies [81, 82], together with a new notion of "Inescapable Configuration Space (ICS) Region" [95] based on a detailed analysis of the geometry of contact constraints in configuration space, to solve these problems and devise efficient algorithms for constructing immobilizing fixtures and grasps, in-hand manipulation sequences and motion plans avoiding collision with obstacles for parts with known geometry. This approach is applied to three different mechanisms: a fixturing device assembled from standard modular elements, a novel reconfigurable gripper, and a team of three mobile robots.

(a)   (b)   (c)
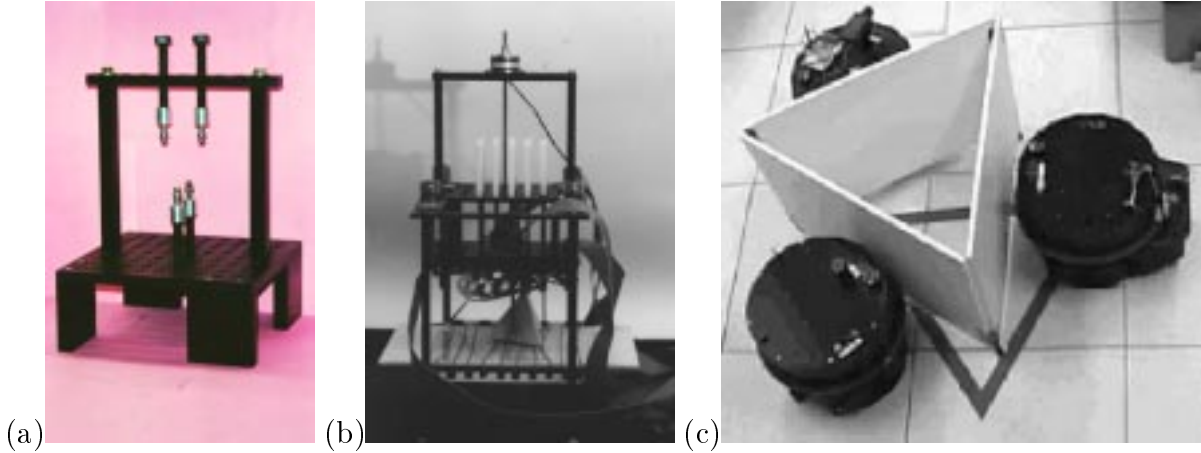
Figure 1.1 The three devices studied in this thesis: (a) a fixturing rig constructed from modular elements; (b) a novel reconfigurable gripper; (c) a team of three mobile robots.

1.2   A New Manipulation Framework

Current approaches to manipulation planning rely on detailed models of friction and contact dynamics to predict the object trajectory during task execution. This is difficult, sometimes unrealistic, and we also believe this is unnecessary. The main theme of this thesis is to develop a method that bypasses such modeling and prediction. We propose a new framework for object manipulation that is guaranteed to work in the absence of jamming. The proposed methodology is based on the new concept of Inescapable Configuration Space (or ICS) region for which kinematic constraints (imposed by the fact that solid objects cannot penetrate each other) are used to characterize the spectrum of joint object/robot configurations guaranteed to capture and immobilize the object.

More specifically, an ICS region is defined to be a pocket of free configurations that can be shrunk, without being broken, to an immobilizing configuration as the robots perform some command. This is illustrated by Figure 1.2 that shows a snapshot of the execution of a grasp of a triangle by three robots (shown as black disks). The two robots at the bottom are fixed and the commanded action is the motion of the top robot along the line segment. In the right part of the figure, the object is immobilized by the three robots. As the top robot moves along the vertical line, the object may move but not escape. The corresponding pocket of free configurations of the object is shown in the

bottom half of each figure (the configuration space is in 3-D but the pocket is drawn in 2-D for simplicity). As we move the top robot closer to the other two robots, the corresponding pocket gets smaller and smaller (as the object has less and less space to move) and finally the pocket contains only an immobilizing configuration when the top robot is at A. Because the pocket is never broken during the sequence, once it is known that the configuraton of the object is contained in the pocket we will be able to guarantee that the object cannot escape regardless of the position of the top robot on the line segment from A to C and of the configuration of the object inside the corresponding pocket. This pocket is the ICS region associated with the command to move the robot along the line segment from A to C.
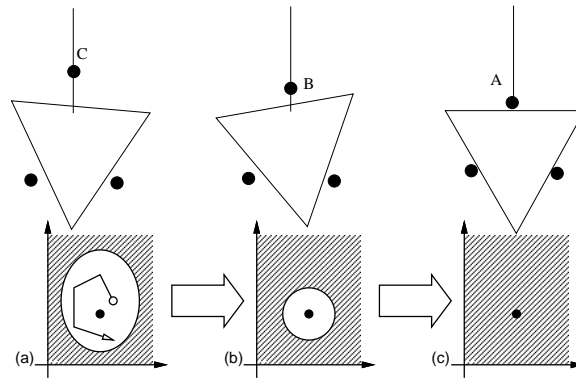
Figure 1.2 Definition of ICS.

The illustration given above is for a command with one degree of freedom. In general, the concept of ICS region can be applied to cases for which commanded actions have more degrees of freedom. We will consider commands with degrees of freedom ranging from two to six in Chapter 5 and 6.

We propose to use the concept of ICS regions to manipulate objects by computing a sequence of the commanded actions to bring the objects from an immobilizing configuration to another. This can be done by constructing a *capture graph* where nodes are the immobilizing configurations of the object and the robots, and there is an arc from node n' to node n'' if n' lies in the ICS region of n''. In the diagram shown in Figure 1.3, immobilizng configurations are denoted by lowercase letters, and their ICS regions are

depicted by ovals labels by the corresponding uppercase letters: the immobilizing config-
urations b and c both lie in the ICS region B associated with immobilizing configuration
b. Given the corresponding graph (shown in the right part of the figure), we can conclude
that an object lying at any point p inside A can be moved to e by four atomic motions:
$p \rightarrow a, a \rightarrow b, b \rightarrow d$ and $d \rightarrow e$.
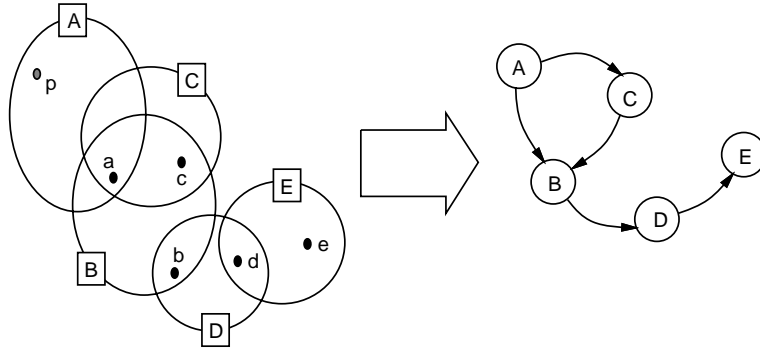
Figure 1.3 Immobilizing configurations and their ICS regions form a directed *capture graph*. In this example an object located at a point p of the ICS region A can be brought to the immobilizing configuration e by a sequence of four actions.

Constructing the capture graph does not require maintaining a global boundary rep-
resentation of the configuration space obstacles. Indeed, tasks such as grasping or part
re-orientation can be parameterized by a small number of variables (e.g., finger posi-
tions): as illustrated by Figure 1.4, the maximal free region of parameter space cor-
responds to a *critical* value of these variables for which the corresponding ICS pocket
becomes unbounded. Once this value is known, all that is needed is efficient algorithms
for determining the immobilizing configurations lying inside the associated ICS region
and testing whether some configurations lie inside the region, which is much simpler than
constructing an explicit description of this region.

We will present in Chapter 4 an efficient in-hand manipulation planner based on
the capture graph idea. The algorithm searches the graph for a sequence of appropriate
gripper configurations (pin triples and pin heights) that can bring the object from a given
initial configuration to one of the immobilizing configurations. A varient of this approach
is applied in Chapter 5 and Chapter 6 to the problem of manipulating polygons using
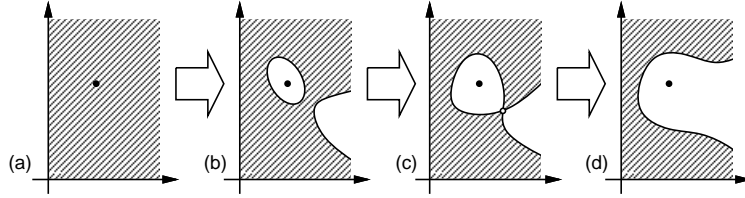
Figure 1.4 ICS region: (a) an immobilizing configuration; (b) a pocket is formed; (c) the pocket merges with an unbounded region of free space at a critical point; (d) the pocket does not exist anymore.

three disc-shaped robots. The manipulation planning for this problem is done without explicitly constructing the capture graph and the graph search is implicit by using only a single grasping configuration.

1.3   Thesis Organization

We review in Chapter 2 the classical concepts of equilibrium, force and form closure, and the newer theory of second-order mobility of rigid bodies [81, 82]. We also present the notion of ICS region in more detail.

We consider the problem of fixturing a three-dimensional object using simple modular elements in Chapter 3. Conceptually, the fixturing rig consists of two parallel plates with locator holes drilled along a rectangular grid, and of a set of spherical locators with integer height and radius. Four of these locators can be selected to form a fixture, and the rig has one continuous degree of freedom (the plate separation) and twelve discrete ones (the integer position and height of the locators). Standard modular elements such as the ones available from the QU CO kit can be used to implement this fixturing device (Figure 1.1(b)), and as shown in Chapter 3, second-order mobility theory can be used to derive simple sufficient conditions for the immobility of the fixtured part [81, 82] and the stability of the fixture [64, 38, 83]. In turn, these conditions are the basis for an algorithm that enumerates all of the stable immobilizing fixtures and grasps of a given polyhedron.

We then introduce in Chapter 4 a new reconfigurable gripper (Figure 1.1(b)) that consists of two parallel plates whose distance can be adjusted by a computer-controlled actuator. The bottom plate is a bare plane, and the top plate carries a rectangular grid of actuated pins that can translate in discrete increments under computer control. We have finished the construction of a prototype of the gripper as part of this thesis. A detailed analysis of the geometry of contact constraints in configuration space is used to devise a much more efficient variant of the fixturing algorithm and apply it to the problem of immobilizing a part with the gripper. This analysis also allows us to characterize the inescapable configuration space (ICS) regions associated with given gripper parameters [80] and to devise in-hand manipulation strategies that, unlike previous approaches to similar problems, do not require strong (and a priori unverifiable) assumptions on contact dynamics [1, 26, 33, 49, 55]. Simulation and actual experimental results are reported.

In Chapter 5, we apply again the concept of ICS to the problem of grasping, capturing and manipulating a polygonal object with three disc-shaped robots in the plane (Figure 1.1(c)). We characterize the range of possible motions of the object within the capture of the robots when two of the robots are fixed and the other one is allowed to move in the plane with two degrees of freedom. The algorithm for generating manipulation sequences has been implemented and both simulation and experimental results with Scout Normadics robots are included.

In Chapter 6, we revisit the same problem but this time all three robots move simultaneously. We present a new set of constraints allowing us to define regions in which the robots can simultaneously move freely while keeping the object from escaping. Although these new constraints are only sufficient and thus only approximate ICS regions, their simplicity enables us to prove the system controllability which in turn leads to a novel algorithm for planning manipulation sequences in the presence of obstacles.

Obviously, when the robots can perform the commanded actions perfectly, we can always bring the object from any configuration in an ICS region to the associated immobilizing configuration. This assumes perfect modeling and control. We report a number of successful experiments with real devices but it is clear that in general modeling and

control will not be perfect and that, in addition, friction may cause jamming. We assume frictionless contact through most of this thesis. This is a common (if sometimes implicit) assumption, since most grasping techniques, for example, assume that an object will not move at all during grasping, or will somehow move into the desired position. The frictionless assumption is mainly to ensure that the object reaches a desired immobilizing configuration when being grasped which is critical to the manipulation planning approach based on the capture graph search mentioned previously. However, in practice, friction may be significant enough to induce jamming. This motivates us to model the effect of friction in Chapter 7. We assume Coulomb friction and characterize the jamming configurations of a polygonal object being grasped by three robots. The purpose of this study is to gain a better understanding of the relationship between friction and the occurance of jamming with the goal to develop manipulation planning techniques that can accomodate relatively high friction loads without jamming.

Finally, we conclude the thesis in Chapter 8 with a summary of the thesis contributions and a discussion of future research plans.

CHAPTER 2

RIGID BODY MOBILITY THEORY

In this chapter, we review results of classical and modern kinematics that characterize the mobility (or lack thereof) of rigid bodies. In particular we present elementary concepts of screw theory [5], introduce the notions of form and force closure [59, 79], and discuss the concept of second-order immobility recently introduced by Rimon and Burdick [81, 84, 85]. We also clarify the relationship between these various notions, and introduce the notion of *inescapable configuration space* (or *ICS*) regions.

2.1   Screw Theory

We recall some elementary notions of screw theory. The following is largely based on Roth's excellent introduction [86]. See [5, 39, 8, 65, 66, 56] for more details.

A *screw* is a straight line with a pitch. The pitch is a linear magnitude that can be thought of as the rectilinear distance through which a nut attached to an ordinary screw is translated parallel to the screw axis while the nut is rotated through a unit angle [5].

Screws provide a unified representation for displacements and forces: from Chasles' theorem, any displacement of a rigid body can be described by a single rotation about a unique axis, combined with a unique translation parallel to this axis. The rotation axis is called the screw axis, and the ratio of the linear translation to the rotation angle is the pitch of the screw. The displacement is referred to as a *twist* about a screw. Its

magnitude is the angular rotation about the screw axis. Infinitesimal displacements and rigid body motions can also be described by twists.

From Poinsot's theorem, any system of forces and moments applied to a rigid body can be uniquely replaced by a single force and a couple, such that the force is parallel to the axis of the couple. In turn, these can be represented by a unique screw axis, a moment about this axis, and a force along it. The pitch of the screw is the ratio of the moment to the force. This combination of force and couple is called a *wrench* acting on a screw. The magnitude of the wrench is the magnitude of the associated force.

Algebraically, a screw can be represented by a sextuple of *screw coordinates*:

$$s = (u, x \times u + pu),$$

where u is a non-zero vector parallel to the screw axis, x denotes the coordinate vector of an arbitrary point on the axis, and p is the screw pitch. Alternatively, we can write the screw coordinates as $s = (u, v)$, where u, v are three-dimensional vectors.

Screw coordinates are homogeneous and a screw does not have a meaningful magnitude; in other words, screws form a five-dimensional projective space. However, screw coordinates can also be used to represent twists and wrenches, which are truly six-dimensional entities. In this case the magnitude of the screw coordinate vector is the magnitude of the associated twist or wrench.

We are now in a position to define force and form closure, but before closing this section, let us note that the wrench associated with a pure force (with no torque component) has a zero pitch; in other words, its screw coordinates are those of a line.

2.2 Force Closure, Form Closure and Equilibrium

We consider *positive grips* [59, 60] constructed as non-negative linear combinations of primitive wrenches (this amounts to assuming non-sticky fingers), and associate with a system of n primitive wrenches $w_1, \ldots, w_n$ the wrench set

$$\mathcal{W} = \{\sum_{i=1}^{n} \xi_i w_i : \xi_i \geq 0 \text{ for } i = 1, \ldots, n\}.$$

Definition 1 *A system of n wrenches $\boldsymbol{w}_1, \ldots, \boldsymbol{w}_n$ is said to achieve force closure when the corresponding wrench set $\mathcal{W}$ is equal to $I\!\!R^6$.*

Intuitively, a system of wrenches achieves force closure when any external load can be balanced by a non-negative combination of the primitive wrenches. Force closure is sometimes called *force/torque closure* [59, 60]. A related notion is *form closure* (also called *complete restraint*) [79, 43, 87]: a system of wrenches acting on some object is said to achieve form closure when it prevents all motions (including infinitesimal ones) of this object. Force and form closure are dual of each other, in the same sense as wrenches and infinitesimal twists are dual notions [86] and, as noted in [63, 60] for example, force-closure grasps are form-closure and vice versa.

Let us note that there is unfortunately no general agreement on terminology in the grasping literature (see [98, 57] for discussions of this problem): for example, Reulaux [79], Salisbury [87], Ji [41], Markenscoff *et al.* [52], and Trinkle [98] use the expression form closure for what we call force closure, and reserve the expression force closure for grasps that can only balance certain external loads. Our definitions match the ones used by Mishra et al. [59], Nguyen [63], and Murray et al. [62].

A somewhat weaker notion is equilibrium, defined below.

Definition 2 *A system of n wrenches $\boldsymbol{w}_1, \ldots, \boldsymbol{w}_n$ is said to achieve equilibrium when the convex hull of the points $\boldsymbol{w}_1, \ldots, \boldsymbol{w}_n$ in $I\!\!R^6$ contains the origin.*

In other words, a given system of wrenches achieves equilibrium when the equation

$$\sum_{i=1}^{n} \xi_i \boldsymbol{w}_i = 0 \tag{2.1}$$

admits a non-trivial, non-negative solution.

Mishra, Schwartz, and Sharir [59] have shown that a necessary and sufficient condition for a system of wrenches to achieve force closure is that the origin of $I\!\!R^6$ lies in the *interior* of the convex hull of the primitive wrenches. In particular, force closure implies equilibrium but there are wrench systems that achieve equilibrium but not force closure.[1]

---

[1]These systems of wrenches are called *strong force-closure* systems by Trinkle [98]. Of course, as noted before, his notion of force closure is different from ours.

In the frictionless case, Reulaux [79], Somov [91] and, much later, Lakshminarayana [43] have shown that four (resp. seven) fingers are *necessary* to achieve force closure of a 2D (resp. 3D) object. In turn, Mishra, Schwartz, and Sharir [59] have shown that six (resp. twelve) fingers are always *sufficient* for objects without rotational symmetries, and Markenscoff, Ni, and Papadimitriou [52] have tightened this result by showing that under very general conditions, four (resp. seven) fingers are sufficient to achieve a force-closure grasp of a 2D (resp. 3D) object without rotational symmetries. They have also shown that when Coulomb friction is taken into account, three fingers are sufficient in the 2D case, and four are sufficient in the 3D case.

2.3 Second-Order Immobility

Paradoxically, there exist grips which are not form-closure yet actually immobilize the grasped object: for example, three frictionless fingers positioned at the centers of the edges of an equilateral triangle cannot prevent an infinitesimal rotation of the triangle about its center of mass, yet prevent any finite motion. More generally, Czyzowicz, Stojmenovic and Urrutia have shown that three point contacts in the plane and four contacts in the three-dimensional case are sufficient to immobilize (i.e., prevent any *finite* motion of) a polyhedron [18].

Rimon and Burdick [81, 84, 85] have clarified the notion of immobility by re-casting it in terms of the *configuration space* $\mathcal{C}$ [48, 46] representing all possible positions and orientations of the manipulated body B. In this framework, B maps onto a point $\mathcal{B}$ of $\mathcal{C}$, while the fingers maps onto volumes (obstacles) $\mathcal{O}_i$. Contact between a finger and the object is achieved when $\mathcal{B}$ is on the surface of the corresponding obstacle $\mathcal{O}_i$, and the wrench exerted by the finger in this case is the normal to the surface of $\mathcal{O}_i$. Fingers are in simultaneous contact with the object when the surfaces of the corresponding obstacles intersect in $\mathcal{B}$, and immobilized configurations simply correspond to isolated points of the free space of $\mathcal{C}$.

This solves the paradox mentioned earlier: at equilibrium, the tangent planes to the various obstacles are linearly dependent. Force (hence form) closure is achieved when the normals to the obstacles positively span $\mathbb{R}^d$ where $d = 3$ in the plane and $d = 6$ in three dimensions, so the inner half-spaces associated with the tangent planes effectively isolate the point lying at their intersection. With fewer than $d + 1$ fingers, the normals cannot positively span $\mathbb{R}^d$, and since they are linearly dependent, there is at least a one-dimensional escape route for the object in the intersection of the half-spaces. Of course, the actual surfaces of the configuration space obstacles are curved, and the intersection of these obstacles may very well isolate the point $\mathcal{B}$ even if the half-spaces associated with their tangent planes do not. In other words, form closure is only a *sufficient* condition for immobility, based on a first-order approximation of the obstacles' surfaces by their tangent planes.

Rimon and Burdick have gone further and shown that a sufficient condition for immobility is that the relative curvature form associated with an essential equilibrium [2] grasp or fixture and defined by (see [84, Def. 4 and Eq. (8)]):

$$\kappa_{\text{rel}} = \sum_{i=1}^{d} \lambda_i |\boldsymbol{w}_i| \kappa_i$$

be negative definite. Here the weights λ_i are the equilibrium weights of (3.1), and $|\boldsymbol{w}_i|$ is the magnitude of the wrench exerted by finger number i. The coefficient κ_i is the curvature form associated with the corresponding contact; it is defined by (see [84, eq. (20)]):

$$\kappa_i = \frac{1}{|\boldsymbol{w}_i|}(\boldsymbol{v}^T, \boldsymbol{\omega}^T)(\mathcal{C}_i^T \mathcal{L}_i \mathcal{C}_i + \mathcal{D}_i)\begin{pmatrix} \boldsymbol{v} \\ \boldsymbol{\omega} \end{pmatrix},$$

where
$$\mathcal{L}_i = \begin{pmatrix} \mathcal{L}_{B_i}(\mathcal{L}_{O_i} + \mathcal{L}_{B_i})^{-1}\mathcal{L}_{O_i} & -\mathcal{L}_{O_i}(\mathcal{L}_{O_i} + \mathcal{L}_{B_i})^{-1} \\ -(\mathcal{L}_{O_i} + \mathcal{L}_{B_i})^{-1}\mathcal{L}_{O_i} & -(\mathcal{L}_{O_i} + \mathcal{L}_{B_i})^{-1} \end{pmatrix},$$

---

[2]Essential equilibrium is achieved when the coefficients λ_i in (3.1) are uniquely defined and strictly positive [84].

$\mathcal{L}_{B_i}$ and $\mathcal{L}_{O_i}$ denote respectively the second fundamental forms [21] of the surfaces of body B and finger O_i at the contact point (in the workspace), and

$$\mathcal{C}_i = \begin{pmatrix} \mathcal{I} & -[\boldsymbol{p}_{i\times}] \\ 0 & [\boldsymbol{n}_{i\times}] \end{pmatrix}, \quad \mathcal{D}_i = \begin{pmatrix} 0 & 0 \\ 0 & -([\boldsymbol{n}_{i\times}]^T[\boldsymbol{p}_{i\times}])^S \end{pmatrix},$$

where, by definition, $\mathcal{A}^S = \frac{1}{2}(\mathcal{A} + \mathcal{A}^T)$, and $[\boldsymbol{a}_\times]$ denotes the skew-symmetric matrix such that $[\boldsymbol{a}_\times]\boldsymbol{x} = \boldsymbol{a} \times \boldsymbol{x}$.

2.4 Inescapable Configuration Space Regions

As observed in the previous section, the immobilized configurations of a rigid object B correspond to isolated points of the free part $\mathcal{F}$ of its configuration space $\mathcal{C}$. More generally, for a given configuration of the fingers (or obstacles) O_i, we will call a compact connected component of $\mathcal{F}$ an *inescapable configuration space* (or *ICS*) region, since any object trajectory starting in such a region cannot escape this region. For polygonal objects and obstacles in the plane, the rational representation of trigonometric functions can be used to represent the boundaries of the ICS regions by algebraic ruled surfaces of low degree in $\mathbb{R}^3$ [12], and it follows that ICS regions can be identified by classical algebraic cell-decomposition methods [2, 17, 88].

In the approach to object manipulation presented in Chapters 4, 5 and 6, we will focus on the case of polygonal or polyhedral objects resting on a plane, with a small and fixed number of circular or spherical fingers (obstacles), and will give a simple characterization of the ICS regions in that case. In particular, we will show that appropriate motions of the fingers monotonically reduce the ICS regions to isolated points of $\mathcal{F}$ (i.e., immobilized configurations). Conversely, we will also characterize the *maximal* ICS regions, i.e., the critical finger configurations for which the free space stops being compact and the object is free to escape to infinity. This will allow us to plan manipulation sequences by efficiently constructing and exploring the adjacency graph formed by overlapping maximal ICS regions, and to effect a desired object motion by changing the finger configurations so the object goes from one immobilizing configuration to the next.

For an ICS region, there is an associated immobilizing configuration. Identifying the immobilizing configuration is the first crucial step in applying the concept of ICS region to a manipulation problem. In the next chapter, we will consider the problem of immobilizing an object. This requires calculating device parameters that reduce the set of possible positions and orientations of the object compatible with the contact constraints to a single point. This method for identifying immobilizng configurations will be used throughout the remaining of the thesis.

CHAPTER 3

MODULAR FIXTURES

3.1 Introduction

We address the problem of immobilizing an object through a few contacts with simple modular fixturing elements, with applications in manufacturing. Our approach is based on the notion of second-order immobility introduced by Rimon and Burdick [81, 84, 85], and it is related to recent work in fixture planning by Wallack and Canny [102, 103], Brost and Goldberg [10], Wagner, Zhuang, and Goldberg [101], and Brost and Peters [11].

For concreteness, let us consider the fixturing device shown in Figure 3.1: it consists of two parallel plates with locator holes drilled along a rectangular grid, and of a set of spherical locators with integer height and radius. Four of these locators can be selected to form a fixture; either two of them are mounted on each plate (type I configuration, Figure 3.1(a)), or three locators are mounted on the first plate, the last one being mounted on the second plate (type II configuration, Figure 3.1(b)). The distance between the plates is a continuously adjustable degree of freedom of the device. (This device is a generalization of the two-dimensional fixturing vise proposed by Wallack and Canny [102, 103].)

Our goal is to compute the locator configurations (i.e., placements and heights) as well as the plate separation that will guarantee that a polyhedral part in frictionless contact with the locators is immobilized. To solve this problem, we must (1) formulate operational conditions for immobility, (2) enumerate all of the locator configurations

15
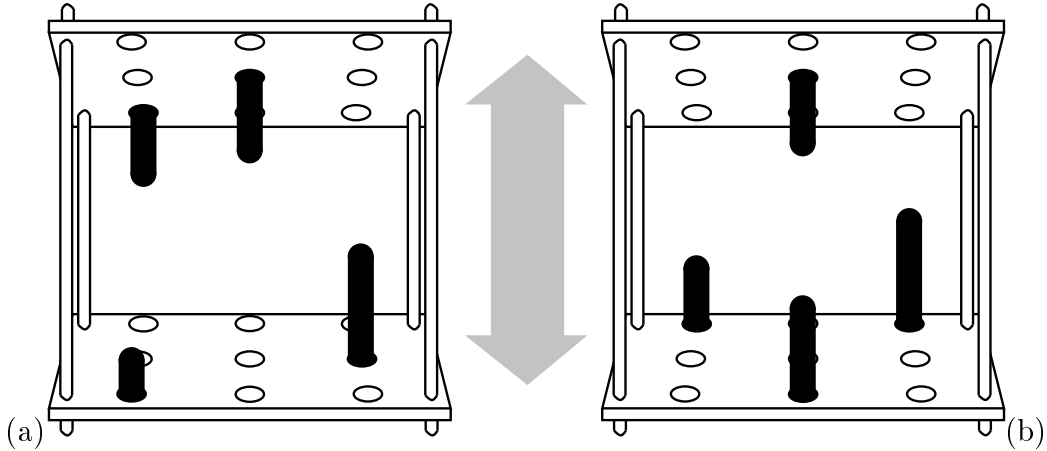
Figure 3.1 The proposed fixturing device: (a) type I configuration, (b) type II configuration.

that may achieve immobility, and (3) for each of these configurations, decide whether there exists a pose of the fixtured object that simultaneously achieves contact with the four locators and guarantees immobility. Our approach to step (1) is to specialize the conditions formulated by Rimon and Burdick to the class of fixturing elements and objects of interest. Step (2) can then be reduced to solving a combinatorial problem, so we can attack step (3) using numerical algebraic methods [50, 51, 61].

It should be noted that the conceptual design shown in Figure 3.1 can be implemented using standard modular fixturing elements such as the ones available in the QU CO kit: for example, a type I configuration can be constructed using two spherical locators mounted on a plate and two additional locators mounted on a beam clamp (Figure 3.2). A similar assembly with three locators and an adjustable vertical clamp can be used for type II configurations.

The rest of this chapter is organized as follows. Previous work in fixture planning is reviewed in Section 3.2. Our approach is described in Section 3.3 and 3.4: sufficient conditions for immobility and stability are derived in Section 3.3; they are used in Section 3.4 to design an efficient algorithm for enumerating all immobilizing stable fixtures of a given polyhedral object using the device shown in Figure 3.1. Preliminary experiments are presented in Section 3.5.

16

(a)   (b)
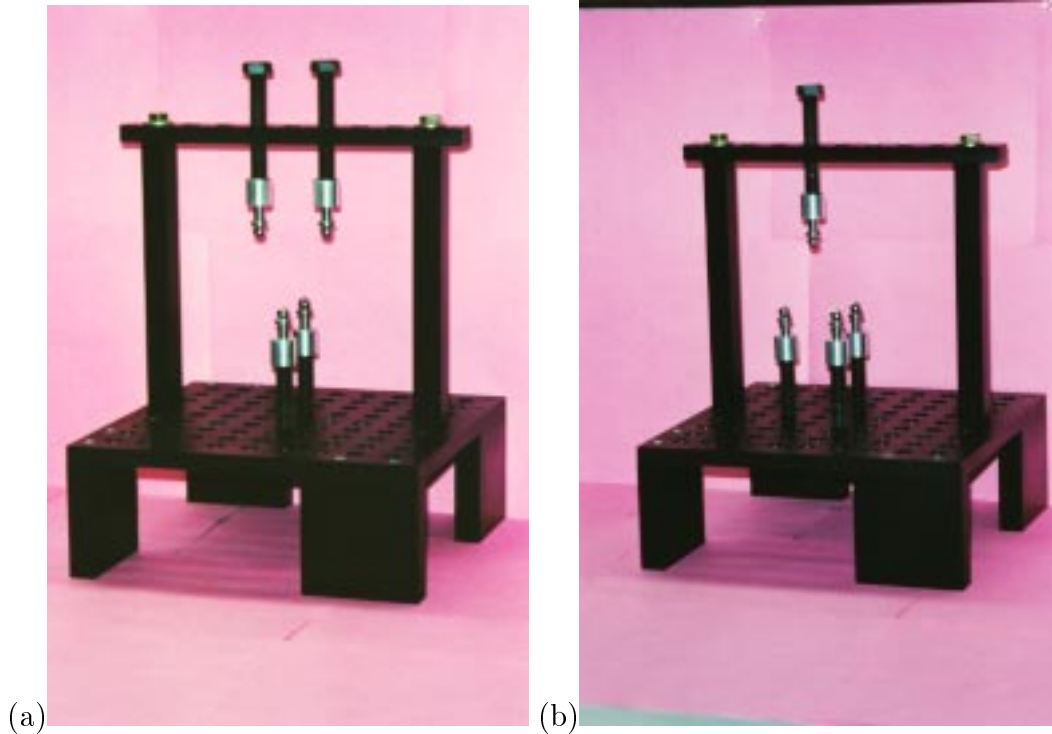
Figure 3.2 Implementing type I and type II configurations of the proposed fixturing device using standard modules from the QU CO kit.

3.2   Related Work

Modular fixturing systems consist of a kit of modules that can be reconfigured to fixture different parts. They have the potential of avoiding the costs associated with the design of custom fixtures, but pose the problem of automatically planning the module configurations adequate for a given part geometry. Traditionally, fixture designers have relied on heuristics such as the *3:2:1 fixturing principle* [35, 89]: the object to be fixtured is first positioned relative to a plane (*primary datum*) defined by three contact points; it is then positioned relative to a line (*secondary datum*) defined by two additional contact points, and finally positioned relative to a last point contact (*tertiary datum*). When the six points have been chosen correctly, the position of the fixtured object is completely determined as long as the contacts are maintained (*deterministic positioning* [3]). The object is then clamped into place by one or several additional contacts (*total constraint* [3]). Positioning is typically achieved through contact with *passive* fixturing elements

such as plates, vee blocks, and locators, while clamping is achieved through contact with *active* fixturing elements, such as vises, toe clamps, or chucks.

The theoretical justification for such an approach finds its roots in the dual role of fixtures: immobilizing a part and resisting the forces and torques involved in manufacturing tasks such as assembly or machining.[1] Since screw theory [5, 39, 66] can be used to represented both displacements (*twists*) and forces and moments (*wrenches*), it is an appropriate tool for analyzing and designing fixtures. Indeed, it is known that six independent contact wrenches are necessary to prevent any infinitesimal displacement which maintains contact, and that a seventh one is required to ensure that contact cannot be broken (these correspond to the positioning and clamping contacts introduced above) [43, 91]. As discussed in Chapter 2, such a fixture prevents any infinitesimal motion of the object, and it is said to achieve form closure [66, 79, 87]. Form closure implies force closure [60, 63], and fixtures achieving form/force closure also fulfill their second role as devices capable of resisting external forces and torques.

Past approaches to fixture planning have been based on expert systems [28, 34, 54], kinematic analysis and screw theory [3, 6, 16, 58], or a combination of both [25, 30]: Markus *et al.* have used a rule-based system to interactively design fixtures for box-type parts and to select appropriate fixture modules [54]. Ferreira and Liu have used a generate-and-evaluate approach to determine the orientation of workpieces for machining operations [28]. Hayes and Wright have proposed *Machinist*, an expert-system-based process planner that incorporates fixturing information in the construction of a machining plan [34].

While expert systems are limited in their ability to generate fixture configurations based on analytical considerations, approaches based on screw theory can accurately predict the performance of fixture designs: Asada and By have proposed the *Automatically Reconfigured Fixturing (ARF)* system, which uses a detailed kinematic analysis to derive conditions for deterministic positioning, part accessibility and detachability, and

---

[1]There are of course other issues involved in fixturing, for example the analysis of part deformation under clamping, see [19, 37] for approaches using finite-element methods.

total constraint [3]. Their approach has been integrated into a robotic assembly cell. Chou, Chandru, and Barash have developed a mathematical method based on screw theory for analyzing and synthesizing fixtures, and used linear programming to generate optimal clamp positions constrained to lie within convex contact polygons [16]. Bausch and Youcef-Toumi have introduced the notion of *motion stop* which represents the geometric resistance of a contact point to a given screw motion, and they have used it to compare fixture configurations. Their approach is integrated with the CATIA CAD system and is capable of synthesizing optimal fixture configurations from a discrete set of candidates.

Finally, it should be noted that some systems bridge the gap between expert systems and kinematic and force analysis: Gandhi and Thompson have proposed a methodology that relies on expert knowledge, force analysis, and geometric reasoning to synthesize and analyze modular fixture configurations [30]. Englert has also combined analytical considerations and knowledge-based methods to identify tradeoff relations between part production attributes and propose a control structure for planning part setup and clamping [25].

As noted by Wallack [103], there has recently been a renewed interest in the academic robotics community for manufacturing problems in general and fixturing in particular. Mishra has studied the problem of designing fixtures for rectilinear parts using toe clamps attached to a regular grid, and proven the existence of fixtures using six clamps [58] (this result has since then been tightened to four clamps by Zhuang, Goldberg, and Wong [107]). In keeping with the idea of *Reduced Intricacy Sensing and Control (RISC)* robotics of Canny and Goldberg [13], Wallack and Canny [102, 103] and Brost and Goldberg [10] have recently proposed very simple modular fixturing devices and efficient algorithms for constructing form-closure fixtures of two-dimensional polygonal and curved objects. Wagner, Zhuang, and Goldberg [101] have also proposed a three-dimensional seven-contact fixturing device and an algorithm for planning form-closure fixtures of a polyhedron with pre-specified pose.

All of the approaches discussed so far are based on the concepts of form and force closure. A different notion is *stability*: a part is said to be in stable equilibrium if it returns to its equilibrium position after having been subjected to a small displacement. Stability is very important in real mechanical systems which cannot be expected to have perfect accuracy. Nguyen has shown that force (or form) closure implies stability [64], but Donoghue, Howard and Kumar have shown that there exist stable grasps or fixtures which do not achieve form closure [23, 38]. As discussed in Chapter 2, Rimon and Burdick have introduced the notion of *second-order immobility* [81, 84, 85] and shown that certain equilibrium grasps (or fixtures) of a part which do not achieve form closure effectively prevent any *finite* motion of this part through curvature effects in configuration space. They have given operational conditions for immobilization and proven the dynamic stability of immobilizing grasps under various deformation models [85]. An additional advantage of this theory is that second-order immobilization can be achieved with fewer fingers (four contacts for convex fingers) than form closure (seven contacts [43, 91]). As detailed in the next section, we propose to exploit second-order immobility in fixture planning for three-dimensional polyhedral objects.

In this chapter, we first derive simple sufficient conditions for immobility and stability in the case of contacts between spherical locators and polyhedral objects (Section 3.3). We then use these conditions in Section 3.4 to design an efficient algorithm for planning stable immobilizing fixtures of a polyhedral object with the device shown in Figure 3.1.

3.3   Sufficient Conditions for Immobility and Stability

3.3.1   A sufficient Condition for Immobility

Let us consider a rigid object and the contacts between d locators and this object. Let us also denote by $\boldsymbol{p}_i$ $(i = 1, .., d)$ the positions of the contacts in a coordinate frame at-

tached to the object, and by $\boldsymbol{n}_i$ ($i = 1, .., d$) the unit inward normals to the corresponding faces.

As before, we say that equilibrium is achieved when the contact wrenches balance each other, i.e.,

$$\sum_{i=1}^{d} \lambda_i \begin{pmatrix} \boldsymbol{n}_i \\ \boldsymbol{p}_i \times \boldsymbol{n}_i \end{pmatrix} = 0, \tag{3.1}$$

for some $\lambda_i \geq 0$ ($i = 1, .., d$) with $\sum_{i=1}^{d} \lambda_i = 1$.

We now specialize Rimon's and Burdick' sufficient condition for second-order immobility to the case of a polyhedron in contact with d spherical locators. As shown in Chapter 2, the relative curvature form is defined by

$$\kappa_{\mathrm{rel}} = \sum_{i=1}^{d} \lambda_i |\boldsymbol{w}_i| \kappa_i$$

be negative definite. Here the weights λ_i are the equilibrium weights of (3.1), $|\boldsymbol{w}_i|$ is the magnitude of the wrench exerted by locator number i, and κ_i is the curvature form associated with the corresponding contact; this quadratic form is defined by:

$$\kappa_i = \frac{1}{|\boldsymbol{w}_i|} (\boldsymbol{v}^T, \boldsymbol{\omega}^T)(\mathcal{C}_i^T \mathcal{L}_i \mathcal{C}_i + \mathcal{D}_i) \begin{pmatrix} \boldsymbol{v} \\ \boldsymbol{\omega} \end{pmatrix},$$

where $\boldsymbol{v}$ and $\boldsymbol{\omega}$ denote the translational and rotational parts of an infinitesimal twist, $\mathcal{L}_i$ is a matrix related to the surface curvatures of the body and locator at the contact points, and the matrices $\mathcal{C}_i$ and $\mathcal{D}_i$ depend only on the position $\boldsymbol{p}_i$ of the contact point and the normal to $\boldsymbol{n}_i$ to the body's surface in $\boldsymbol{p}_i$.

Specializing the above equations to equilibrium contacts between spherical locators and polyhedra yields:

$$\kappa_{\mathrm{rel}} = \sum_{i=1}^{d} \lambda_i \boldsymbol{\omega}^T \mathcal{K}_i \boldsymbol{\omega}, \quad \text{where} \quad \mathcal{K}_i = ([\boldsymbol{n}_{i\times}]^T [\boldsymbol{p}_{i\times}])^S - r_i [\boldsymbol{n}_{i\times}]^T [\boldsymbol{n}_{i\times}], \tag{3.2}$$

and r_i denotes the locator's radius. Note that there is no term involving the translation $\boldsymbol{v}$ in this case. It follows from (3.2) that a sufficient condition for immobility is that the 3×3 symmetric matrix

$$\mathcal{K} = \sum_{i=1}^{d} \lambda_i \mathcal{K}_i$$

is negative definite.

3.3.2   A Sufficient Condition for Stability

We prove a sufficient condition for the stability (in the sense of Nguyen [64], see also [23, 38]) of a fixture configuration, and show that it is equivalent to the immobility condition derived in the previous paragraph (see [85] for a more general statement of the dynamic stability of immobilizing grasps).

Each locator is modeled as a sphere of radius r_i attached to a linear spring whose axis is aligned with the inward normal to the corresponding contact face. As the solid moves, the sphere slides on the contact face and translates along the corresponding spring (Figure 3.3).
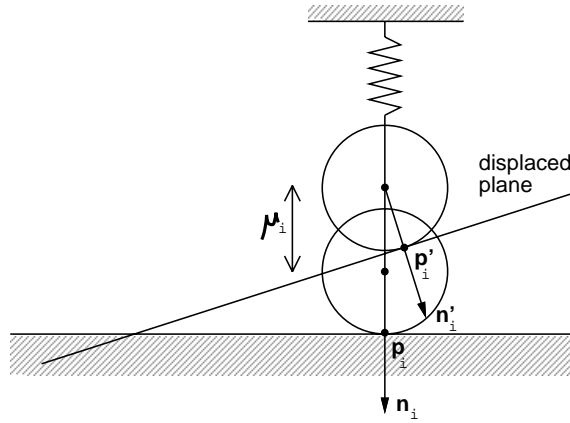
Figure 3.3 Small displacement of a plane in contact with a sphere mounted on a spring.

The potential energy of the fixture is the sum of the potential energies of the individual springs, i.e.,

$$U = \sum_{i=1}^{d} \frac{1}{2}\sigma_i^2,$$

where σ_i is the displacement of the spring associated with locator number i from its position at rest (we assume a unit spring constant for each locator). In general we can write $\sigma_i = -\lambda_i + \mu_i$, where λ_i is the compression at equilibrium (which is of course equal to the coefficient λ_i in (3.1)) and μ_i denotes the displacement of the sphere along $\boldsymbol{n}_i$ corresponding to a given displacement of the solid. An equilibrium fixture will be stable

when it corresponds to a local minimum of the potential energy (as a function of small displacements of the object).

A rigid displacement is specified by a rotation $\mathcal{R}$ of axis $\boldsymbol{a}$ and angle θ, and a translation $\boldsymbol{v}$. Following Nguyen [64], we use a second-order Taylor expansion of the exponential definition of rotations, and parameterize μ_i by the twist $(\boldsymbol{v}, \boldsymbol{\omega})$, where $\boldsymbol{\omega} = \theta \boldsymbol{a}$.

The gradient and Hessian of the potential energy are respectively

$$\nabla U = \sum_{i=1}^{d}(-\lambda_i + \mu_i)\nabla\mu_i \quad \text{and} \tag{3.3}$$

$$\nabla^2 U = \sum_{i=1}^{d} \nabla\mu_i\nabla\mu_i^T + (-\lambda_i + \mu_i)\nabla^2\mu_i.$$

A simple calculation shows that the gradient of μ_i at the origin is the wrench $(\boldsymbol{n}_i^T, \boldsymbol{p}_i \times \boldsymbol{n}_i^T)^T$, and it follows as expected that the fixture is in equilibrium if and only if equation (3.1) is satisfied. To decide whether the equilibrium is stable, we must examine the Hessian of the potential function. Computing the Hessian of μ_i at the origin and substituting in (3.3) yields:

$$\nabla^2 U|_{0,0} = \mathcal{F} + \mathcal{S},$$

$$\text{where} \quad \mathcal{F} = \sum_{i=1}^{d} \begin{pmatrix} \boldsymbol{n}_i \\ \boldsymbol{p}_i \times \boldsymbol{n}_i \end{pmatrix} \begin{pmatrix} \boldsymbol{n}_i \\ \boldsymbol{p}_i \times \boldsymbol{n}_i \end{pmatrix}^T, \quad \text{and} \quad \mathcal{S} = -\sum_{i=1}^{d} \lambda_i \begin{pmatrix} 0 & 0 \\ 0 & \mathcal{K}_i \end{pmatrix}.$$

The equilibrium is stable when $\mathcal{F}+\mathcal{S}$, the Hessian of the potential function, or *stiffness matrix*, is positive definite. The matrix $\mathcal{F}$ is of course positive semi-definite, its zeros being the twists reciprocal to the wrenches exerted by the locators (which are guaranteed to exist for frictionless fixtures when $d \leq 6$). These twists satisfy the equations

$$\boldsymbol{v} \cdot \boldsymbol{n}_i + \boldsymbol{\omega} \cdot (\boldsymbol{p}_i \times \boldsymbol{n}_i) = 0 \quad \text{for} \quad i = 1, \ldots, d. \tag{3.4}$$

For equilibrium fixtures, only three of the above equations are independent, and for any choice of $\boldsymbol{\omega}$ there exists in general a vector $\boldsymbol{v}$ such that (3.4) is satisfied. Thus $\nabla^2 U$ is positive definite if and only if the matrix $\mathcal{K}$ is negative definite. This condition is the same as the sufficient condition for immobility derived earlier.

3.4 Planning Four-Locator Immobilizing Fixtures of Polyhedral Objects

In this section, we focus on the four-locator case and present an efficient algorithm for enumerating all immobilizing fixtures of a polyhedral object that can be achieved with the device of Figure 3.1. To simplify this planning process, we reduce the problem of achieving contact between a spherical locator and a plane to the problem of achieving point contact with a plane. This is done without loss of generality by growing the object to be fixtured by the locator radius and shrinking the spherical end of the locator into its center (see [10, 102, 103] for similar approaches in the two-dimensional case). For the sake of conciseness, we restrict our attention here to type II fixture configurations. Planning type I configurations involves analogous methods and has the same cost.

The algorithm can be summarized as follows. For each quadruple of faces do:

1. Test whether they can be held in essential equilibrium.

2. Enumerate all locator configurations potentially achieving equilibrium through contacts with the selected faces.

3. For each such configuration, compute the pose of the object and test the immobilization condition.

3.4.1 Testing Essential Equilibrium

For a polyhedral object, the normals $\boldsymbol{n}_i$ are fixed vectors. To ensure essential equilibrium, we restrict our attention to quadruples of faces such that no three of them have coplanar normals. This ensures that the coefficients λ_i in (3.1) are uniquely defined, and it allows us to compute them from the equation $\sum_{i=1}^{4} \lambda_i \boldsymbol{n}_i = 0$ and to test whether they all have the same sign. If they do not, the four candidate faces are rejected. If they do, we obtain three independent *linear* constraints on the positions of the locators on the

faces:

$$\sum_{i=1}^{4}(\lambda_i \boldsymbol{n}_i) \times \boldsymbol{p}_i = 0. \tag{3.5}$$

(Note that the coefficients λ_i are now constants depending only on the choice of faces.)

We can parameterize each contact $\boldsymbol{p}_i$ by two variables u_i, v_i. Assuming convex faces, the fact that the contact points actually belong to the faces can be written as a set of linear inequalities on u_i, v_i:

$$f_{ij}(u_i, v_i) \leq 0, \quad j = 1, .., k_i, \tag{3.6}$$

where k_i is the number of edges that bound face number i.

Given a choice of four faces, a necessary and sufficient condition for the existence of contact points within those faces which achieve equilibrium is that there exists a solution to (3.5) subject to the constraints (3.6). This can be tested using linear programming. If the test is negative, the quadruple of faces is rejected.

For quadruples passing this second test, there is only (in general) a subset of each face that can participate in an equilibrium configuration. The subset corresponding to face number i is determined by projecting the five-dimensional polytope defined by (3.5) and (3.6) onto the plane (u_i, v_i). Several algorithms can be used to perform this projection, including Fourier's method [29], the convex hull and extreme point approaches of Lassez and Lassez [45, 44], and the Gaussian elimination and contour tracking techniques of Ponce *et al.* [75].

For faces with a bounded number of edges, all of these algorithms run in constant time, and they can be used to construct sub-faces that can be passed as input to the rest of the algorithm.

3.4.2   Enumerating Locator Configurations

An exhaustive search of all possible grid coordinates would be extremely expensive: consider an object of diameter D (measured in units equal to the distance between successive plate holes); there are $O(D^8)$ type II possible configurations: one locator is at

the origin with zero length, two locators have three integer coordinates, the last locator has only two. A similar line of reasoning also applies to type I configurations, and it yields the same order of complexity.

This has prompted us, like Wallack and Canny [102, 103] and Brost and Goldberg [10] in the two-dimensional case, to use bounds on the distance between two faces to restrict the set of grid coordinates under consideration. The minimum and maximum distances between pairs of points belonging to two given faces can be computed in constant time as follows: the maximum distance between two faces is always achieved for a pair of vertices. The minimum distance, on the other hand, may be achieved for any pair of face, edge, or vertex points (Figure 3.4). The first two cases shown in Figure 3.4 (face-face and edge-face pairs) only occur when two faces are parallel or when one edge is parallel to a face, and they reduce to computing the distance between a vertex and a face. Thus, there are only three non-trivial cases: the vertex-face, edge-edge, and vertex-edge pairs, and the corresponding distances are easily computed by constructing the unique straight line orthogonal to the pair of features of interest.
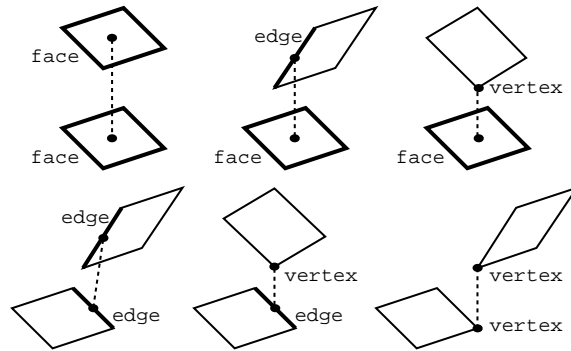
Figure 3.4 A list of the feature combinations yielding the minimum distance between two faces.

Let us position the first locator at the origin with zero length. The integer point corresponding to the second locator is then constrained to lie within the spherical shell centered at the origin with inner radius equal to the minimum distance between the two corresponding faces and outer radius equal to the maximum distance. Given the position of the second locator, the third locator is now constrained to lie within the region formed

by the intersection of the two shells associated with the first and second locator. Finally, given the position of the third locator, the fourth locator is constrained to lie within a region formed by the intersection of three shells. The projection of this region onto the first plate yields the set of integer coordinates of the locator. Its last coordinate δ is determined at the next stage of the algorithm.

3.4.3 Computing the Pose Associated with a Given Locator Configuration

To avoid imposing a particular parameterization of the object's pose, we take advantage of the fact that a tetrahedron is completely determined by the lengths of its six edges.

We define the tetrahedron whose vertices are the four contacts by six quadratic equality constraints of the form

$$|\boldsymbol{p}_i - \boldsymbol{p}_j|^2 = l_{ij}^2, \text{ with } i = 1, 2, 3 \text{ and } i < j \leq 4, \tag{3.7}$$

which specify the lengths of the tetrahedron's edges.

At this point, the integer grid coordinates of the locators are fixed, and the coefficients l_{ij} are only functions of the variable δ. Thus the equalities (3.5) and (3.7) form a system of nine equations in the nine unknowns u_i, v_i ($i = 1, .., 4$) and δ. Since three of these equations are linear, and the remaining six are quadratic, this system admits at most $2^6 = 64$ solutions which can easily be computed using homotopy continuation [61] or the toolkit for algebraic computation described in [50].

Once the solutions have been found, we can check whether they satisfy the linear inequalities (3.6) defining the contact faces, then check whether they achieve immobilization. Note that the object pose corresponding to a given locator configuration and plate distance is easily computed: since one of the locators is at the origin, we only need to compute the rotation mapping the fixturing device's coordinate frame onto the object's coordinate frame. Since we know the positions of the contacts in both coordinate systems, it is a simple matter to compute the corresponding rotation.

3.4.4 Algorithm Analysis.

For each quadruple of faces, enumerating the locator configurations amounts to determining the integer positions falling in regions defined by the intersection of two, four, or six half-spaces bounded by spheres. A naive approach to that problem is to test every grid point against the constraints defining the regions of interest with cost $O(D^8)$, where D is as before the diameter of the object measured in units equal to the distance between two successive holes.

A better approach is to use a three-dimensional scan-line conversion algorithm to determine the integer points within a region in (optimal) time proportional to the number V of these points: scan-line conversion algorithms are used in computer graphics to render polygonal and curved shapes by enumerating pixels within these shapes one row at a time; they only require the ability to trace the shape boundaries and find their extrema in the horizontal and vertical dimension, and they have a time complexity linear in the size of their output. It is relatively straightforward to generalize these algorithms to the three-dimensional case: we can construct an explicit representation of the region boundaries by a procedure akin to boundary evaluation in constructive solid geometry. This process is simplified by the fact that in our case the boundary elements are sphere patches, circular arcs (intersections of two spheres), and vertices (intersections of three spheres). Constructing the boundary representation and its extrema in any direction can be done in constant time (given our bounded number of half-spaces), and scan-line conversion can then proceed, one plane at a time, in time proportional to V (Figure 3.5). Thus, the time complexity of our overall algorithm is $O(N^4 V)$ where N is the number of faces of the polyhedron. Of course, V is still, in the worst case, $O(D^8)$.

We can assume without loss of generality that each face can be inscribed in a disc of diameter d (note that $d \leq D$ and that in practice, we may have $d \ll D$). The volume of a spherical shell is then $O(D^2 d)$, and the area of the intersection of two such shells is also at worse $O(D^2 d)$. The area of the projection of the intersection of three shells is itself $O(Dd)$. Thus the total complexity of the algorithm is $O(N^4 D^5 d^3)$.
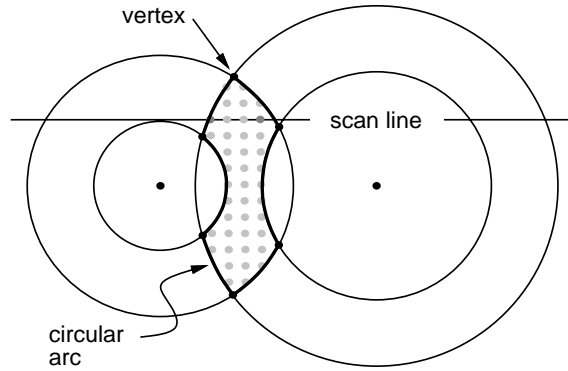
Figure 3.5 Illustration of scan-line conversion in the 2D case: spans between consecutive boundary elements are filled one scan-line at a time.

To obtain a more realistic estimate of the algorithm's behavior, let us further assume that the polyhedron under consideration has total area A with faces all having the same area, so $d^2 = O(D^2/N) = O(A/N)$. Under this assumption, the complexity of the algorithm becomes $O(N^2\sqrt{N}A^4)$. It should also be noted that, in practice, we will often have $d \ll D$, so the volume of the intersection of two shells will be proportional to Dd^2 instead of D^2d, and the area of the projection of the intersection of three shells will often be d^2 instead of Dd (Figure 3.6). More experiments will allow us to conduct an empirical evaluation of this model.
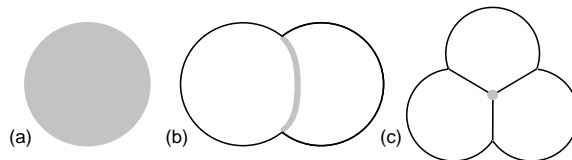
Figure 3.6 The regions shown in grey correspond to the position of: (a) the second locator, (b) the third locator, (c) the fourth locator.

3.5 Implementation and Results

We have fully implemented the proposed fixturing algorithm. The implementation has been written in C, and it includes the two pruning stages proposed in Section 3.4: the subsets of the faces that may participate in an immobilizing grasp are first found

by projecting the polytope defined by the equilibrium constraints (3.5) and (3.6) onto the parameter space of the faces. Candidate configurations that satisfy the distance constraints associated with these subsets of the faces are then enumerated by scan-converting the volumes bounded by the corresponding spherical shells.

Figure 3.7 shows some simulation results. The test object is a tetrahedron, and each result is shown from two different viewpoints. As shown in Figure 3.2, we have also constructed the proposed four-locator fixturing device using modular fixturing elements from the QU CO kit. We have used an aluminum base plate with an array of threaded holes, compatible threaded bolts and nuts, removable spherical locator tips, and a horizontal beam. The bolts and spherical tips are used as locators, and different locator heights are implemented by attaching different number of nuts to the bolts before screwing them through the threaded holes of the base plate. The horizontal beam is used as a support for the top locators.

Table 3.1 shows some quantitative results for different grid resolutions. In our experiments we have used a $K \times K$ grid with various values of K, as well as locators whose height may take ten discrete values. Table 3.1 shows the results obtained without any pruning (N), using spherical shell pruning only (S), and combining the projection- and shell-pruning stages (P+S).

K	# Candidates		
	N	S	P+S
3	6,377,292	267,868	223,224
4	63,700,992	4,429,772	3,601,440
5	379,687,500	20,720,018	17,709,408
6	1,632,586,752	297,104,432	237,683,544

Table 3.1 Quantitative results using a tetrahedron as a test object.

We have used homotopy continuation [61] to solve the polynomial system of degree 64 that determines the poses of an object compatible with a given locator configuration. Our distributed implementation of continuation takes roughly 2.5 seconds on two networked four-processor SUN SPARCstations 10 to solve this system. Thus we have not been able

a)

b)

c)

d)
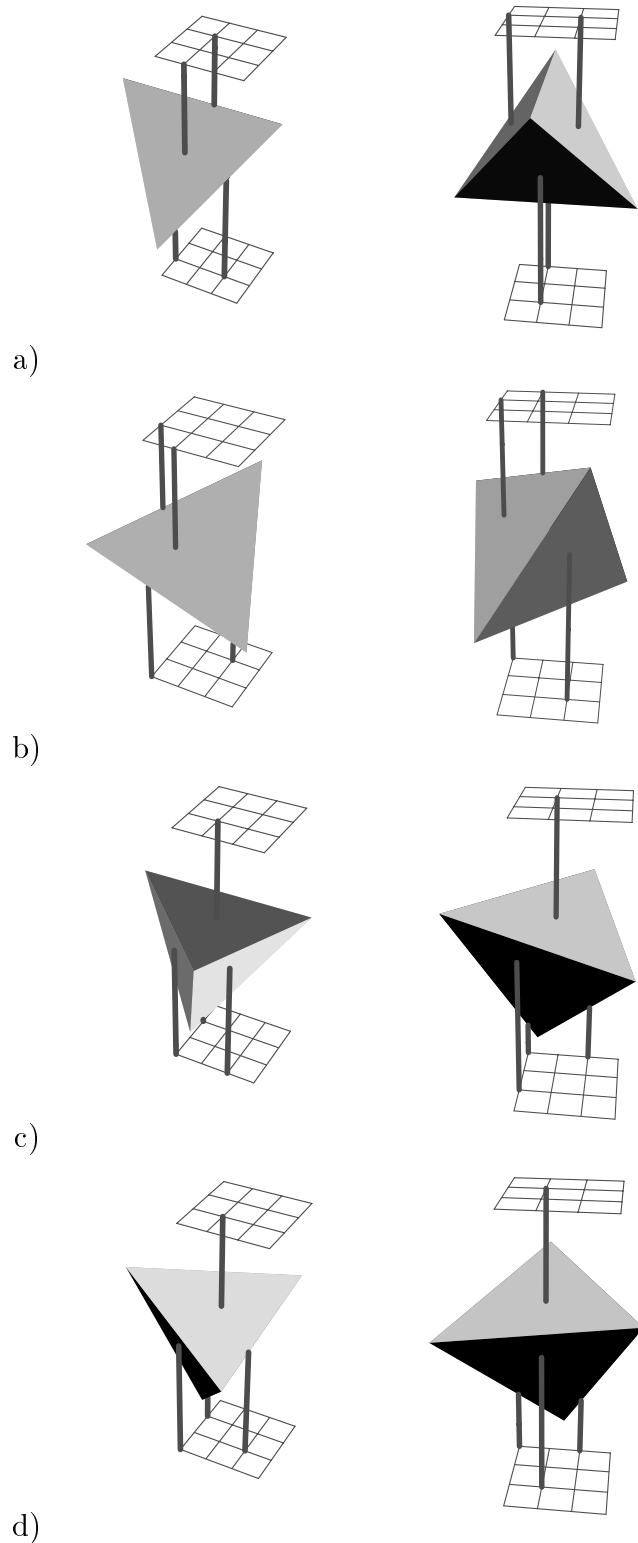
Figure 3.7 Some solutions for the four-locator fixturing device.

(a)   (b)
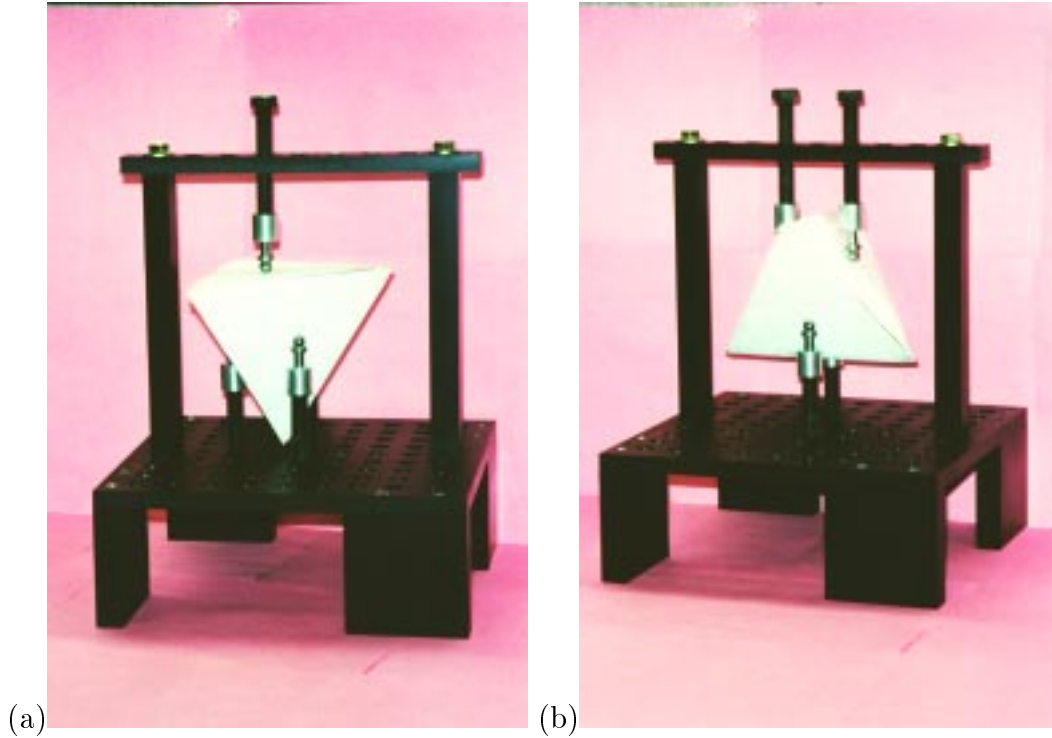
Figure 3.8 The fixturing device immobilizing a tetrahedron.

in our actual experiments with moderate grid resolutions to compute in a reasonable time all of the achievable fixtures. Instead, we have stopped the computation once a few immobilizing fixtures had been found. The statistics given in Table 3.1 have been obtained by running only the part of the algorithm that enumerates all possible locator configurations.

3.6   Conclusions

We have given sufficient conditions for the immobility and stability of modular fixtures, and proposed and implemented an algorithm for fixturing three-dimensional polyhedra. To the best of our knowledge, this algorithm is the first ever proposed for fixturing true three-dimensional objects with arbitrary pose (see [101, 11] for related work using prismatic fixturing elements and three-dimensional objects with pre-specified pose). In-

teresting future research includes finding a lower-degree to pose computation in the fixture planning and considering a wider, more realistic class of fixturing situations.

Fixturing and grasping are two problems with the same objective, which is immobilizing objects. It is therefore an obvious step to modify the fixturing rig presented in this chapter for grasping purpose. In the next chapter, we propose a new reconfigurable gripper which is a motorized version of the fixture.

CHAPTER 4

A RECONFIGURABLE GRIPPER

4.1 Introduction

Classical parallel-jaw grippers are unable to adapt to a wide variety of workpiece geometries; although dextrous hands have been proposed by the academic robotics community [40, 87], they are too expensive and cumbersome for typical manufacturing applications. Thus different grippers are used for different parts (hundreds of different models are indeed listed by gripper manufacturers). This calls for the design of reconfigurable grippers which combine the flexibility of dextrous hands with the cost-effectiveness and simplicity of parallel-jaw grippers, and for the development of accompanying software to reconfigure these grippers according to part geometry. We propose a new reconfigurable gripper which is simply a motorized version of the fixture presented in the previous chapter.

We address in this chapter the problem of grasping and manipulating three-dimensional polyhedral objects using the new reconfigurable gripper. The gripper consists of two parallel plates whose distance can be adjusted by a computer-controlled actuator (Figure 4.1). The bottom plate is a bare plane, and the top plate carries a rectangular grid of actuated pins that can translate in discrete increments under computer control.

As part of this thesis work, we have completed the construction of a prototype of this gripper. Figure 4.1(b)-(d) shows some pictures of our prototype: it is equipped with a grid of twenty five fingers, each one of them being mounted on the lead screw of a separate

linear actuator. The top and lower plate assemblies can be moved relative to each other using a large linear actuator. To avoid friction as much as possible, the bottom plate is covered with a series of strings of metal beads, which lets the manipulated part roll with minimal resistance. We should stress that designs that are simpler, more reliable and more accurate, are of course possible: for example, we only need three pins to move at any time, which does not require one actuator per pin. Our main goal here is to demonstrate that manipulation tasks can actually be performed using our approach.
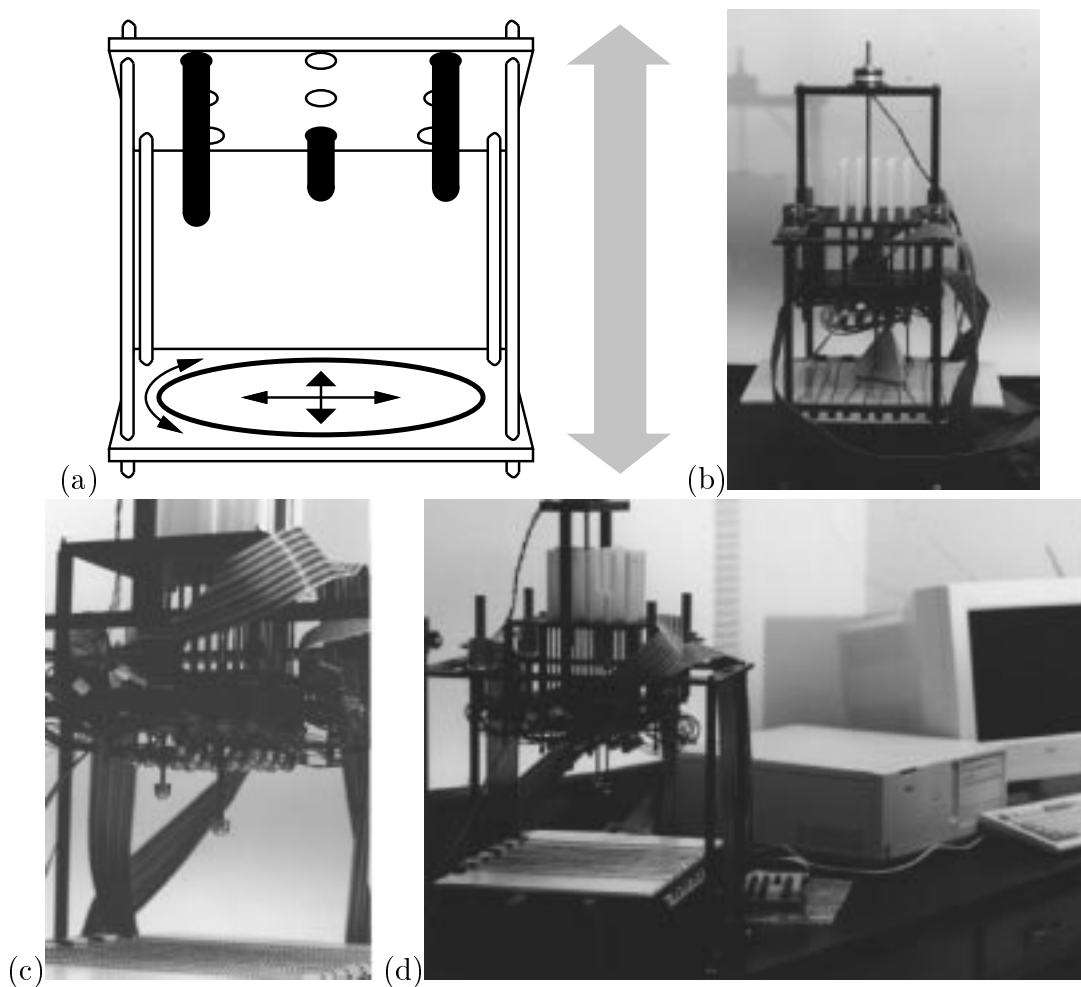
Figure 4.1 A reconfigurable gripper: (a) conceptual design and (b)-(d) actual prototype.

We propose to use this gripper to immobilize objects through frictionless contacts with three of the pins and the bottom plate, and to manipulate an object within a grasp

35

by planning the sequence of pin configurations that will bring this object to a desired position and orientation.

Our approach is based on the notion of second-order immobility introduced by Rimon and Burdick [81] and on a detailed analysis of the geometry of the joint object/gripper configuration space. Characterizing the range of possible object motions associated with a grasp configuration allows us to identify the "minimal" configurations for which the object is totally immobilized as well as the "maximal" ones for which there is a non-empty open set of object motions within the grasp, but no escape path to infinity. The minimal configurations are the basis for grasping, and the maximal ones are the basis for in-hand manipulation. In addition, our analysis decouples the continuous and discrete degrees of freedom of the gripper, which allows us to devise efficient algorithms for grasp and manipulation planning.

The rest of this chapter is organized as follows. Previous work on grasp and manipulation planning is briefly reviewed in Section 4.2. We attack the problem of planning immobilizing grasps with our reconfigurable gripper in Section 4.3 by first studying the contact geometry in configuration space (Section 4.3.1) then using the results of this study to devise an efficient grasp planning algorithm (Section 4.3.2). Simulation results are presented in Section 4.3.3. We turn in Section 4.4 to the problem of planning in-hand manipulation sequences, and again study the geometry of the problem (Section 4.4.1) before presenting an efficient manipulation planning algorithm (Section 4.4.2). Simulation results are presented in Section 4.4.3. Section 4.5 generalizes our in-hand manipulation approach to the case of continuous finger motions, and Section 4.7 concludes the chapter.

4.2   Related Work

The notions of form and force closure are the traditional theoretical basis for grasp planning algorithms. Mishra, Schwartz, and Sharir [59] have proposed linear-time algorithms for computing a finger configuration achieving force closure for frictionless polyhedral objects. Markenscoff and Papadimitriou [53] and Mirtich and Canny [57] have

proposed algorithms for planning grasps which are optimal according to various criteria [27]. In each of these works, the grasp-planning algorithm outputs a single grasp for a given set of contact faces. Assuming Coulomb friction [63], Nguyen has proposed instead a geometric method for computing *maximal independent* two-finger grasps of polygons, i.e., segments of the polygonal boundary where the two fingers can be positioned independently while maintaining force closure, requiring as little positional accuracy from the robot as possible. This approach has been generalized to handle various numbers of fingers and different object geometries in [7, 15, 68, 71, 72, 75]

Robotic grasping and fixture planning are related problems (in both cases, the object grasped or fixtured must, after all, be held securely), but their functional requirements are not the same: as remarked by Chou, Chandru, and Barash [16], machining a part requires much better positional accuracy than simply picking it up, and the range of forces exerted on the parts are very different. The role of friction forces is also different: in the grasping context, where fingers are often covered with rubber or other soft materials, friction effects can be used to lower the number of fingers required to achieve form closure from seven to four; in the fixturing context, on the other hand, it is customary to assume frictionless contact, partly due to the large magnitude and inherent dynamic nature of the forces involved [16] (see, however [47] for an approach to fixture planning with friction). Finally, the kinematic constraints on the positions of the contacts are also quite different: in particular, dextrous grippers have *continuous* degrees of freedom, corresponding to the various finger joints, while modular fixtures have mostly *discrete* degrees of freedom, corresponding for example to the position of pins on an integer grid attached to a fixturing plate.

In Chapter 3, we introduced a new approach to modular fixture planning, based on the notion of second-order immobility. In this chapter, we propose to bridge the gap between fixture and grasp planning by considering a new class of reconfigurable grippers with mostly discrete degrees of freedom, which have the potential of achieving the same level of flexibility as dextrous robotic hands for a fraction of the cost. We also give an algorithm for grasp planning and introduce a new approach to in-hand manipulation.

Unlike previous approaches to similar problems, this approach does not require strong (and a priori unverifiable) assumptions on contact dynamics [1, 26, 33, 49, 55].

4.3 Grasp Planning

In this section, we consider the problem of grasping a three-dimensional polyhedral object with our gripper and derive geometric conditions for contact, equilibrium, and immobility. We then use these conditions in an efficient algorithm for enumerating all immobilizing grasps of a polyhedral object.

4.3.1 Geometry of the Problem

Although we consider manipulating objects in the plane, the contact constraints are very similar to those in the previous chapter. More precisely, our gripper can be used to hold a polyhedral object through contacts with three of the top plate pins, and either a face, an edge-and-vertex, or a three-vertex contact with the bottom plate. Let us assume for the sake of simplicity that the faces of the polyhedron are triangular (convex faces can be handled in similar ways, see [16] for a related approach). Any wrench exerted at a contact point between a face and the bottom plate can be written as a positive combination of wrenches at the vertices. Likewise, the wrenches corresponding to an edge-and-vertex contact are positive combinations of wrenches exerted at the end-points of the line segment and at the vertex. Thus equilibrium configurations can be found, in general, by writing the equilibrium equation (3.1) for six elementary wrenches.

We detail the case of a contact between the bottom plate and a triangular face f with inward unit normal $\boldsymbol{n}$ and vertices $\boldsymbol{v}_i$ ($i = 1, 2, 3$), and assume in all the sequel that the remaining faces f_i ($i = 1, 2, 3$) are convex, with inward unit normals $\boldsymbol{n}_i$ (Figure 4.2). We also assume without loss of generality that the four vectors $\boldsymbol{n}$ and $\boldsymbol{n}_i$ ($i = 1, 2, 3$) *positively span* $\mathbb{R}^3$, i.e., that a strictly positive linear combination of these vectors is equal to zero (this is a necessary condition for essential equilibrium). Finally, given the physical layout of our gripper, contact between the upper-jaw pins and faces such that

$\boldsymbol{n} \cdot \boldsymbol{n}_i > 0$ is of course impossible, and we further assume without loss of generality that $\boldsymbol{n} \cdot \boldsymbol{n}_i < 0$ for $i = 1, 2, 3$.
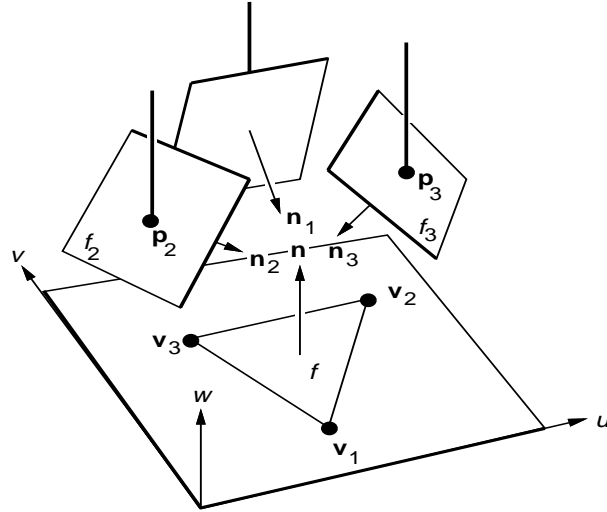
Figure 4.2 The four faces involved in a grasp.

Under these assumptions, we can choose a coordinate system (u, v, w) attached to the object with w axis parallel to $\boldsymbol{n}$, and write in this coordinate system

$$\boldsymbol{n} = \begin{pmatrix} 0 \\ 0 \\ 1 \end{pmatrix} \quad \text{and} \quad \boldsymbol{n}_i = \frac{1}{l_i} \begin{pmatrix} a_i \\ b_i \\ -1 \end{pmatrix}, \quad \text{where} \quad l_i = \sqrt{1 + a_i^2 + b_i^2}.$$

Likewise, since the vectors $\boldsymbol{n}$ and $\boldsymbol{n}_i$ $(i = 1, 2, 3)$ positively span $\mathbb{R}^3$, we can write $\boldsymbol{n} = -\sum_{i=1}^{3} \mu_i \boldsymbol{n}_i$, where $\mu_i > 0$ for $i = 1, 2, 3$. To complete the specification of the faces f_i $(i = 1, 2, 3)$, we will denote by c_i the height of f_i at the origin, so the plane of this face can be parameterized by $w_i = a_i u_i + b_i v_i + c_i$. Finally, since we assume convex faces, we will express the fact that the point associated with the parameters u_i, v_i actually belongs to f_i by a set of linear inequalities on u_i, v_i:

$$a_{ij} u_i + b_{ij} v_i + c_{ij} \leq 0, \quad j = 1, .., k_i, \tag{4.1}$$

where k_i is the number of edges that bound face number i.

4.3.1.1 Contact

We reduce the problem of achieving contact between a spherical pin and a plane to the problem of achieving point contact with a plane. This is done without loss of generality by growing the object to be fixtured by the pin radius and shrinking the spherical end of the pin into its center. We attach a coordinate system (q, r, w) to the gripper, and denote by $\mathcal{R}$ and $\boldsymbol{t}$ the rotation of angle θ about $\boldsymbol{n}$ and the translation (x, y) in the plane orthogonal to $\boldsymbol{n}$ that map the (q, r, w) coordinate system onto the (u, v, w) coordinate system.

If $\boldsymbol{p}_i$ and $\boldsymbol{q}_i$ denote respectively the positions of the tip of pin number i in the object's and gripper's coordinate frames, we can write

$$\boldsymbol{p}_i = \begin{pmatrix} u_i \\ v_i \\ a_i u_i + b_i v_i + c_i \end{pmatrix}, \quad \boldsymbol{q}_i = \begin{pmatrix} q_i \\ r_i \\ \delta - h_i \end{pmatrix} \quad \text{and} \quad \boldsymbol{q}_i = \mathcal{R}\boldsymbol{p}_i + \boldsymbol{t}, \tag{4.2}$$

where q_i, r_i and h_i denote respectively the integer pin position on the bottom plate grid and its height, and δ is the jaw separation.

Equation (4.2) is a condition for contact between pin number i and the corresponding face. It can be rewritten as $\mathcal{C}_i(x, y, \theta, \delta) = 0$, where

$$\mathcal{C}_i(x, y, \theta, \delta) \stackrel{\text{def}}{=} (x - q_i)\cos(\theta + \alpha_i) + (y - r_i)\sin(\theta + \alpha_i) + d_i\delta - e_i = 0, \tag{4.3}$$

and $\alpha_i = \text{Arg}(a_i, b_i)$ and $d_i = 1/\sqrt{a_i^2 + b_i^2}$, and $e_i = d_i(c_i + h_i)$.[1] Note that α_i is simply the angle between the u axis and the projection of $\boldsymbol{n}_i$ onto the u, v plane (Figure 4.3(a)).

For a given jaw separation δ, the set $S_i(\delta)$ of object configurations (x, y, θ) for which $\mathcal{C}_i(x, y, \theta, \delta) = 0$ forms a ruled surface: indeed, its intersection with a plane $\theta = \text{constant}$ is a line $L_i(\delta, \theta)$ at distance $e_i - d_i\delta$ from the fixed point (q_i, r_i) of the x, y plane, and the angle between the x axis and the normal to this line is $\theta + \alpha_i$ (Figure 4.3(b)). Changing θ corresponds to rotating the line about the point (q_i, r_i), while changing δ corresponds to translating the line.

---

[1]Here, abusing the usual mathematical notation, $\text{Arg}(c, s)$ is the angle a such that $\cos(a) = c/\sqrt{c^2 + s^2}$ and $\sin(a) = s/\sqrt{c^2 + s^2}$.
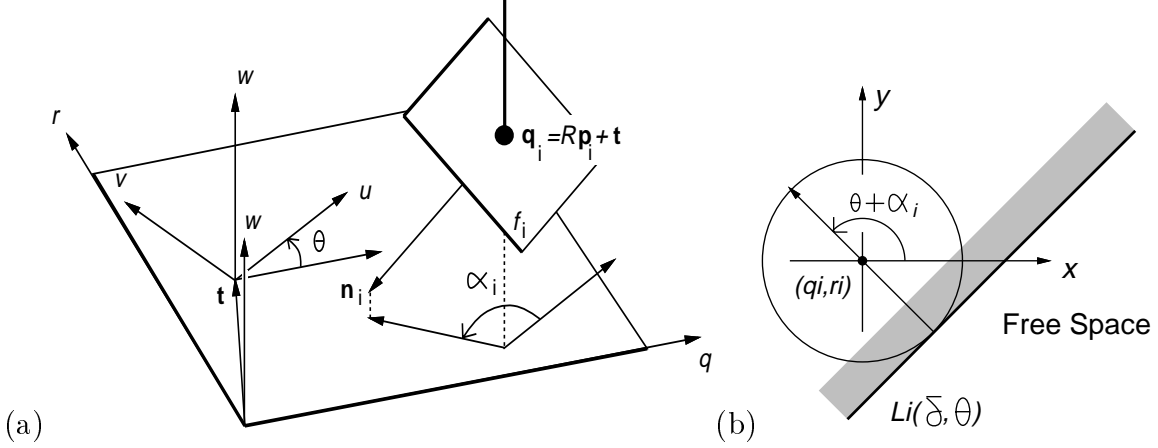
Figure 4.3 Contact between a pin and a face: (a) in workspace; (b) in x, y configuration space.

The three pins will be in contact with the corresponding faces when (4.3) is satisfied for $i = 1, 2, 3$. In particular, if

$$\mathcal{E}(\delta, \theta) \stackrel{\text{def}}{=} \sum_{i=1}^{3} \frac{\mu_i}{d_i l_i} \mathcal{C}_i(x, y, \theta, \delta),$$

then $\mathcal{E}(\delta, \theta) = 0$ whenever the three contacts are achieved simultaneously. A simple calculation exploiting the relation $\boldsymbol{n} = -\sum_{i=1}^{3} \mu_i \boldsymbol{n}_i$ shows that

$$\mathcal{E}(\delta, \theta) = \delta - A \cos(\theta - \alpha) - B, \tag{4.4}$$

where

$$\begin{cases} A = \sqrt{C^2 + S^2}, \quad \alpha = \operatorname{Arg}(C, S), \quad B = \sum_{i=1}^{3} \frac{\mu_i}{l_i}(c_i + h_i) \\ \\ C = \sum_{i=1}^{3} \frac{\mu_i}{l_i}(a_i q_i + b_i r_i), \quad \text{and} \quad S = \sum_{i=1}^{3} \frac{\mu_i}{l_i}(-b_i q_i + a_i r_i). \end{cases}$$

Note that (4.4) justifies the notation $\mathcal{E}(\theta, \delta)$ since the value of $\mathcal{E}$ is independent of x and y. More importantly, it is now clear that a necessary condition for the existence of an object position achieving contact with the three pins is that the point (θ, δ) lies on the *contact sinusoid* defined by $\mathcal{E}(\delta, \theta) = 0$. This condition is also sufficient: for given values of θ and δ on this sinusoid, the three linear equations $\mathcal{C}_i(x, y, \theta, \delta)$ $(i = 1, 2, 3)$ in the two unknowns x and y are linearly dependent, and thus admit a common solution.

41

4.3.1.2 Equilibrium

Here we take advantage of the fact that the overall scale of the wrenches is irrelevant to rewrite the equilibrium equation (3.1) as

$$\begin{cases} \sum_{i=1}^{3} \lambda_i \begin{pmatrix} \boldsymbol{n} \\ \boldsymbol{v}_i \times \boldsymbol{n} \end{pmatrix} + \sum_{i=1}^{3} \mu_i \begin{pmatrix} \boldsymbol{n}_i \\ \boldsymbol{p}_i \times \boldsymbol{n}_i \end{pmatrix} = 0, \\ \lambda_1 + \lambda_2 + \lambda_3 = 1, \end{cases} \quad (4.5)$$

where $\lambda_i \geq 0$ $(i = 1, 2, 3)$.

In turn, using the fact that $\boldsymbol{n} = -\sum_{i=1}^{3} \mu_i \boldsymbol{n}_i$, forming the dot product of the above expression with $\boldsymbol{n}$, and using elementary properties of triple products yields

$$\sum_{i=1}^{3} \mu_i [(\mathcal{R}^{-1} \boldsymbol{q}_i) \times \boldsymbol{n}] \cdot \boldsymbol{n}_i = 0,$$

which can be rewritten in the coordinate system (q, r, w) as

$$\sum_{i=1}^{3} \frac{\mu_i}{l_i} [(-b_i q_i + a_i r_i) \cos \theta - (a_i q_i + b_i r_i) \sin \theta] = 0 \iff \sin(\theta - \alpha) = 0.$$

It follows that a necessary and sufficient condition for three pins in contact with the corresponding faces of the object to achieve equilibrium is that $\theta = \alpha$ or $\theta = \alpha + \pi$. Note that these values of θ are independent of the heights of the pins, which will prove extremely important in the grasp planning algorithm presented in Section 4.3.2.

4.3.1.3 Immobility

We now examine the sufficient condition for immobility derived in Chapter 3 in the case of our gripper. Since the radii corresponding to the planar contacts are effectively infinite, it is obvious that $\boldsymbol{\omega}^T \mathcal{K} \boldsymbol{\omega}$ is negative for any vector $\boldsymbol{\omega}$ which is not parallel to $\boldsymbol{n}$. Thus we must determine the sign of

$$\boldsymbol{n}^T \mathcal{K} \boldsymbol{n} = M \sum_{i=1}^{3} \mu_i [(\boldsymbol{n}_i \times \boldsymbol{n}) \cdot (\boldsymbol{P}_i \times \boldsymbol{n}) - r |\boldsymbol{n}_i \times \boldsymbol{n}|^2], \quad (4.6)$$

where r is the common radius of the pins and $M = 1/(1 + \sum_{i=1}^{3} \mu_i)$ is a scale factor used to balance the fact that we have chosen $\lambda_1 + \lambda_2 + \lambda_3 = 1$ in our formulation of equilibrium.

Note that we have used $\boldsymbol{P}_i$ instead of $\boldsymbol{p}_i$ to denote the position of the contact point because (4.6) is valid in the coordinate system of the *original object*: as noted earlier, we assume in the rest of this paper that the object has been grown by the pin radius, while the spherical end of the pin has been shrunk into its center. This implies that $\boldsymbol{P}_i = \boldsymbol{p}_i + r\boldsymbol{n}_i$. In turn, using (4.2) allows us to rewrite (4.6) as

$$\boldsymbol{n}^T\mathcal{K}\boldsymbol{n} = M\sum_{i=1}^{3}\mu_i(\boldsymbol{n}_i \times \boldsymbol{n}) \cdot [(\mathcal{R}^{-1}(\boldsymbol{q}_i - \boldsymbol{t})) \times \boldsymbol{n}],$$

or equivalently

$$\boldsymbol{n}^T\mathcal{K}\boldsymbol{n} = M\sum_{i=1}^{3}\frac{\mu_i}{l_i}[(a_iq_i + b_ir_i)\cos\theta + (-b_iq_i + a_ir_i)\sin\theta] = AM\cos(\theta - \alpha),$$

and it follows that $\mathcal{K}$ is negative definite if and only if $\theta = \alpha + \pi$.

4.3.1.4 Main Results

We can now summarize the results obtained in this section with the following lemma.

Lemma 1: For given integer pin positions and heights q_i, r_i and h_i ($i = 1, 2, 3$), a sufficient condition for an object at configuration (x_0, y_0, θ_0) to be immobilized by a grasp with jaw separation δ_0 is that:

(1) $\theta_0 = \alpha + \pi$,

(2) $\mathcal{C}_i(x_0, y_0, \theta_0, \delta_0) = 0$ for $i = 1, 2, 3$, and

(3) $a_{ij}[(q_i - x_0)\cos\theta_0 + (r_i - y_0)\sin\theta_0] + b_{ij}[-(q_i - x_0)\sin\theta_0 + (r_i - y_0)\cos\theta_0] + c_{ij} \leq 0$ for $i = 1, 2, 3$ and $j = 1, .., k_i$.

This lemma is an obvious corollary of the results obtained in Sections 4.3.1.1, 4.3.1.2 and 4.3.1.3, the third condition simply expressing the fact that the contacts must occur within the faces.

4.3.2 Algorithm

According to Lemma 1, all continuous degrees of freedom of a grasp (object orientation, jaw separation and object position) can be computed once the grasp's discrete degrees of freedom (pin positions and heights) have been set. This yields the following naive algorithm for grasp planning: for each quadruple of faces, enumerate all grid positions and heights of the three pins, then compute the remaining grasp parameters and check whether they satisfy condition (3) of Lemma 1. This algorithm is similar to the fixture planning technique, and its complexity is $O(N^4D^6)$, where N is the number of faces of the grasped polyhedron, and D is its diameter measured in units equal to the distance between successive grid points.

A better approach is the following algorithm, which has the same overall structure as the naive one, but limits the number of faces and gripper configurations under consideration by exploiting a number of geometric constraints, most notably the fact that the orientation of an object held in an immobilizing grasp depends only on the pins' positions and not on their heights:

For each quadruple of faces do

1. Test whether they can be held in equilibrium.

2. Enumerate all pin positions that may immobilize the object and compute the corresponding object orientation.

3. For each such position, enumerate the pin lengths that immobilize the object and compute the remaining grasp parameters.

The first step of the algorithm uses linear programming and polytope projection techniques [29, 45, 44, 75] to prune gripper configurations that cannot achieve equilibrium. The second step uses distance constraints to reduce the enumeration of the pin positions that may yield equilibrium grasps to the scan-line conversion of circular shells (see [102, 103, 10] for related approaches to fixture planning for two-dimensional objects). Finally,

the third step of the algorithm uses condition (3) of Lemma 1 to reduce the enumeration of pin heights that yield immobilizing grasps to polygon scan conversion.

The three steps of the algorithm are detailed in Sections 4.3.2.1 to 4.3.2.3. Section 4.3.2.4 shows that its complexity is $O(N^4 D^2 d^4)$ where d is the maximum diameter of the object's faces. Empirical results are presented in Section 4.3.3.

4.3.2.1   Testing the Existence of Equilibrium Configurations

We first check that the four surface normals positively span $\mathbb{R}^3$. This is easily done by checking that any three of the normals are linearly independent, then using the equation $\boldsymbol{n} = -\sum_{i=1}^{3} \mu_i \boldsymbol{n}_i$ to compute the coefficients μ_i and check whether they have the same sign. If they do not, the quadruple of faces under consideration is rejected. If they do, the normals positively span $\mathbb{R}^3$, and (4.5) provides four linear equations in the the nine unknowns λ_i, u_i, v_i $(i = 1, 2, 3)$.

We can now test the existence of equilibrium configurations by using linear programming to determine whether the five-dimensional polytope defined by (4.5) and the inequality constraints (4.1) and $\lambda_i \geq 0$ is empty. When this polytope is not empty, there is only (in general) a subset of each face that can participate in an equilibrium configuration. As in the fixturing case, the subset corresponding to face number i is determined by projecting the polytope defined onto the plane (u_i, v_i) [29, 45, 44, 75].

4.3.2.2   Enumerating Pin Positions

As shown by Lemma 1, given a quadruple of faces, we can first enumerate all possible pin locations on the lower plate and compute the corresponding rotations, then enumerate the corresponding pin heights and compute the corresponding jaw separation and object pose.

An exhaustive search of all possible grid coordinates would be extremely expensive: consider an object of diameter D (measured in units equal to the distance between successive grid points); there are a priori $O(D^4)$ different pin locations, since we can position one pin at the origin and the other two pins at arbitrary locations on the grid.

Instead, we use an approach similar to the algorithms presented by Wallack and Canny [102, 103] and Brost and Goldberg [10], using bounds on the distance between two faces to restrict the set of grid coordinates under consideration. Clearly, each pin must lie within the horizontal projection of each face. Thus if we position the first pin at the origin, the integer point corresponding to the second pin is constrained to lie within the circular shell centered at the origin with inner radius equal to the minimum distance between the projections of the two corresponding faces and outer radius equal to the maximum distance. Given the position of the second pin, the third pin is now constrained to lie within the region formed by the intersection of the two shells associated with the first and second pin.

Enumerating the pin locations thus amounts to determining the integer positions falling in planar regions defined by a circular shell or the intersection of two such shells. This can be done as before in optimal time proportional to the number V of these points by using a scan-line conversion algorithm.

4.3.2.3 Enumerating Pin Lengths

Once the position of the pins has been chosen and the corresponding rotation has been computed, we can align the gripper's and object's coordinate systems so they are only separated by the horizontal translation (x, y). This allows us to rewrite the contact equations as

$$a_i(x - q_i) + b_i(y - r_i) + \delta - c_i - h_i = 0 \quad \text{for} \quad i = 1, 2, 3. \tag{4.7}$$

Equation (4.7) holds whenever the three pins are in the planes of the faces f_i of the grasped object. Writing that the pins actually lie within the faces constrains the possible values of the translation $\boldsymbol{t}$ between the gripper and object coordinate frames: let us denote by by f_i' the convex polygon $\{(x, y) | a_{ij}(x - q_i) + b_{ij}(y - r_i) - c_{ij} \geq 0$ for $j = 1, .., k_i\}$ (geometrically, f_i' can be constructed by projecting f_i onto the (u_i, v_i) plane, then applying to the projection a symmetry with respect to the origin and a translation by (q_i, r_i)). Using once again (4.2) shows that the point (x, y) is restricted to lie within

46

the polygon $F' = f_1' \cap f_2' \cap f_3'$ (Figure 4.4(a)). Substituting into (4.7) and using the fact that we can choose $q_1 = r_1 = h_1 = 0$ now yields

$$\begin{pmatrix} h_2 \\ h_3 \end{pmatrix} \in \{\mathcal{A} \begin{pmatrix} x \\ y \end{pmatrix} + \boldsymbol{b} | \begin{pmatrix} x \\ y \end{pmatrix} \in F'\}$$

where

$$\mathcal{A} = \begin{pmatrix} a_2 - a_1 & b_2 - b_1 \\ a_3 - a_1 & b_3 - b_1 \end{pmatrix}, \quad \boldsymbol{b} = \begin{pmatrix} c_1 - (a_2 q_2 + b_2 r_2 + c_2) \\ c_1 - (a_3 q_3 + b_3 r_3 + c_3) \end{pmatrix}.$$
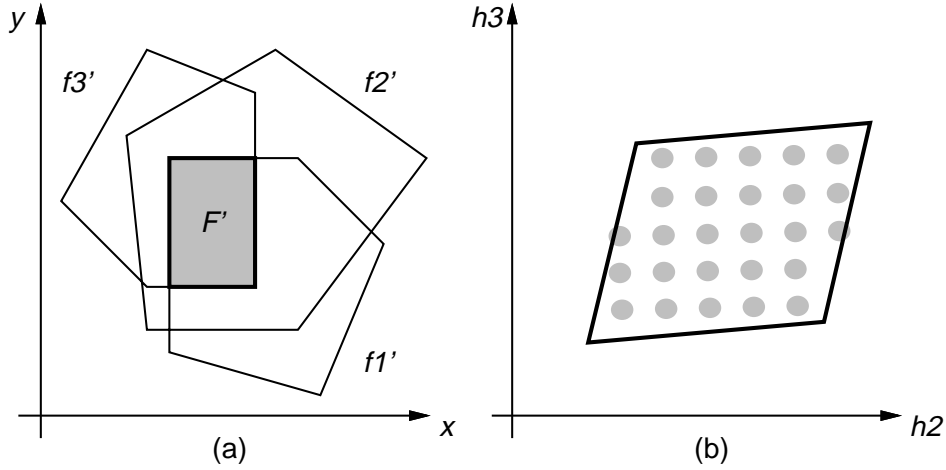
Figure 4.4 Enumerating pin lengths: (a) the polygon F' defined in the x, y plane by the intersection of the faces f_i', and (b) the corresponding convex polygon in the h_2, h_3 plane, along with the integer points inside it.

In other words, the possible values of (h_2, h_3) are simply the integer points that lie in the polygon defined by the above equation, which is obtained from F' by an affine transformation (Figure 4.4(b)). These points can once again be determined in optimal time proportional to their actual number using a polygon scan-line conversion algorithm.

Now, for a given configuration (location plus length) of the pins, (4.7) forms a system of three linear equations in the three variables x, y, and δ. This system is readily solved to yield the pose of the object and the separation of the plates. Note that the values of the coefficients λ_i are easily computed from (4.5) if required.

Note that the gripper configurations found by our algorithm will automatically ensure that the contacts between the three pins and the planes of the corresponding faces occur within the faces.

4.3.2.4   Algorithm Analysis

Without any assumption on the geometry of the grasped object, the complexity of our algorithm is clearly $O(N^4D^6)$. To obtain a more realistic estimate of the algorithm behavior, let us assume without loss of generality that each face can be inscribed in a disc of diameter d (note that $d \leq D$ and that in practice, we may have $d \ll D$). The area of a circular shell is then $O(Dd)$, and the area of the intersection of two such shells is also at worse $O(Dd)$. Finally, the area of the polygon F is $O(d^2)$. Thus the total complexity of the algorithm is $O(N^4D^2d^4)$. As noted in the Introduction, this is an improvement over the algorithm proposed in [69, 94], whose complexity is $O(N^4D^4d^2)$ since it does not decouple the enumeration of the pin positions and pin lengths.

For polyhedra with total area A whose faces all have approximately the same area, we have $d^2 = O(D^2/N) = O(A/N)$, and it follows that the complexity of our algorithm is $O(N^2A^3)$.

Note that if we assume that $d \ll D$, the area of the intersection of two shells will in general be proportional to d^2 instead of dD. More experiments will allow us to conduct an empirical evaluation of this model.

4.3.3   Implementation and Results

In this section, we present some simulation results. Some results of the experiments with the gripper prototype is presented in Section 4.6. The implementation has been written in C. Figures 4.5 and 4.6 show some of the grasps of a tetrahedron and of a polyhedron with 10 faces that our algorithm has found using a 5×5 grid.

Table 4.1 gives some quantitative results. We have used a $K \times K$ grid with various values of K, as well as pins whose height may take ten discrete values. The table shows the results obtained without any pruning (N), using circular shell pruning only (S), and combining the projection- and shell-pruning stages (P+S). All run times have been measured on a SUN SPARCstation 10. The table shows that, as could be expected, pruning eliminates a much larger percentage of the possible configurations in the case
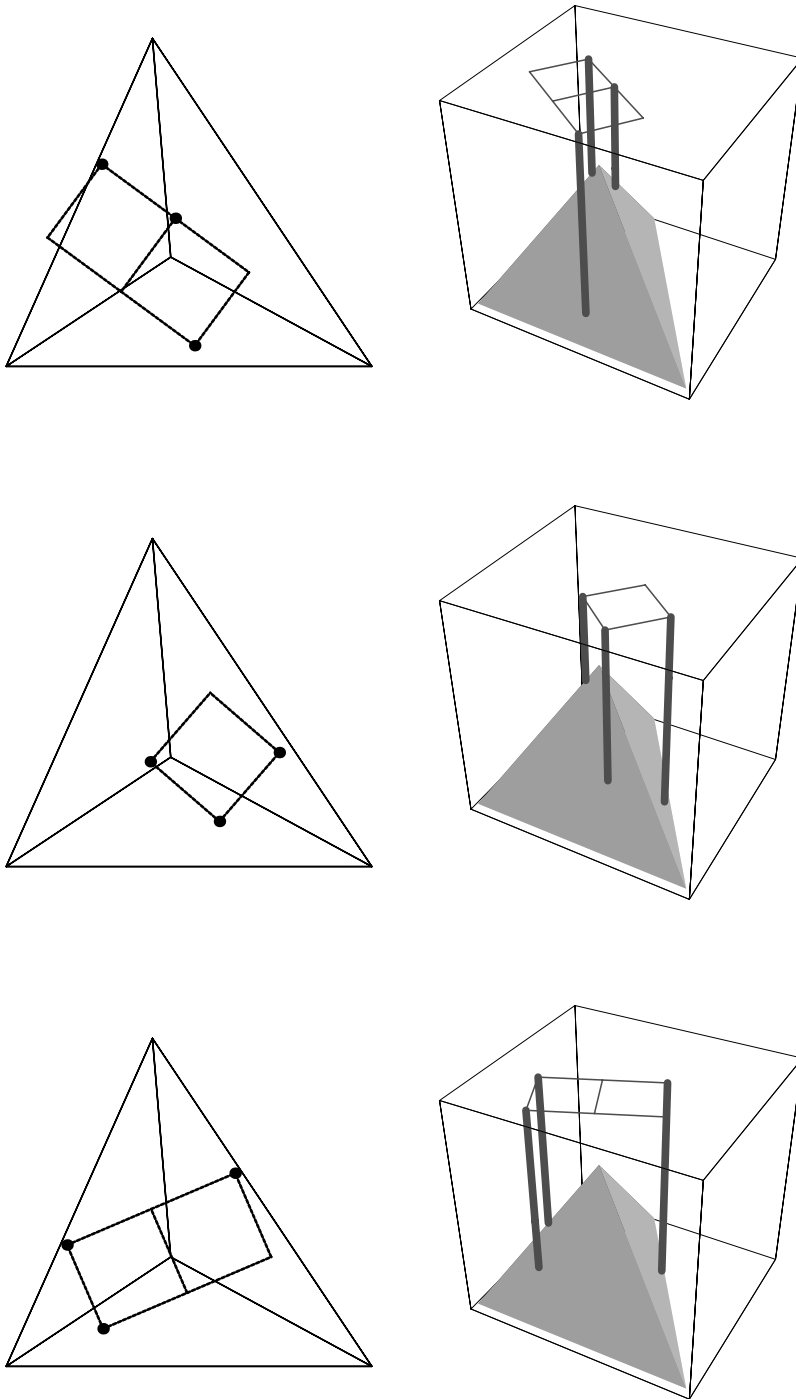
Figure 4.5 Grasping a tetrahedron: some solutions for a 5×5 grid.
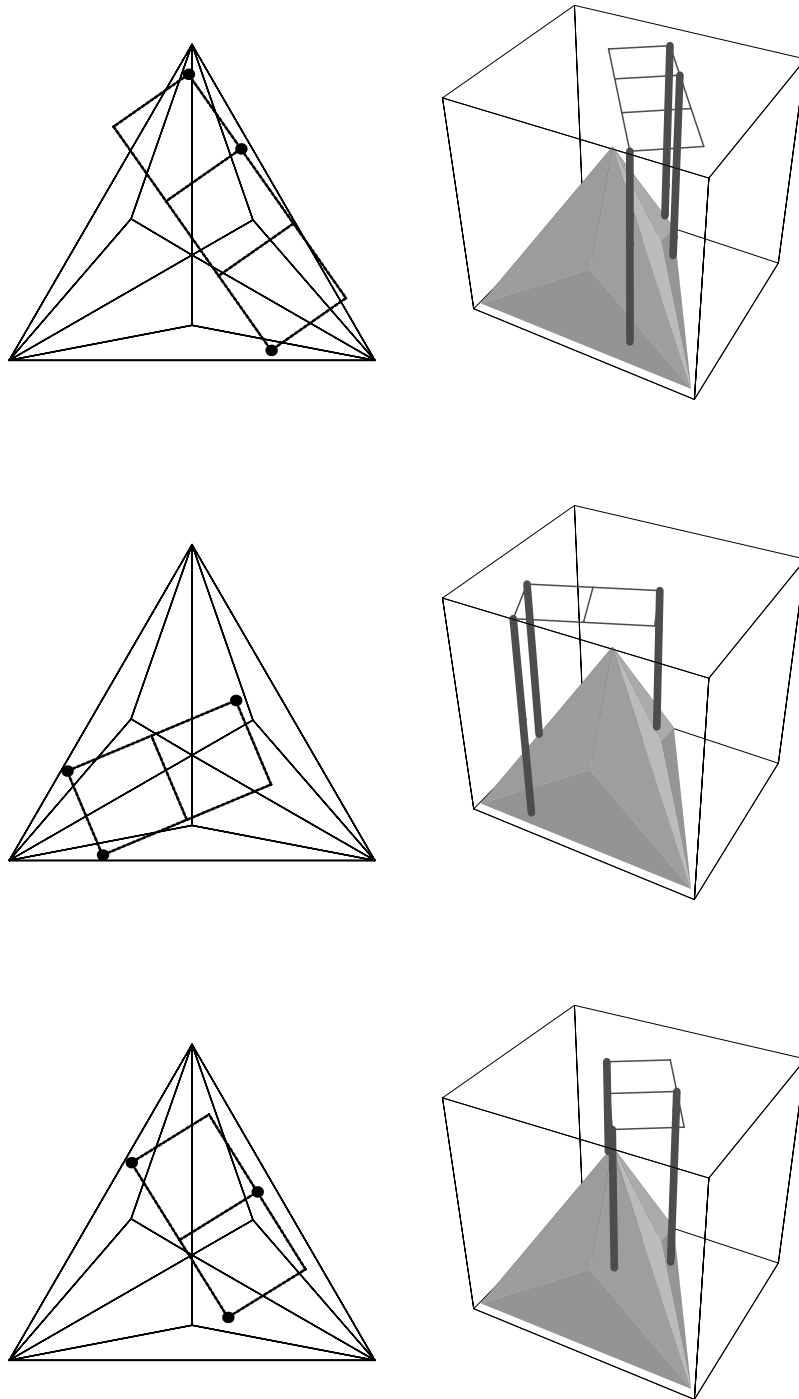
Figure 4.6 Grasping a 10-face polyhedron: some solutions for a 5×5 grid.

of the polyhedron with 10 faces than in the case of the tetrahedron, corresponding to the fact that, for most choices of faces, the range between the minimum and maximum distances is smaller for the polyhedron with 10 faces.

Tetrahedron							
K	Number of	Run Time (s)			# Candidates		
	Solutions	N	S	P+S	N	S	P+S
3	0	1	1	1	33	10	10
4	160	1	1	1	141	42	40
5	704	2	1	2	411	145	135
6	1,963	4	2	2	927	391	378
7	4,263	8	4	4	1,839	795	751

Polyhedron with 10 Faces							
K	Number of	Run Time (s)			# Candidates		
	Solutions	N	S	P+S	N	S	P+S
3	0	20	1	2	2,772	750	712
4	189	47	3	4	11,844	2,213	2,102
5	794	72	9	9	34,524	3,819	3,537
6	2,326	142	20	20	77,868	7,811	7,125
7	5,046	341	43	41	154,476	16,259	14,951

Table 4.1 Quantitative results for two test objects.

4.4 In-Hand Manipulation

We present a new approach to in-hand manipulation based on the concept of *inescapable configuration space region*, i.e., on the idea of characterizing the regions of configuration space for which the object is not immobilized but is constrained to lie within a closed region of the free configuration space (see [80] for related work in the two-dimensional, two-finger case). This allows us to plan in-hand planar motions as sequences of gripper configurations: as the gripper's jaws open from an initial immobilized configuration, the object stays in place under the action of gravity; then as the jaws close, starting in some inescapable region of configuration space, the object is moved to

51

a new immobilizing position and orientation. Note that this approach does not require modeling what happens when contact occurs, but it indeed requires frictionless contacts to avoid wedging.

4.4.1 Geometry of the Problem

4.4.1.1 Free Configuration Space Regions

Let us consider an immobilizing configuration of the gripper, defined by the position q_i, r_i and height h_i of the pins $(i = 1, 2, 3)$, by the position x_0, y_0 and orientation θ_0 of the object in the gripper's coordinate system, and by the jaw separation δ_0. We assume that the values of q_i, r_i and h_i are held constant and examine what happens when the separation of the jaws changes.

Note that for a given jaw separation $\delta \geq 0$, the ruled surface $S_i(\delta)$ defined in Section 4.3.1.1 splits the three-dimensional space $\mathbb{R}^2 \times S^1$ of configurations x, y, θ into a "free" half-space $V_i(\delta)$ and a "forbidden" half-space $W_i(\delta)$ where pin number i penetrates the plane of f_i. Furthermore, $V_i(\delta)$ (resp. $W_i(\delta)$) is characterized by $\mathcal{C}_i(x, y, \theta, \delta) \geq 0$ (resp. ≤ 0).

Now let us consider the volume $V(\delta) = V_1(\delta) \cap V_2(\delta) \cap V_3(\delta)$. Given the form of $C_i(x, y, \theta, \delta)$, it is obvious that if a configuration lies in free space for some value δ_1 of δ, it also lies in free space for any other value $\delta_2 \geq \delta_1$. In other words, $V(\delta_1) \subset V(\delta_2)$ when $\delta_2 \geq \delta_1$ (this is also intuitively obvious since increasing δ corresponds to opening the jaws). In particular, the immobilizing configuration (x_0, y_0, θ_0) is always in free space for $\delta \geq \delta_0$.

The intersection of $V(\delta)$ with a plane $\theta = \text{constant}$ forms a triangular region $T(\delta, \theta)$. Note that the triangles corresponding to various values of θ are all homothetic since their edges make constant angles with each other. However, their size, position, and orientation varies with θ. Note also that these triangles, although possibly empty, are not degenerate: indeed, it is easy to verify that a necessary and sufficient for two edges of $T(\delta, \theta)$ to be parallel is that the normals to the corresponding faces be either equal

or symmetric with respect to the vector $\boldsymbol{n}$, which contradicts the assumption that the directions $\boldsymbol{n}_i$ ($i = 1, 2, 3$) and $\boldsymbol{n}$ positively span $\mathbb{R}^3$.

As shown in Figure 4.7, the region $T(\delta, \theta)$ may contain an open subset (Figure 4.7(a)), be reduced to a single point (Figure 4.7(b)), or be empty (Figure 4.7(c)).

(a)   (b)   (c)
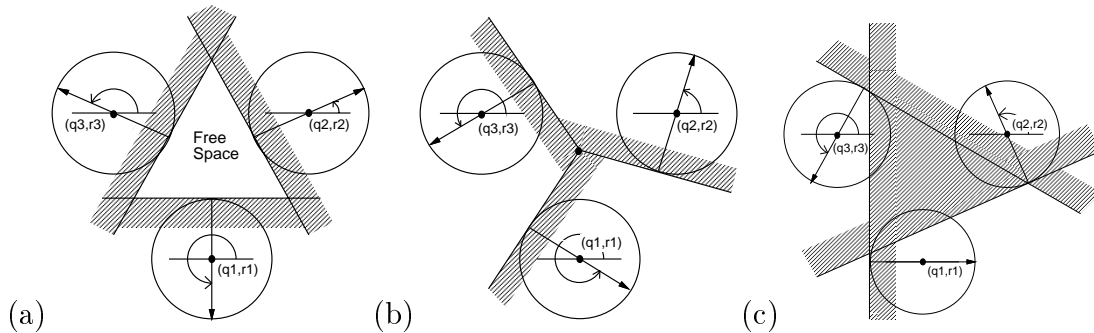
Figure 4.7 Possible configurations of the intersection $T(\delta, \theta)$ of $V(\delta)$ with a plane $\theta =$ constant: (a) $T(\delta, \theta)$ contains an open neighborhood; (b) it is reduced to an isolated point of the x, y plane; (c) it is empty.

In the second case (Figure 4.7(b)), the three pins simultaneously touch the corresponding faces, and $\mathcal{E}(\delta, \theta) = 0$. In fact, it is easy to show that a necessary and sufficient condition for $T(\delta, \theta)$ to contain at least one point is that $\mathcal{E}(\delta, \theta) \geq 0$: the condition is clearly necessary: since $\mathcal{E}(\delta, \theta)$ is by construction a convex combination of the functions $\mathcal{C}_i(x, y, \theta, \delta)$, the fact that $\mathcal{E}(\delta, \theta) < 0$ implies that, for any x, y, there exists some $i \in \{1, 2, 3\}$ such that $\mathcal{C}_i(x, y, \theta, \delta) < 0$. To show that the condition is also sufficient, let us assume that $T(\delta, \theta)$ is empty. This implies that, for any x, y, there exists some $i \in \{1, 2, 3\}$ such that $\mathcal{C}_i(x, y, \theta, \delta) < 0$. In particular, if (x_{12}, y_{12}) is the point where the two lines associated with the faces f_1 and f_2 intersect (as remarked earlier, these lines are not parallel), we must have $\mathcal{E}(\delta, \theta) = (\mu_3/l_3)\mathcal{C}_3(x_{12}, y_{12}, \theta, \delta) < 0$.

This result allows us to characterize qualitatively the range of orientations θ for which $T(\delta, \theta)$ is not empty (Figure 4.8): for a given δ, the condition $\mathcal{E}(\delta, \theta) = 0$ is an equation in θ that may have zero, one, or two real solutions: a double root occurs at the minimum $\delta = \delta_0$ or at the maximum $\delta = \delta_{\max}$ of the sinusoid. In the former case, $\mathcal{E}$ is strictly positive everywhere except at $\theta = \alpha$ where it is equal to zero, and the range of orientations is S^1. In the latter case, the range of orientations reduces to a single point $\theta_0 = \alpha + \pi$.

For any value δ_1 in the open interval $]\delta_0, \delta_{\max}[$, there are two distinct roots θ', θ'', and the range of orientations is the arc bounded by these roots and containing θ_0. Finally, for values of δ outside the $[\delta_0, \delta_{\max}]$ interval, there is no solution: either δ is strictly smaller than δ_0 and the range of orientations is empty (at least one of the pins penetrates the plane of the corresponding face), or δ is strictly larger than $\delta_{\max}$, and the range of orientations is S^1.
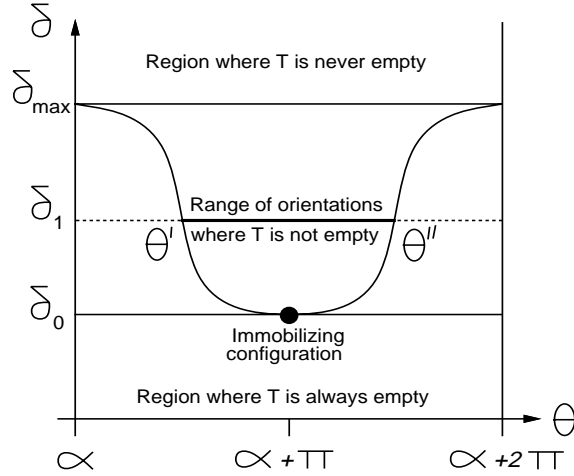
Figure 4.8 Regions of θ, δ space delimited by the sinusoid $\mathcal{E}(\delta, \theta) = 0$.

In particular, since the volume $V(\delta)$ is a stack of contiguous triangles $T(\delta, \theta)$, it is clear at this point that, for $\delta \geq \delta_0$, $V(\delta)$ is a non-empty, connected, compact region of $\mathbb{R}^2 \times S^1$. The analysis conducted in this section also gives some geometric insight on the immobility conditions derived earlier. In particular, it confirms that the minimum point $(\alpha + \pi, \delta_0)$ of the contact sinusoid corresponds to an isolated point of configuration space or equivalently to an immobilizing configuration: indeed, the triangle $T(\delta_0, \alpha + \pi)$ is reduced to a point, and $T(\delta, \theta)$ is empty for any $\theta \neq \theta_0$. Likewise, although the maximum $(\alpha, \delta_{\max})$ of the sinusoid corresponds to an equilibrium grasp, it does not yield an immobilizing grasp since the object is free to undergo arbitrary rotations.

4.4.1.2   Inescapable Configuration Space Regions

The discussion so far has characterized the contacts between the pins and the planes of the corresponding faces, ignoring the fact that each face is in fact a convex polygon in its plane. Let us construct a parameterization of the set $E_i(\delta, \theta)$ of configurations (x, y) for which the tip of pin number i belongs to the corresponding face. Obviously, $E_i(\delta, \theta)$ is a subset of $L_i(\delta, \theta)$. This line is at distance $-d_i\delta + e_i$ from the point (q_i, r_i), with a normal whose orientation is $\theta + \alpha_i$; hence, it can be parameterized by

$$
\begin{pmatrix} x \\ y \end{pmatrix} = \begin{pmatrix} q_i \\ r_i \end{pmatrix} + (-d_i\delta + e_i) \begin{pmatrix} \cos(\theta + \alpha_i) \\ \sin(\theta + \alpha_i) \end{pmatrix} + \eta \begin{pmatrix} -\sin(\theta + \alpha_i) \\ \cos(\theta + \alpha_i) \end{pmatrix}, \quad \eta \in \mathbb{R}.
$$

Using this parameterization and (4.2) yields

$$
\begin{pmatrix} u_i \\ v_i \end{pmatrix} = (d_i\delta - e_i) \begin{pmatrix} \cos\alpha_i \\ \sin\alpha_i \end{pmatrix} - \eta \begin{pmatrix} -\sin\alpha_i \\ \cos\alpha_i \end{pmatrix}.
$$

In turn, substituting these values in the inequalities (4.1) defining f_i yields a set of linear inequalities in η and δ. Actual contact occurs for pairs (η, δ) lying in the convex polygon defined by these constraints. It follows that for given values of δ and θ, $E_i(\delta, \theta)$ is a line segment, and the parameters η' and η'' associated with its endpoints are piecewise-linear functions of δ.

Now let us consider the three segments $E_i(\delta, \theta)$ ($i = 1, 2, 3$) together (Figure 4.9): if $E_i(\delta, \theta)$ and $E_j(\delta, \theta)$ intersect for all $i \neq j$, then the three segments completely enclose the triangle $T(\delta, \theta)$ (Figure 4.9(a)). We say that the corresponding configuration satisfies the *enclosure condition* since there is no escape path for the object in the x, y plane with the corresponding orientation θ. More generally, when all triples of segments in the range of orientations associated with a given jaw separation δ satisfy the enclosure condition, $V(\delta)$ itself is an *inescapable configuration space* (ICS) region: in other words, the object is free to move within the region $V(\delta)$, but remains imprisoned by the grasp and cannot escape to infinity.
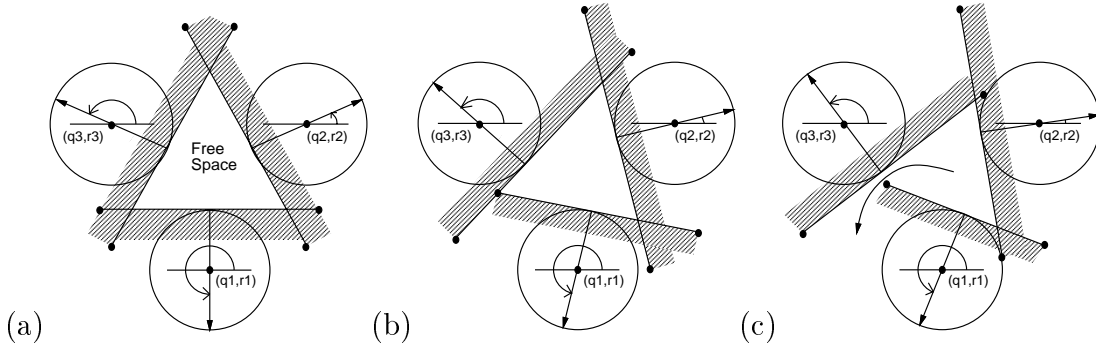
Figure 4.9 Triangle configurations: (a) three segments enclosing a triangle; (b) a critical configuration; (c) an opened triangle and an escape path.

4.4.1.3 Maximum ICS Regions

Here we address the problem of characterizing the maximum value δ^* for which $V(\delta)$ forms an ICS region for any δ in the $[\delta_0, \delta^*]$ interval. We know that at $\delta = \delta_0$ the three segments intersect at the immobilizing configuration, forming an ICS region reduced to a single point. Thus the enclosure condition holds at $\delta = \delta_0$. On the other hand, as $\delta \to +\infty$, the whole configuration space becomes free of obstacles, thus there must exist a critical point for some minimal value of δ greater than δ_0. This guarantees that δ^* has a finite value.

As shown by Figure 4.9(b), a critical event occurs when one of the endpoints of a segment lies on the line supporting another segment. After this event, the line segments fail to enclose the triangle $T(\delta, \theta)$ and the object can escape the grasp (Figure 4.9(c)).

According to the results established in the previous section, we can parameterize the coordinates of one of the endpoints of the segment $E_i(\delta, \theta)$ by

$$\begin{pmatrix} x \\ y \end{pmatrix} = \begin{pmatrix} q_i \\ r_i \end{pmatrix} + (-d_i\delta + e_i) \begin{pmatrix} \cos(\theta + \alpha_i) \\ \sin(\theta + \alpha_i) \end{pmatrix} + (f_i\delta + g_i) \begin{pmatrix} -\sin(\theta + \alpha_i) \\ \cos(\theta + \alpha_i) \end{pmatrix}, \qquad (4.8)$$

on the appropriate δ interval, with constants f_i and g_i determined by the coefficients a_{ij}, b_{ij} and c_{ij} of (4.1).

A critical event occurs when the endpoint under consideration is on the line $L_j(\delta, \theta)$ for some $j \neq i$. Substituting (4.8) into (4.3) yields, after some simple algebraic manipulation

$$A_{ij}\cos(\theta + \beta_{ij}) + B_{ij}\delta + C_{ij} = 0, \qquad (4.9)$$

56

where

$$
\begin{cases}
A_{ij} = \sqrt{(q_i - q_j)^2 + (r_i - r_j)^2}, \\
\beta_{ij} = \alpha_j - \mathrm{Arg}(q_i - q_j, r_i - r_j), \\
B_{ij} = d_j - d_i \cos(\alpha_j - \alpha_i) + f_i \sin(\alpha_j - \alpha_i), \\
C_{ij} = -e_j + e_i \cos(\alpha_j - \alpha_i) + g_i \sin(\alpha_j - \alpha_i).
\end{cases}
$$

In other words, critical configurations form a second sinusoid in θ, δ space, called the *critical sinusoid* in the rest of this presentation.

We seek the minimum value of $\delta^* > \delta_0$ for which the range of orientations includes one of the critical orientations. As discussed above, we know that δ^* exists. Let us suppose first that a critical value lies in the interior of the range of orientations associated with some $\delta_1 \geq \delta_0$, and denote by $\delta_{\min}$ the minimum value of δ on the critical sinusoid. By definition, we have $\delta_1 \geq \delta_{\min}$. Suppose that $\delta_1 > \delta_{\min}$. Then by continuity, there exists some δ_2 such that $\delta_{\min} < \delta_2 < \delta_1$ and the corresponding range of orientations also contains a critical orientation (Figure 4.10). The argument holds for any value of $\delta > \delta_{\min}$. In other words, either the range of orientations of $\delta_{\min}$ contains a critical orientation, in which case $\delta^* = \delta_{\min}$ (Figure 4.10(a)), or it does not, in which case the critical value associated with δ^* must be one of its range's endpoints (Figure 4.10(b)). This is checked by intersecting the contact sinusoid and the critical one. Note that this process must be repeated for each segment/vertex pair to select the minimum value of δ^*.

4.4.1.4 Main Result

The following lemma follows immediately from the results established in Sections 4.4.1.1, 4.4.1.2 and 4.4.1.3 and summarizes the findings of these sections.

Lemma 2: For given integer pin positions and heights q_i, r_i and h_i $(i = 1, 2, 3)$ and an immobilizing configuration $(x_0, y_0, \theta_0, \delta_0)$, there exists a critical jaw separation δ^* such that:

(1) for any $\delta > \delta^*$, there exists a path allowing the object to escape the grasp,
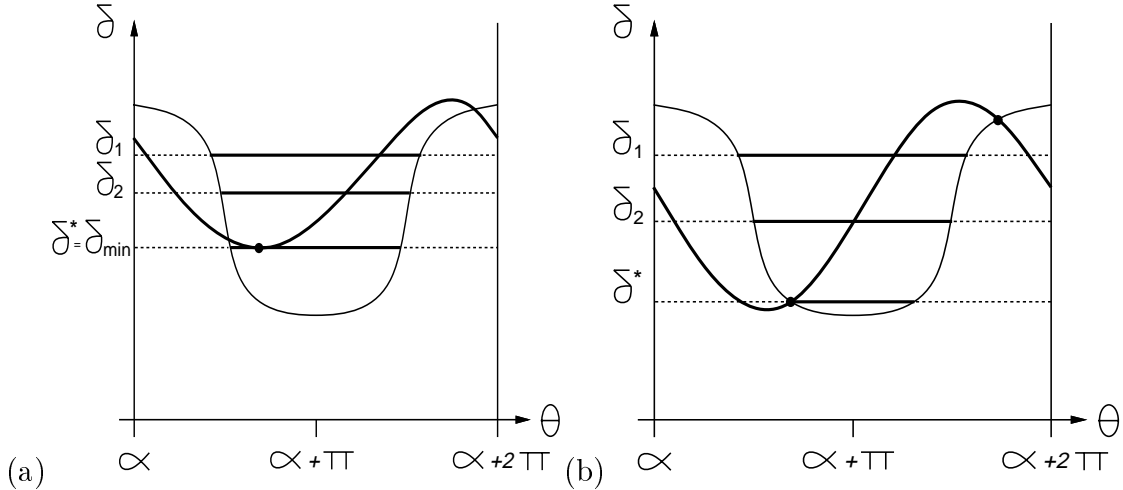
Figure 4.10 Critical configurations: (a) the critical configuration is the minimum of the critical sinusoid (shown as the thicker curve); (b) the critical configuration is the minimum intersection of the critical sinusoid and the contact sinusoid.

(2) for any δ in the interval $[\delta_0, \delta^*]$, the volume $V(\delta)$ is an inescapable region of configuration space,

(3) for any $\delta' \leq \delta''$ in the interval $[\delta_0, \delta^*]$, $V(\delta') \subset V(\delta'')$, and

(4) δ^* can be computed in closed form as the minimum of a sinusoid or the intersection of two sinusoids.

4.4.2 Algorithm

Lemma 2 can be used as a basis for in-hand manipulation by remarking that an object anywhere in the ICS region associated with some gripper configuration can be moved to the corresponding immobilized position and orientation by closing the gripper jaws (this follows immediately from properties (2) and (3) in Lemma 2). Thus we can plan manipulation sequences from one immobilized configuration to another by using the following algorithm:

Off-line:

(1) Compute the set S of all immobilizing configurations of the object.

(2) Construct a directed graph G whose vertices are the elements of S and whose edges are the pairs (s, s') of elements of S such that s belongs to the maximum ICS region ICS(s') associated with s'.

On-line:

(3) Given two configurations i and g in S, search the graph G for the shortest path going from the initial configuration i to the goal configuration g.

Once a path has been found, the corresponding manipulation sequence can be executed: starting from the configuration i, each edge (s, s') in the path allows us to move the object from s to s' by opening the jaws and retracting the pins associated with s, then lowering the pins associated with s' and closing the jaws.

4.4.2.1 Triples of Pins: Prototypes and Shifts

The grasp planning algorithm of Section 4.3.2 can be used to enumerate all immobilizing object/gripper configurations and implement Step (1). There is however a difference between grasping and manipulation applications: during grasp planning, one can always assume that the first pin is at the origin with zero height. Of course, when a grasp is actually executed, the pin positions and heights, along with the jaw separation, all have to be shifted so that the corresponding variables are all positive and the pin positions remain within the extent of the top plate. Nonetheless, gripper configurations that only differ by a shift of the three pin positions are equivalent for grasping purposes. This is not the case for in-hand manipulation, where the goal is to move the object held by the gripper across the bottom plate: this forces us to take into account all shifted configurations of a grasp.

We will say that a triple of pin positions with the first pin located at the origin is a *prototype*, and that all positions of the triple within the bottom plate are the *shifts* of this prototype. For each prototype, we can define the minimum rectangle aligned with the (p, q) coordinate axes and enclosing the pins. If W and H denote the width and height of this rectangle, and K^2 is the total number of grid elements, the prototype admits

$(K - W)(K - H)$ different shifts, which can trivially be computed in time proportional to their number. As shown in Section 4.3.2.4, there are $O(D^2 d^2)$ immobilizing prototypes, to which correspond $O(D^2 d^4 K^2)$ shifted object/gripper configurations. If we assume that the manipulated object fits completely on the gripper's bottom plate, note that we will have $d \leq D \leq K$.

4.4.2.2 Constructing the Graph

Constructing the graph G requires the ability to decide whether an immobilizing configuration s_a lies in the region ICS(s_b) associated with another configuration s_b. Let θ_a denote the orientation of the configuration s_a, and δ_b^* denote the critical jaw separation associated with s_b. A necessary condition for s_a to belong to ICS(s_b) is of course that s_a belongs to the range of orientations associated with δ_b^*.

When this necessary condition is fulfilled, let $T(\delta_b^*, \theta_a)$ denote the slice of ICS(s_b) at $\theta = \theta_a$. Then s_a will belong to ICS(s_b) if and only if s_a is inside $T(\delta_b^*, \theta_a)$. Note that constructing $T(\delta_b^*, \theta_a)$ does *not* require constructing an explicit boundary representation of ICS(s_b) then intersecting it with the plane $\theta = \theta_a$: instead, we construct the triangle directly from the lines $L_i(\delta_b^*, \theta_a)$ as explained in Section 4.4.1.1.

Thus constructing the graph only requires the ability of computing δ^* and the corresponding range or orientations, constructing the triangles $T(\delta^*, \theta)$ for discrete values of θ, and testing whether a point belongs to one of these triangles. Each one of these computations can be done in constant time.

From Section 4.3.1.2, we know that for a given triple of pins, all immobilizing configurations of a given object will have the same orientation, independent of the pin heights. Of course, the immobilized orientation of the object remains the same when the triple of pins is arbitrarily shifted on the grid. Thus we can associate to each immobilizing prototype a plane $\theta =$ constant of the object's configuration space, and all the corresponding immobilizing configurations will lie in that plane. In other words, the vertices of the graph G will form layers of immobilized configurations corresponding to as many prototypes.

We now give an efficient algorithm for constructing the edges of the graph G. Let S_a and S_b be the sets of immobilized configurations corresponding to the layers $\theta = \theta_a$ and $\theta = \theta_b$ of the configuration space. We want to find all pairs of configurations s_a in S_a and s_b in S_b such that s_a lies within $\mathrm{ICS}(s_b)$ or equivalently within $T(\delta_b^*, \theta_a)$. This can of course be achieved by testing for each point-triangle pair whether the point belongs to the corresponding triangle. Instead, we observe that, following Section 4.4.1.1, the triangles $T(\delta_b^*, \theta_a)$ associated with all the elements of S_b are homothetic and, since θ is fixed, they also have the same orientation. This allows us to derive a more efficient method.

Let us restate the problem: given a set of points $P = \{p_1, p_2, .., p_n\}$, and a set $T = \{t_1, t_2, .., t_m\}$ of homothetic triangles having the same orientation, find all pairs (p_i, t_j) $(i = 1, .., n,\ j = 1, .., m)$ such that the point p_i is inside the triangle t_j (Figure 4.11). This type of query is common in computational geometry: for example, Chazelle gave an optimal $O(\log m + r)$ algorithm for the related problem of finding the subset of m isothetic rectangles which contain a query point, where r is the number of rectangles returned [14].
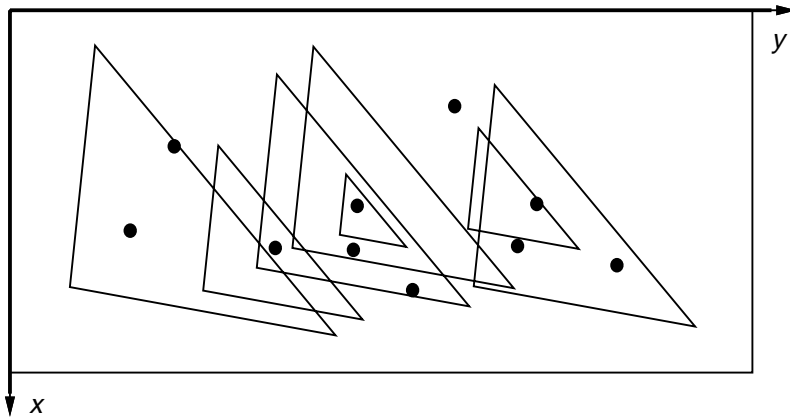
Figure 4.11 Points and triangles within the same layer.

This problem can be mapped onto another classical one through the following transformation: let $\boldsymbol{u}_i$ $(i = 1, 2, 3)$ denote the inward unit normals to the edges of the triangles. Given some choice of origin in the plane, we can associate with any point p its coordinates (x_1, x_2, x_3) along the vectors $\boldsymbol{u}_i$ (Figure 4.12). Likewise, we can associate with

each triangle t the signed distances (y_1, y_2, y_3) between the origin and its edges along the vectors $\boldsymbol{u}_i$. Obviously p is inside t if and only if $x_i \geq y_i$ for $i = 1, 2, 3$. If we define the partial order $\succ$ over $\mathbb{R}^3$ by $(x_1, x_2, x_3) \succ (y_1, y_2, y_3)$ if and only if $x_i \geq y_i$ for $i = 1, 2, 3$, we have reduced our initial problem to the problem of finding the pairs of points p'_i in P' and t'_j in T' such that $p'_i \succ t'_j$, where P' and T' are subsets of $\mathbb{R}^3$ containing respectively n and m points. This is the problem called "3D Merge Dominance" by Preparata and Shamos [76, pp. 357–363], who give a simple divide-and-conquer algorithm for solving this problem in $O((m + n) \log(m + n) + s)$ time and $O(m + n)$ space, where s is the number of pairs found by the algorithm.
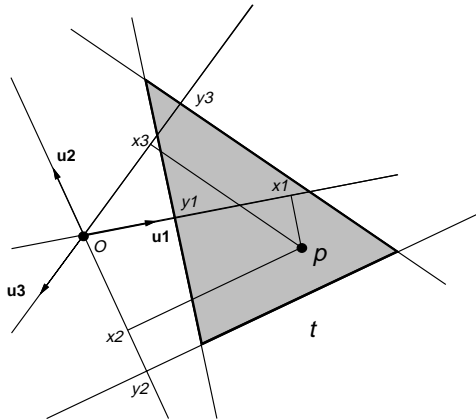
Figure 4.12 Three-dimensional coordinates associated with a point p and a triangle t.

It is not clear whether the time complexity of this algorithm is optimal in the three-dimensional case: indeed, the 1D Merge Dominance problem can be solved in $O((m + n) \log(\min(m, n)) + s)$ as follows: if the number m of elements of T' is smaller than the number n of elements of P', sort the elements of T', then, for each p' element of P', insert this element in the sorted list, returning all the elements of $t' \leq p'$, then delete p' from the sorted list. If $n < m$, sort P' instead and use the same process with the relation $\geq$. This algorithm is more efficient than the 3D algorithm.

4.4.2.3 Algorithm Analysis

The cost of the algorithm is dominated by the construction of the graph. Let V denote the number of immobilizing gripper configurations (or equivalently the number of vertices of G), and let P denote the number of prototypes associated with these configurations. Note that $P = O(D^2 d^2)$ and $V = O(P d^2 K^2)$ according to the analysis of Section 4.3.2.4. Let E denote the number of edges of G. Since each prototype yields $O(d^2 K^2)$ shifted configurations and $d \leq K$, it follows from the analysis of the dominance algorithm that the construction of the graph takes $O(P^2 d^2 K^2 \log K + V + E)$ time. Of course, $E = O(V^2)$.

4.4.3 Implementation and Results

In this section, we present extensive simulation results. Some result of the experiments with the gripper prototype is presented in Section 4.6. We have implemented the manipulation planning algorithm, including its 3D dominance part, and tested our implementation using a 5×5 grid resolution. The program has been written in C, and all run times have been measured on a SUN SPARCstation 10.

Figure 4.13 shows an example of maximum ICS region in the configuration space (x, y, θ) for one of the immobilized configurations of a tetrahedron. Note that this graphical representation is for display only: our algorithm does not construct an explicit boundary representation of the ICS. Instead, we compute the corresponding δ^* value and the associated range of orientations. Our grasp planning program finds 208 prototypes and 33,868 shifted immobilizing configurations, and the corresponding ICS computation takes 13 seconds. The graph G contains 1,247,374 edges, and its construction takes 156 seconds.

Once the graph has been constructed, the search for sequences of gripper configurations is quite efficient: a simple breadth-first approach has been used in our experiments to search the graph G, and the search time is below 1 second in all cases.

Figures 4.14 and 4.15 show two examples. In the first one, the program finds a 4-step sequence to move the object from the configuration shown in Figure 4.14(a) to the one

(a)   (b)   (c)
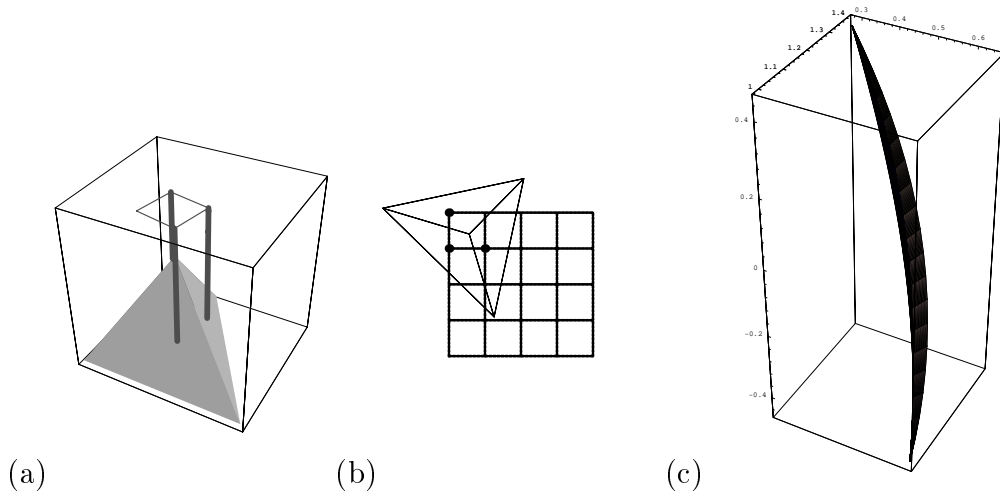
Figure 4.13 An ICS in configuration space: (a)-(b) two views of an immobilized config-
uration of a tetrahedron; (c) the corresponding ICS.

shown in Figure 4.14(b). Note that, although the pin configurations are the same in
Figures 4.14(c) and 4.14(d), the pin lengths are actually different.

(a)   (b)

(c)   (d)
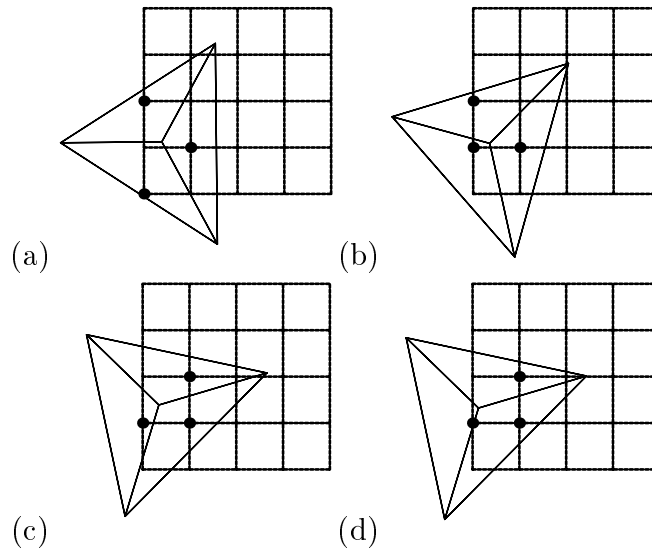
Figure 4.14 The four steps of a manipulation for moving a tetrahedron from configura-
tion (a) to configuration (d).

Figure 4.15 shows a more complicated example, where the program finds a 72-step
sequence of gripper configurations to move the object from the configuration shown in
Figure 4.15(a) to the one shown in Figure 4.15(b).

64

(a)   (b)

(c)
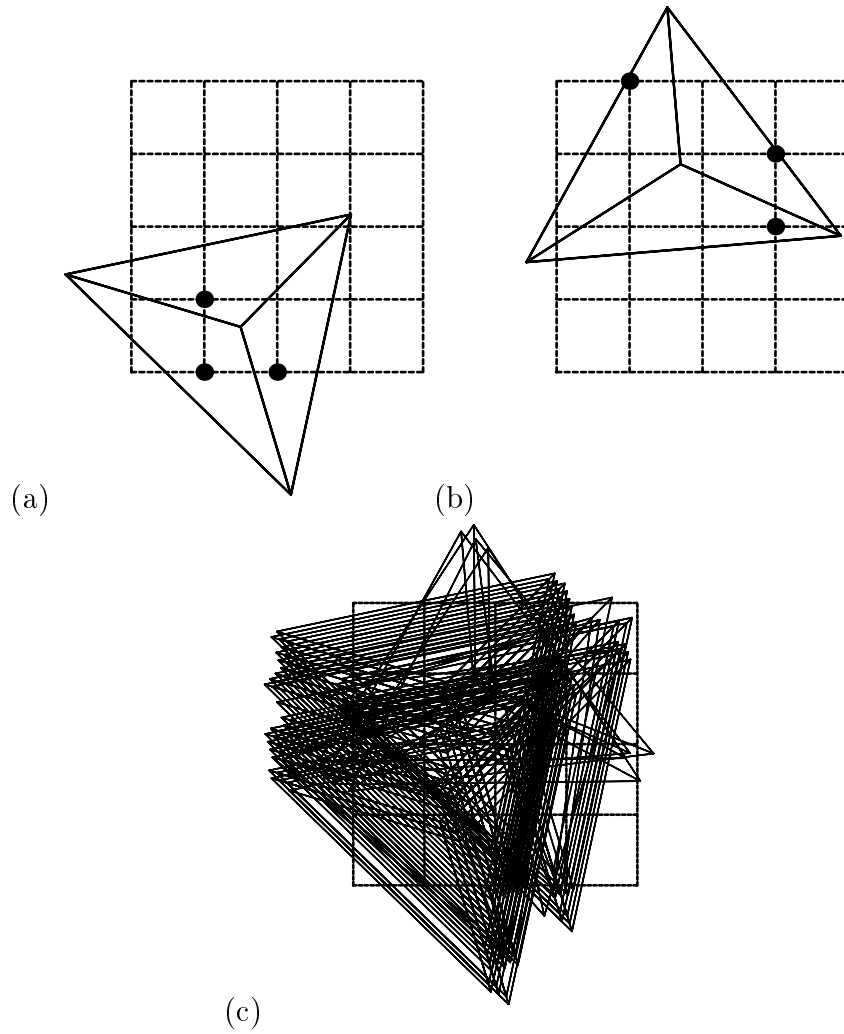
Figure 4.15 Another example: (a) initial configuration, (b) goal configuration, (c) sequence of motions.

4.5 Toward In-Hand Manipulation with Continuous Finger Motions

The pins of our prototype are actuated by high-resolution stepper motors, and therefore capable of virtually continuous motion. Taking this capability into account in the manipulation planning may be complicated but clearly will increase the dexterity of the gripper. In this section, we take the first steps toward solving this problem by introducing the concept of *ICS union* (or *ICSU*).

For a triple of pins $\boldsymbol{t} = (t_1, t_2, t_3)$ and an orientation θ, we define ICSU $\mathcal{T}_{\theta, \boldsymbol{t}}$ to be the set of all object configurations (x, y, θ) that are contained in a maximum ICS region for the triple $\boldsymbol{t}$ at some pin height configuration (h_2, h_3) (as before, without loss of generality, h_1 can be set to zero). Because at an orientation θ, the maximum ICS of a triple of pins $\boldsymbol{t}$ at a pin height configuration (h_2, h_3) is a triangle, therefore $\mathcal{T}_{\theta, \boldsymbol{t}}$ is basically the union of such triangles for all admissible pin height configurations (h_2, h_3).

From the definition above, for an object configuration $\boldsymbol{q}$, when $\boldsymbol{q} \in \mathcal{T}_{\theta, \boldsymbol{t}}$, there exists some pin configuration (h_2, h_3) of the pin triple $\boldsymbol{t}$ by which the object can be immobilized. This leads us to another way for planing a manipulation sequence. Consider ICSU $\mathcal{T}_{\theta_1, \boldsymbol{t}_1}$ and $\mathcal{T}_{\theta_2, \boldsymbol{t}_2}$ where θ_1 and θ_2 are the immobilizing orientations for pin triples $\boldsymbol{t}_1$ and $\boldsymbol{t}_2$ correspondingly. Let $\boldsymbol{q}_1 \in \mathcal{T}_{\theta_1, \boldsymbol{t}_1}$ and $\boldsymbol{q}_2 \in \mathcal{T}_{\theta_2, \boldsymbol{t}_2}$ be two configurations of the object. We can bring the object from configuration $\boldsymbol{q}_1$ to $\boldsymbol{q}_2$ using the following steps: (1) use some pin height configurations of pin triple $\boldsymbol{t}_1$ to translate the object to a configuration in $\mathcal{T}_{\theta_1, \boldsymbol{t}_1} \cap \mathcal{T}_{\theta_1, \boldsymbol{t}_2}$, and (2) switch to pin triple $\boldsymbol{t}_2$ and appropriate pin height to change the orientation of the object to θ_2, and (3) translate the object using appropriate sequence of pin height configuration to bring the object to $\boldsymbol{q}_2$.

We can again reduce in-hand manipulation planning to graph search. Because there we need only one node to represent a pin triple (instead of one node per each pin height configuration in the discrete case), the graph in this case is much smaller than for the discrete case, and hopefully we will have a more efficient planner. In this section, we will

show how to construct an approximation of the ICSU. This is the first step toward the full geometric characterization of the ICSU

Following discussion is for a fixed triple of pins $\boldsymbol{t}$. By considering h_1, h_2 and h_3 as variables, we can parameterize the segment $E_i(\theta, \delta)$ as follows:

$$
\begin{pmatrix} x \\ y \end{pmatrix} = \begin{pmatrix} q_i \\ r_i \end{pmatrix} + (-d_i(\delta_i - h_i) + e_i) \begin{pmatrix} \cos(\theta + \alpha_i) \\ \sin(\theta + \alpha_i) \end{pmatrix} + \eta \begin{pmatrix} \cos(\theta + \alpha_i) \\ \sin(\theta + \alpha_i) \end{pmatrix}, \quad (4.10)
$$

where d_i and e_i are appropriate constants.

When the enclosure condition is satisfied, the line $L_j(\theta, \delta)$ $(j \neq i)$ intersects the segment $E_i(\theta, \delta)$. Substituting the parameterization of x and y in (4.10) into the equation defining the line $L_j(\theta, \delta)$ yields, after some simple algebraic manipulation

$$
\eta = A_{ij} \cos(\theta + \beta_{ij}) + B_{ij}(\delta - h_i) + C_{ij}, \quad (4.11)
$$

where A_{ij}, B_{ij} and C_{ij} are appropriate constants.

Similar to Section 4.4.1.2, we can easily show that the pair $(\eta, \delta - h_i)$ is constrained to lie in a polygon defined by a set of linear inequalities in η and $\delta - h_i$ and any inequality in this set can be written in one of the following forms:

1. $\eta \leq c_k(\delta - h_i) + c'_k$,

2. $\eta \geq c_k(\delta - h_i) + c'_k$,

3. $\delta - h_i \leq c_k$,

4. $\delta - h_i \geq c_k$,

where c_k and c'_k are appropriate constants.

For all inequalities of types 1 and 2, substituting η into (4.11) yields inequalities in θ, δ, h_2 and h_3. For given values of h_2 and h_3, these inequalities, together with the remaining constraints of types 3 and 4, define a region in the (θ, δ) plane for which the enclosure condition is satisfied. By construction, the constraints defining this region can be written in one of the following forms:

(a) $\delta \leq A' \cos(\theta + \beta_{ij}) + B'(h_2, h_3)$,

(b) $\delta \geq A' \cos(\theta + \beta_{ij}) + B'(h_2, h_3)$,

(c) $\delta \leq c_k + h_i$,

(d) $\delta \geq c_k + h_i$,

where A' is a constant and B' is an appropriate linear function of h_2 and h_3.

Let us suppose for a moment that there is only one inequality, and that it is of type (a). Let $\mathcal{L}$ denote the upper boundary curve of the region defined by this inequality. Recall that the equation of the contact sinusoid $\mathcal{E}$ can be written as $\delta = A \cos(\theta + \alpha) + B(h_2, h_3)$, where B is a linear function of h_2 and h_3. As h_2 and h_3 change, the two curves $\mathcal{L}$ and $\mathcal{E}$ translate in the δ direction of the (θ, δ) plane, with an offset linear in h_2 and h_3. Subtracting $B(h_2, h_3)$ from the equations defining $\mathcal{E}$ and $\mathcal{L}$ yields two new curves: $\mathcal{E}'$, which is now fixed in the (θ, δ) plane, and $\mathcal{L}'$ which can translate in the δ direction as a function of $G(h_2, h_3) = B'(h_2, h_3) - B(h_2, h_3)$.

For given values of h_2 and h_3, we call the region above $\mathcal{E}'$ the *allowable region*, and the region below $\mathcal{L}'$ the *valid region*. (The region below $\mathcal{E}'$ is not allowable because it corresponds to configurations for which the object is penetrated by the pins, and the region above $\mathcal{L}'$ is not valid, because it corresponds to configurations for which the enclosure condition is violated.) There are three situations to consider, depending on the value $g = G(h_2, h_3)$ (Figure 4.16).

1. In the first case, shown in Figure 4.16(1), g is not sufficiently large for the minimum of $\mathcal{E}'$ (corresponding to the immobilizing configuration) to be contained in the valid region. As a result, the object cannot be immobilized.

2. In the case shown in Figure 4.16(2), g is sufficiently large for the valid region to contain the minimum of $\mathcal{E}'$. The maximum ICS is associated with the lower intersection of the two curves, and the corresponding range of orientations is the θ interval R shown in the figure.
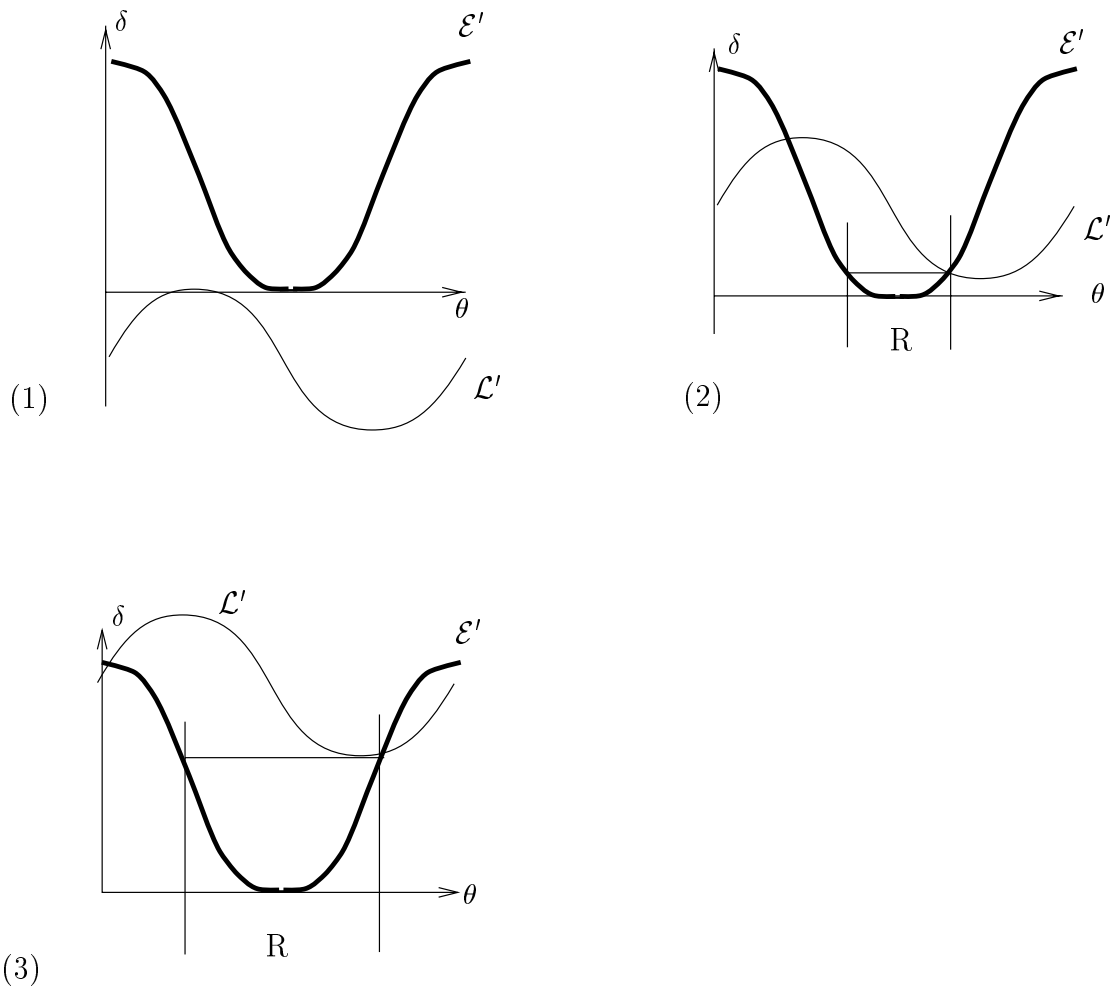
Figure 4.16 The three possible relationships between the curves $\mathcal{E}'$ and $\mathcal{L}'$ (type (a) constraints). See text for details.

3. Finally, in the case shown in Figure 4.16(3), g is also sufficiently large for the allowable region to contain the minimum of $\mathcal{L}'$. The maximum ICS is associated with the minimum of $\mathcal{L}'$, and the corresponding range of orientations is the θ interval R shown in the figure.

We know the range of orientations of the maximum ICS for given h_2 and h_3 values. Let us now draw a diagram of this range as a function of $g = G(h_2, h_3)$. We denote by $R_g = [-\theta_g, \theta_g]$ the range of orientations associated with the value g. Clearly, as g increases, $\mathcal{L}'$ moves up in the (θ, δ) plane, and R_g monotonically expands. In particular, $R_{G(h_2,h_3)}$ contains θ_g when $G(h_2, h_3) \geq g$ (Figure 4.17). This condition defines a half-plane in (h_2, h_3) space, and any point in this half-plane yields an immobilizing configuration (x, y) whose maximum ICS is not empty at $\theta = \theta_g$.
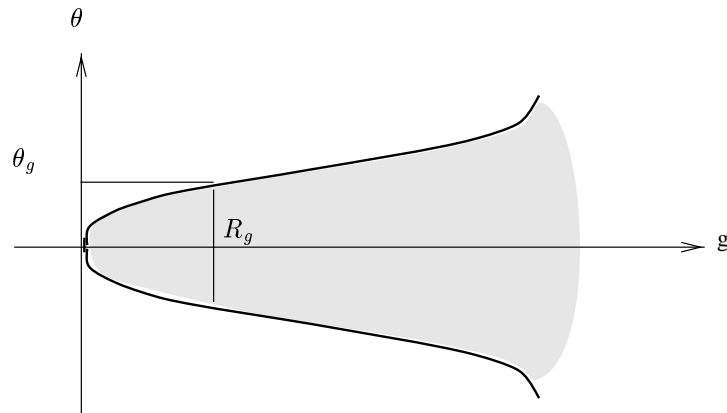
Figure 4.17 The range of orientations of the maximum ICS as a function of g.

So far, we have considered only one inequality of type (a). Of course, we must consider all inequalities (for all possible i, j and k). Together, they define a set of half-planes whose intersection is a convex polygon $\mathcal{P}(\theta_g)$ in the (h_2, h_3) plane. Any point in this polygon determines an immobilizing configuration (x, y) whose maximum ICS is not empty at $\theta = \theta_g$.

Note that inequalities of different types yield range diagrams of different shapes. However, it is easy to verify that they all have the same range monotonicity property.

Let us take a moment to examine a type (b) inequality. This time, we denote by $\mathcal{L}$ the *lower* boundary of the region defined by this inequality. We can define as before a new curve $\mathcal{L}'$ by $\delta = A' \cos(\theta + \beta_{ij}) + G(h_2, h_3)$, where $G(h_2, h_3) = B'(h_2, h_3) - B(h_2, h_3)$. This curve translates in the δ direction as a function of $G(h_2, h_3)$. This time, however, the valid region is *above* $\mathcal{L}'$.

Now, let us show how to draw the diagram of the range of orientations of the maximum ICS in this case (Figure 4.18). At $g = g_{-1}$ (Figure 4.18(1)), the valid region does not include the minimum of the contact sinusoid, and the object cannot be immobilized. As a result, the range of orientations is empty. As g decreases to g_0, as shown in Figure 4.18(2), both curves intersect at the minimum of the contact sinusoid. That is, the maximum ICS contains only the immobilizing configuration, and the range of orientations contains only the immobilizing orientation θ_0. As g continues decreasing, the lower intersection of both curves moves up, and the range of orientations expands. As shown in Figures 4.18(3) and 4.18(4), the range is equal to R_1 when $g = g_1$ and to R_2 when $g = g_2$. For $g < g_2$, the curves do not intersect, and the entire allowable region is contained in the valid region. In other words, the allowable region becomes the maximum ICS, and all orientations are valid. The diagram shown in Figure 4.19 summarizes this construction, and we can use this diagram to obtain another linear constraint on h_2 and h_3 for a given value of θ_g.

Let us go back to the polygon $\mathcal{P}(\theta_g)$ again. Remember that a pair (h_2, h_3) in this polygon determines an immobilizing configuration (x, y) such that the triangular section of the associated maximum ICS by the $\theta = \theta_g$ plane is not empty.

Suppose δ^* is the value of δ associated with the maximum ICS. As we decrease the value of δ from δ, at some point, the ICS triangle in the plane $\theta = \theta_g$ will shrink to a point. This point is contained in the original ICS triangle (when $\delta = \delta^*$) and it corresponds to a configuration where the three pins are simultaneously in contact with the object, and the object is lying at the orientation θ_g (of course, the object is not immobilized unless $\theta_g = \theta_0$). Similar to Section 4.3.2.3 (actually, in the reverse direction), we can compute the position (x, y) associated with this configuration by applying an affine

71
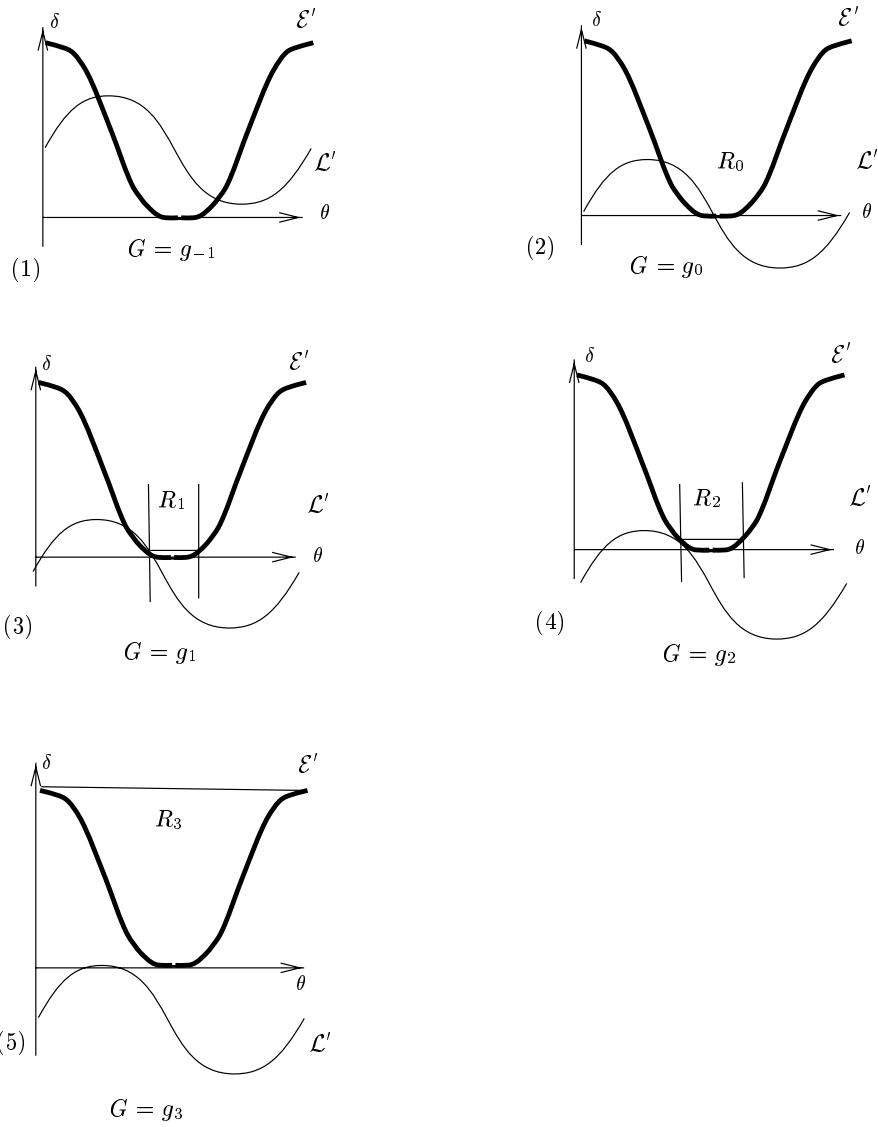
Figure 4.18 The curves $\mathcal{E}'$ and $\mathcal{L}'$ for different values of g (type (b) constraints).
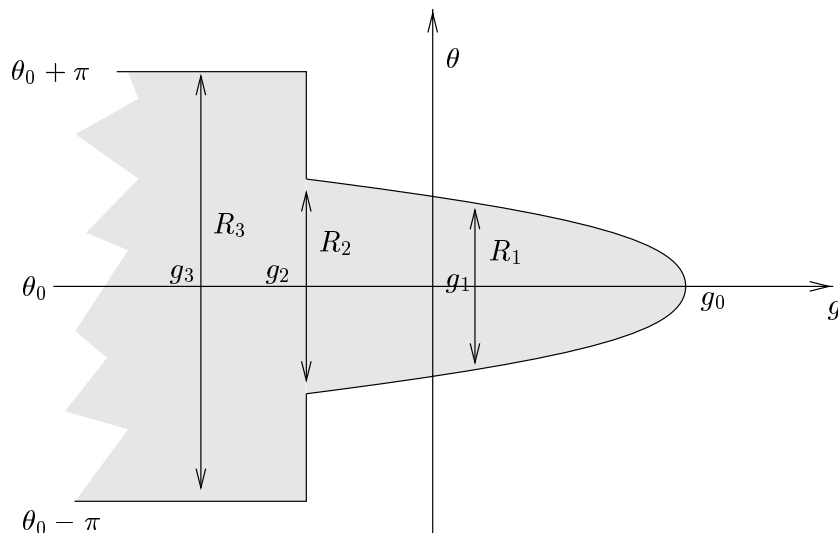
Figure 4.19 The diagram of the range of orientations of maximum ICS with respect to g.

transform to (h_2, h_3). Therefore, we can apply the transform to map $\mathcal{P}(\theta_g)$ in the (h_2, h_3) space to a polygon $\mathcal{P}_{xy}(\theta_g)$ in the plane $\theta = \theta_g$ of the object configuration space. Also, from the construction, it is clear that $\mathcal{P}_{xy}(\theta_g) \subset \mathcal{T}_{\theta_g, \boldsymbol{t}}$. We can thus construct a simple approximation of the ICSU. Interestingly, in many cases, $\mathcal{P}_{xy}(\theta_g) = \mathcal{T}_{\theta_g, \boldsymbol{t}}$.

We have not implemented any manipulation planning algorithm based on this approximation. The main objective of this section is to illustrate an interesting extension of ICS to problems with higher continuous degrees of freedom.

4.6 Experiments with the Prototype

Using the algorithms presented in previous sections, we present here experiments with the gripper prototype. For the experiments given here, it takes 3 seconds to compute all grasps, and 147 seconds to construct the graph for manipulation planning.

4.6.1 Friction

All contacts must be kept as close to frictionless as possible. Strands of metal beads are used to lessen the frictional resistance between the bottom plate and the object. The friction between the pin tips and the object also need to be considered, and we smoothed the surface of the pin tips. This is important because jamming may cause the pins to bend instead of letting the object reach the desired configuration.

4.6.2 Gripper Calibration

To correctly operate, the gripper requires calibration. The calibration has two parts. First, we need to calibrate the large actuator that controls the height of the plate. This is currently performed by manually measuring the actual height of the plate, and passing this parameter to the computer that will command the actuator to a prespecified home position. Once the plate is at the correct home position, we continue with the second part of the calibration. We place a level metal board under the top plate, and keep actuating all the small motors that control the pins until the tips hit the board. Clearly, the height of all pins are now equal at a known value, so we can then send a command to actuate all pins to a desired home position. Note that the actuating power for the calibration of the small actuators must be sufficiently low so that the actuators are not damaged when the pins are stopped when they hit the metal plate while the actuators are still active.

4.6.3 Grasping

In our experiments, a regular tetrahedron is used as a test object. Figure 4.20 and 4.21 show two grasps of this object. The desired configuration viewed from the top is shown in Figure 4.20(a) and 4.21(a). This target configuration is also marked on the lower plate to help verify the successful execution of the task. In Figure 4.20(b) and 4.21(b), the tetrahedron is placed in some arbitrary configuration in the vicinity of the target. When the corresponding grasping operation is executed, we can see that the tetrahedron is moved to and immobilized at the target configuration (Figure 4.20(c) and 4.21(c)). Now

we command the gripper to lift the top plate to the height associated with the maximum ICS of the grasp. We can verify that the tetrahedron is inescapable by trying to move it out of the capture. In this two example, we cannot take the tetrahedron out of the capture without bending the pins. Figure 4.20(d) and 4.21(d) show the most clockwise orientation in the capture, and Figure 4.20(e) and 4.21(e) show the most counterclockwise orientation in the capture. Trying to lower the top plate to the immobilizing height again from these extreme configurations, the tetrahedron again is immobilized exactly at the target configuration (Figure 4.20(f) and 4.21(f)).

4.6.4   In-Hand Manipulation

The first demonstration is a short manipulation sequence. See Figure 4.22. This manipulation has three steps and basically rotates the tetrahedron clockwise about 30 degrees. The targets for the three steps are marked on the board as shown in Figure 4.22(a). First, we place the tetrahedron in some configuration close to the target mark of the first step (Figure 4.22(b)) and execute the manipulation sequence. We can see that for each step in the sequence, the tetrahedron is successfully moved to the desired configuration (Figure 4.22(c)-(e)).

The second demonstration shows a longer manipulation sequence. This sequence contains 39 manipulation steps. All steps are shown in Figure 4.23(a). In the illustration shown in Figure 4.24, the lower plate are marked with initial, final, and three intermediate configurations (Figure 4.23(b)). Again, as shown in Figure 4.24(c)-(e), the tetrahedron successfully reaches the final configuration when the manipulation sequence is executed.
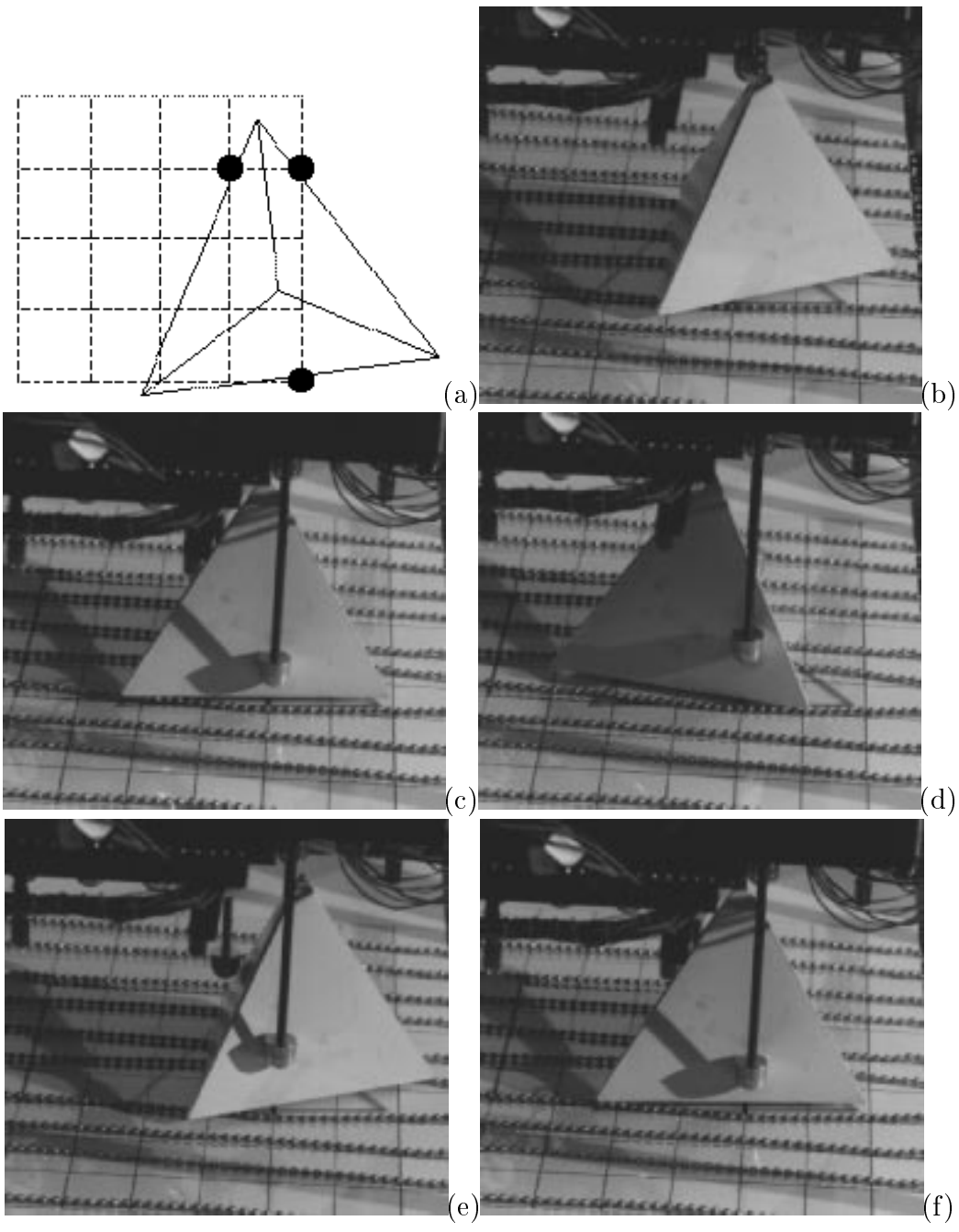
Figure 4.20 A grasp.
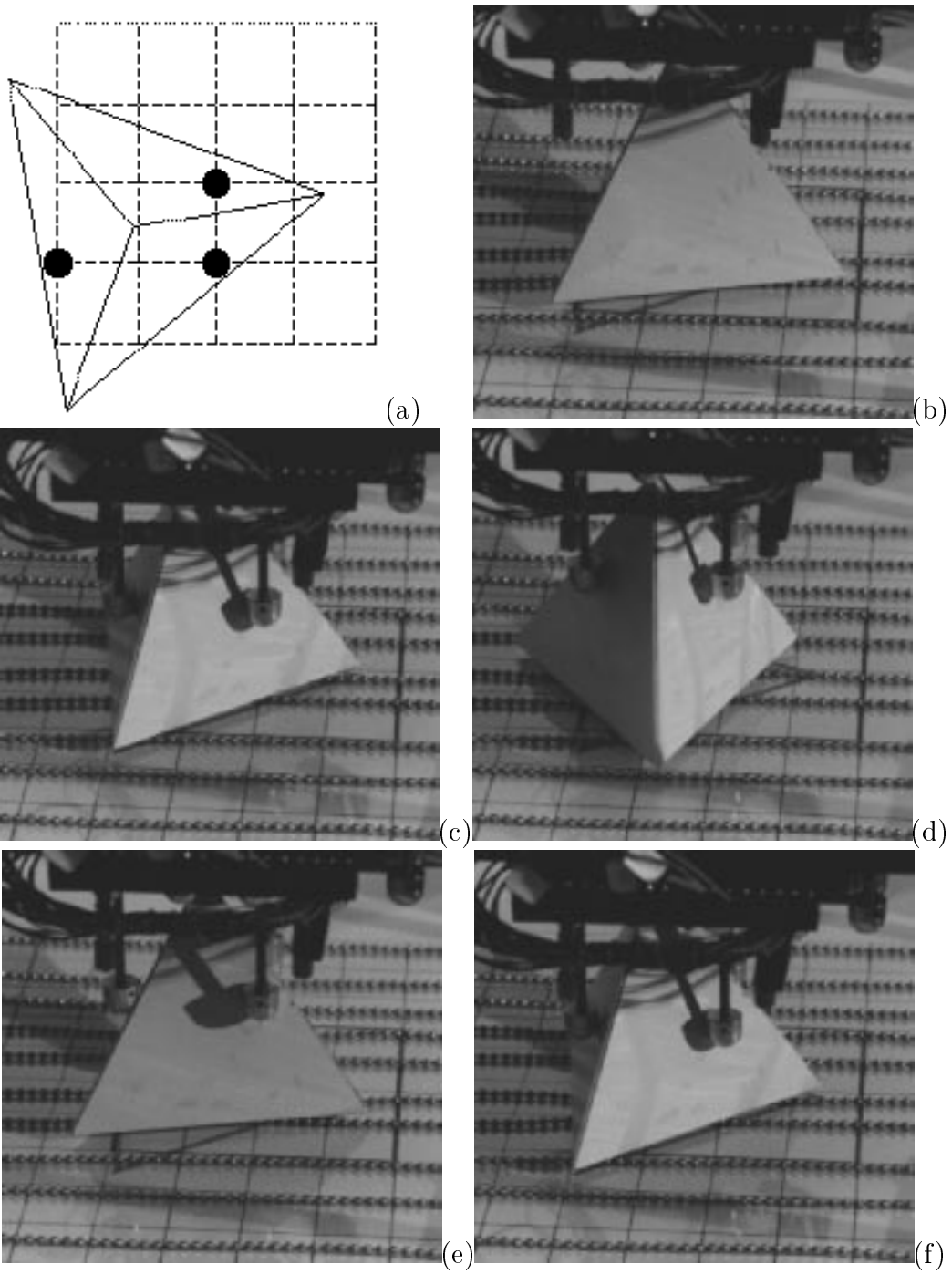
Figure 4.21 Another grasp.

(a)

(b)

(c)

(d)

(e)
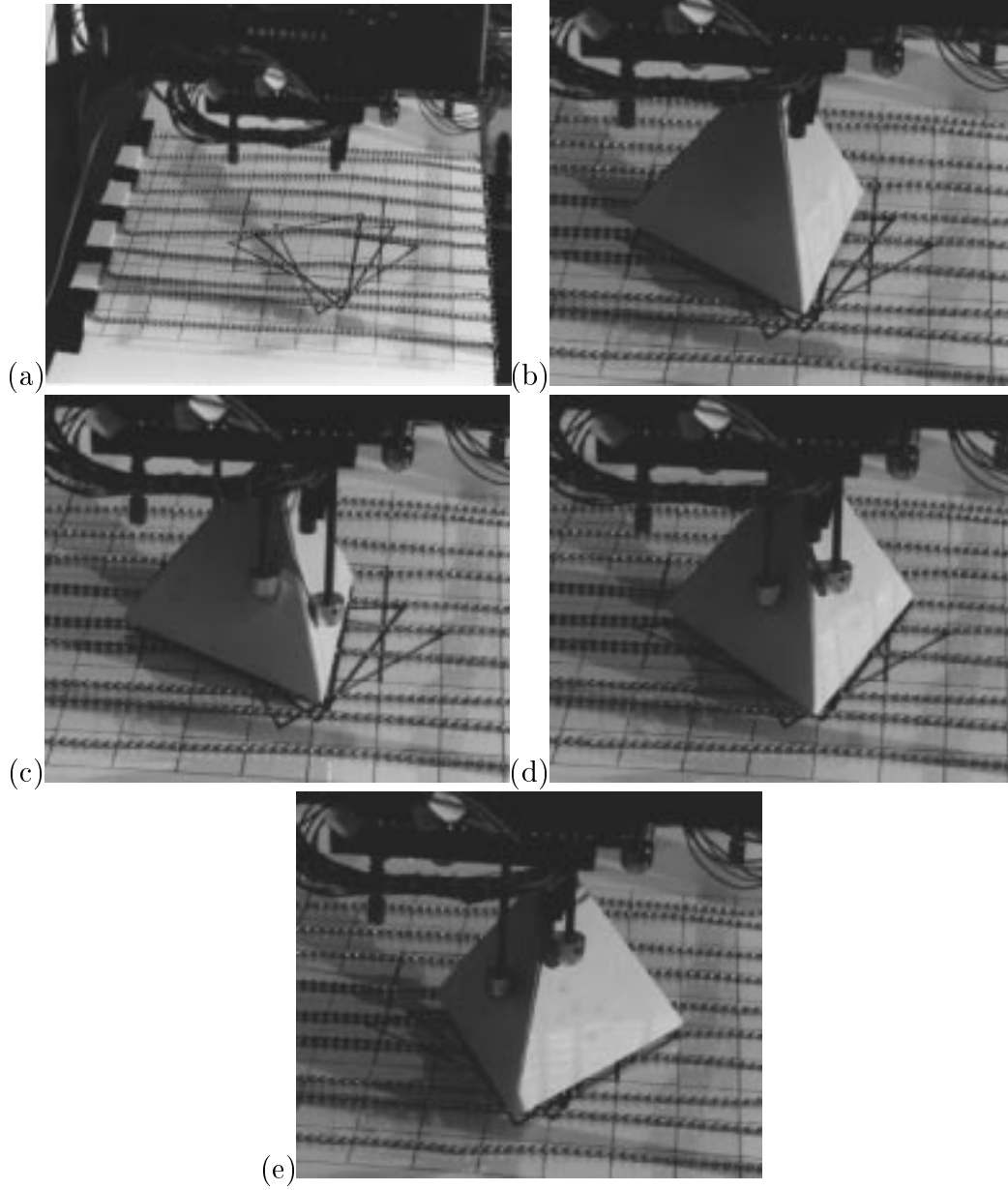
Figure 4.22 A short manipulation sequence.
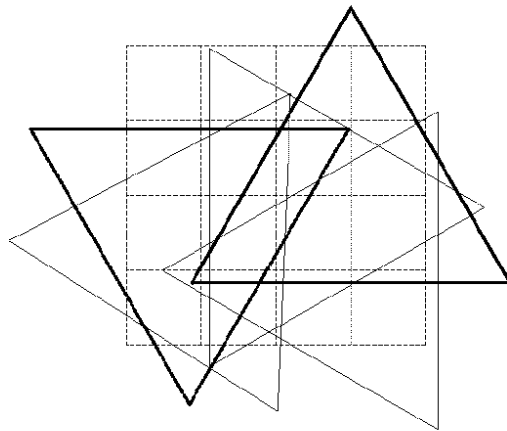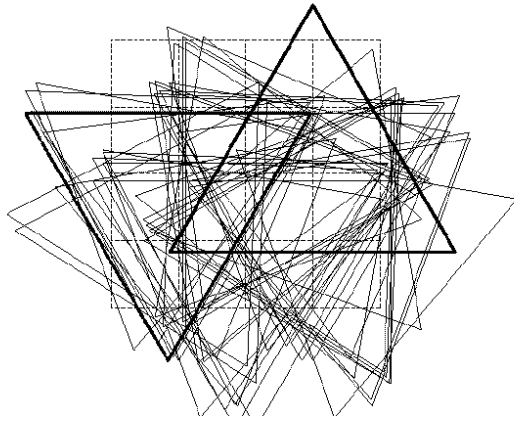
Figure 4.23 Steps in a manipulation.

(a)

(b)

(c)

(d)

(e)

(f)
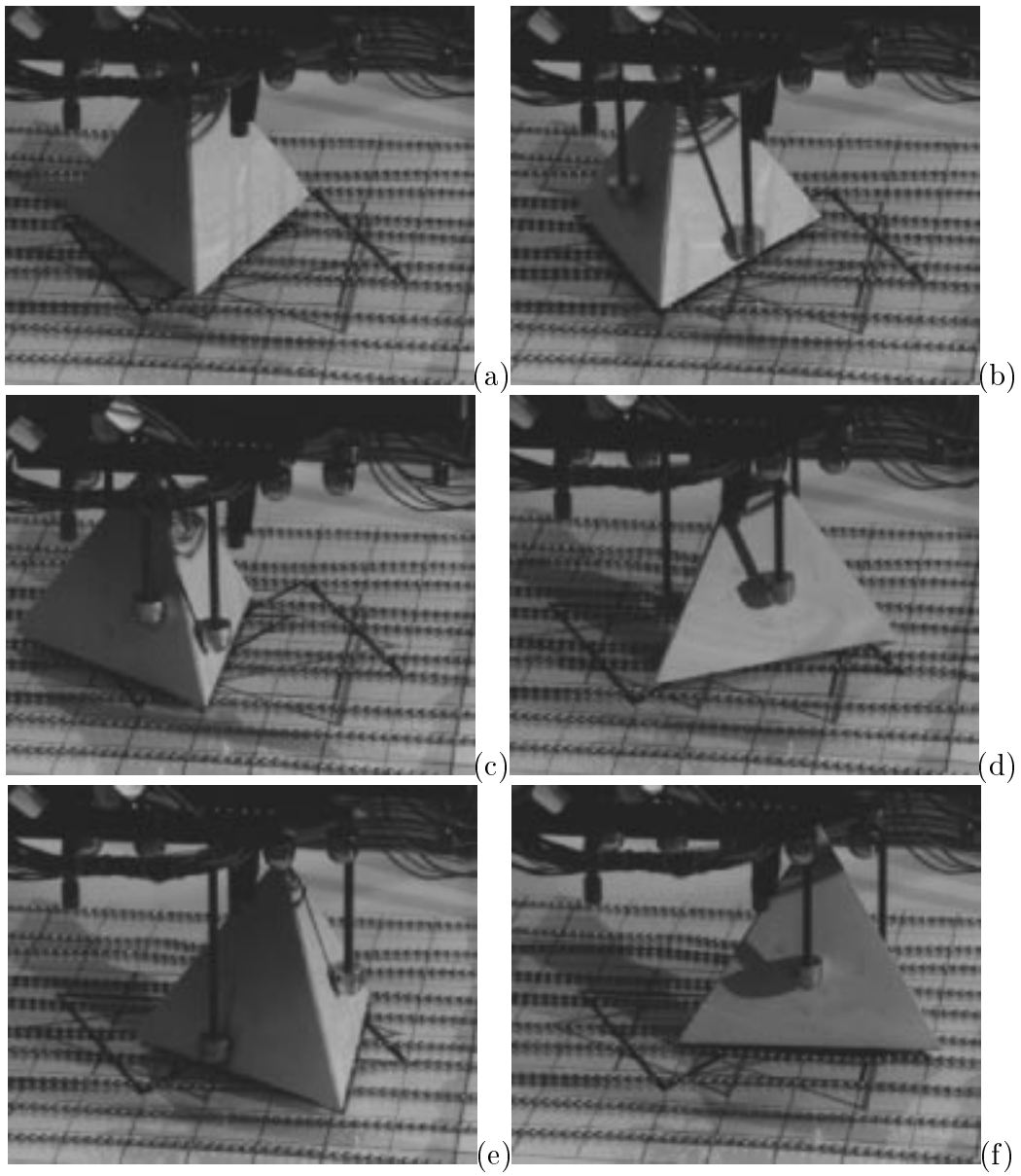
Figure 4.24 Another manipulation sequence.

4.7 Conclusions

We have presented a new reconfigurable gripper. As part of this thesis work, we have also completed the construction of a prototype of this gripper. We proposed to use this gripper to immobilize and manipulate polyhedral objects. We have studied the geometry of these tasks in configuration space, presented efficient grasp and in-hand manipulation planning algorithms, and reported the results from both simulation and experiments with the prototype.

Besides the gripper design and construction, the main contribution of this chapter is the concept of ICS (inescapable configuration space) region which we will use as a framework for object manipulation. In this chapter, we have applied this concept to a manipulation problem with one continuous degree of freedom. In the next chapter, we will show an application of this concept in a manipulation problem with two degrees of freedom.

CHAPTER 5

MOBILE ROBOTS

5.1   Introduction

In this chapter, we apply the concept of ICS presented in Chapter 4 to another problem. We address the problem of manipulating a planar polygonal object with three disc-shaped robots capable of arbitrary straight line and circular arc motions in the plane. In practice, the discs may be the fingertips of a robot hand or mobile platforms.

We propose an algorithm for grasping the object and bringing it to a desired position and orientation through sequences of atomic motions of each robot. This algorithm guarantees that the object will never escape from the robots' grasp, even when contact is broken during the initial grasping phase or the subsequent manipulation stage. It does not require synchronizing the motion of the discs, and only assumes that each one of them can be moved in turn to follow a given straight line or circular arc.

The proposed approach is based on a detailed analysis of the geometry of the joint object/robot configuration space which is along the line of the ICS concept presented in Chapter 4 [95] . Instead of trying to predict the exact motion of the object, we characterize the range of possible motions associated with each position of the robots and identify the "minimal" robot configurations for which the object is totally immobilized as well as the "maximal" ones for which there is a non-empty open set of object motions within the grasp, but no escape path to infinity.

A simulation-based implementation of this general approach was first applied in [93] to the case where the three robots are only allowed to move along straight lines with fixed directions. In this case, individual robot motions have only one degree of freedom, and planning amounts to determining the maximum extent of the translation of each robot along the associated line segment. The new technique proposed in this chapter allows the robots to move in the plane with two degrees of freedom. In turn, this simplifies planning and allows us to construct complex motion plans from many fewer elementary steps. The proposed approach is validated by simulation examples and preliminary experiments with Nomadic Scout robots (Section 5.5).

5.1.1   Related Work

In [93], we showed that ICS regions can be used to manipulate an object by pushing it with three disc-shaped robots moving along straight lines with fixed directions: starting from some immobilizing configuration, we move the robots one at a time in the direction associated with the lead robot, then choose another direction etc.. to achieve the desired translation and/or rotation. The object remains at all times in the ICS region associated with the discs, and the planned manipulation is guaranteed to succeed as long as the friction forces associated with contacts between the robots, the object and its supporting plane are not large enough to cause jamming. In particular, unlike other approaches to manipulation planning (e.g., [1, 26, 33, 49, 55, 67]), this approach does not require that finger/object contact be maintained during grasping or manipulation, nor does it rely on any particular model of friction or contact dynamics.

A limitation of the method presented in [93] (and the related grasp planning techniques of [20, 80]) is that the individual robot motions only have one degree of freedom: each robot can only translate along a straight line with a fixed direction. This severely limits the extent of the translation and forces any complex motion to be decomposed into a large number of atomic elements. The new approach presented in this chapter addresses this difficulty by allowing the robots to move within two-dimensional regions

of the plane. This allows us to construct much larger atomic motions and simplifies planning.

5.2   1-DOF ICS Regions

We apply in this section the concept of an inescapable configuration space region. The analysis proceeds along the lines of Chapter 4 [94] by identifying the constraints imposed by the robots in the configuration space of the polygon. The general approach is the same as in [94] but the setting and the corresponding constraints are of course different.

5.2.1   Contact

We reduce the problem of achieving contact between a disc and a line to the problem of achieving point contact with a line. This is done without loss of generality by growing the object to be grasped by the disc radius and shrinking each disc into its center.

We attach a coordinate system (u, v) to the polygon, and write in this coordinate system the equations of the line supporting the edge e_i $(i = 1, 2, 3)$ as $u \cos \alpha_i + v \sin \alpha_i - d_i = 0$, where α_i is the angle between the u axis and the *internal* normal $\boldsymbol{n}_i$ to the edge, and d_i is the distance between the origin of the (u, v) coordinate system and the edge.

Without loss of generality, we also define a world coordinate system (q, r) such that the r axis is parallel to the motion direction $\boldsymbol{v}$ and goes through the center of the first (moving) disc. We denote by $\boldsymbol{q}_i = (q_i, r_i)^T$ the position of the center of disc number i in this coordinate system. In particular, $q_1 = 0$ and $r_1 = \delta$.

We can write the condition for contact between disc number i and the corresponding line as

$$\boldsymbol{q}_i = \mathcal{R} \boldsymbol{p}_i + \boldsymbol{t}, \tag{5.1}$$

where $\boldsymbol{p}_i = (u_i, v_i)^T$ and $\boldsymbol{q}_i = (q_i, r_i)^T$ denote the positions of the contact point in the two coordinate systems, $\mathcal{R}$ is a rotation matrix of angle θ and $\boldsymbol{t} = (x, y)^T$ is the translation

between the two coordinate frames. Let $c_i = \cos(\theta + \alpha_i)$ and $s_i = \sin(\theta + \alpha_i)$, the above equation can be rewritten as

$$(x - q_i)c_i + (y - r_i)s_i + d_i = 0, \tag{5.2}$$

When the three contacts are achieved simultaneously, we have

$$\begin{pmatrix} c_1 & s_1 & \delta s_1 - d_1 \\ c_2 & s_2 & q_2 c_2 + r_2 s_2 - d_2 \\ c_3 & s_3 & q_3 c_3 + r_3 s_3 - d_3 \end{pmatrix} \begin{pmatrix} x \\ y \\ -1 \end{pmatrix} = 0.$$

For this equation to be satisfied, the determinant of the 3×3 matrix must be zero, which yields (after some simple algebraic manipulation):

$$\delta \sin(\theta + \alpha_1) + A_2 \cos(\theta + \beta_2) + A_3 \cos(\theta + \beta_3) - B = 0, \tag{5.3}$$

where β_2, β_3 and A_2, A_3, B are appropriate constants.

This condition defines a curve in θ, δ space, called the *contact curve*. This curve is defined on the $[0, 2\pi]$ interval, but an actual contact between the first disc and the corresponding edge can only occur when the angle between $\boldsymbol{v}$ and the internal normal to the edge is obtuse, i.e., when $\theta + \alpha_i \in [\pi, 2\pi]$. It follows from the form of its equation that the contact curve is in fact bounded by two vertical asymptotes on that interval.

5.2.2   Equilibrium

At equilibrium, the various forces and moments exerted at the contacts balance each other. This can be written in the object's coordinate system as

$$\sum_{i=1}^{3} \lambda_i \begin{pmatrix} \boldsymbol{n}_i \\ \boldsymbol{p}_i \times \boldsymbol{n}_i \end{pmatrix} = 0, \quad \text{where} \quad \begin{cases} \lambda_1, \lambda_2, \lambda_3 > 0, \\ \lambda_1 + \lambda_2 + \lambda_3 = 1. \end{cases}$$

Using the change of coordinates (5.1) and taking advantage of the fact that $\sum_{i=1}^{3} \lambda_i \boldsymbol{n}_i = 0$ allows us to rewrite this equation as

$$\sum_{i=1}^{3} \lambda_i \begin{pmatrix} \boldsymbol{n}_i \\ (\mathcal{R}^{-1}\boldsymbol{q}_i) \times \boldsymbol{n}_i \end{pmatrix} = 0,$$

which can be interpreted as a 3×3 homogeneous equation in the coefficients $\lambda_1, \lambda_2, \lambda_3$. A necessary and sufficient condition for this equation to have a non-trivial solution is that its determinant be zero, i.e.,

$$\begin{vmatrix} \boldsymbol{n}_1 & \boldsymbol{n}_2 & \boldsymbol{n}_3 \\ (\mathcal{R}^{-1}\boldsymbol{q}_1) \times \boldsymbol{n}_1 & (\mathcal{R}^{-1}\boldsymbol{q}_2) \times \boldsymbol{n}_2 & (\mathcal{R}^{-1}\boldsymbol{q}_3) \times \boldsymbol{n}_3 \end{vmatrix} = 0.$$

Expanding the determinant yields, after some additional algebraic manipulation, the condition

$$\delta \cos(\theta + \alpha_1) - A_2 \sin(\theta + \beta_2) - A_3 \sin(\theta + \beta_3) = 0,$$

and eliminating δ between this equation and the contact constraint (5.3) yields an equation in θ only:

$$\cos(\theta + \alpha_1) = \frac{A_2}{B} \cos(\beta_2 - \alpha_1) + \frac{A_3}{B} \cos(\beta_3 - \alpha_1). \tag{5.4}$$

There are (at most) two solutions for this equation in the $[0, 2\pi]$ interval. When they exist, exactly one of them is in the interval of physically achievable contacts. It is also easy to show that the corresponding solution is a minimum of the contact curve. As in [94], this minimum corresponds to an immobilizing configuration [81].[1]

Figure 5.1 shows an actual example in the object's and disc's coordinate frames. The triangle has to rotate 60 degrees counterclockwise to be immobilized by the matching discs (Fig. 5.1(c)). This is verified on the contact curve shown in Fig. 5.1(e) where the minimum occurs at 60 degrees in the physically realizable interval. The maximum of the curve corresponds to the configuration shown in Fig. 5.1(d), and it cannot be achieved in reality: the first disc would have to lie inside the triangle.

---

[1]The object will be immobilized even if there is no friction: although this appears to contradict classical screw theory, which states that three fingers are not sufficient to immobilize a two-dimensional object in that case [43], recall that screw theory is concerned with *infinitesimal* motions: there exists an escape velocity but no finite escape motion. See [81] for details.
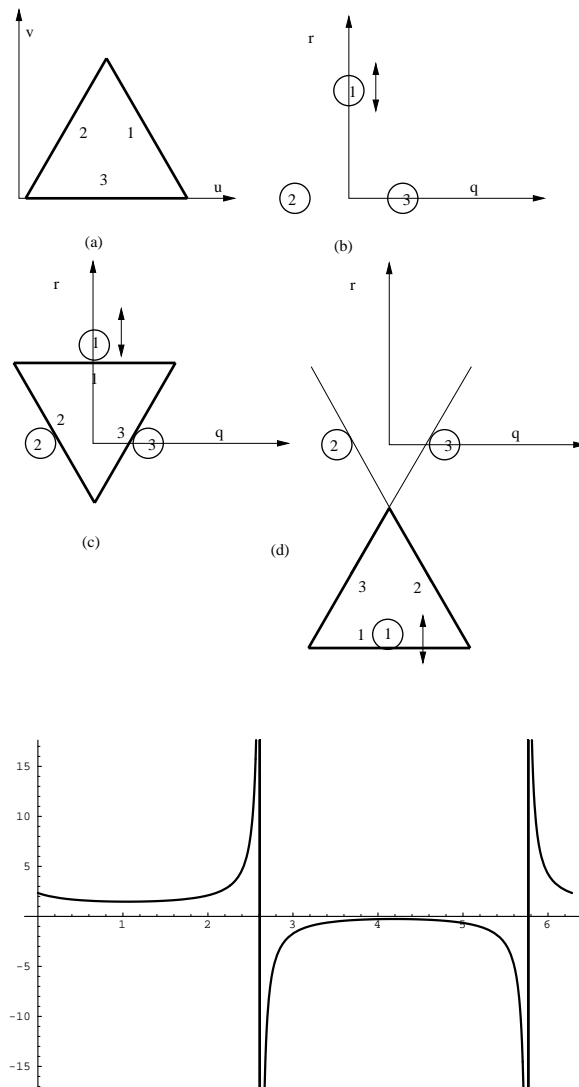
Figure 5.1 A grasp and the corresponding contact curve.

87

5.2.3 Free Configuration Space Regions

Let us consider an immobilizing configuration of the robots, and denote by $x_0, y_0, \theta_0, \delta_0$ the corresponding values of x, y, θ, δ. Let us also assume that the positions of robots 2 and 3 are held constant while the δ coordinate of the first robot may change.

We denote by S_i the set of object configurations (x, y, θ) for which contact between disc number i and the corresponding object edge is achieved. From (5.2), this is a ruled surface in (x, y, θ) space, whose intersection with a plane $\theta = $ constant is a line $L_i(\theta)$ at distance $-d_i$ from the fixed point (q_i, r_i) of the x, y plane, and the angle between the x axis and the normal to this line is $\theta + \alpha_i$. Changing θ corresponds to rotating each line about the point (q_i, r_i). Changing δ amounts to translating the line $L_1(\theta)$.

Together, the three ruled surfaces S_1, S_2 and S_3 bound a volume V of free configuration space. Given the setup of the robots, it is obvious that if a configuration lies in free space for some value δ_1 of δ, it also lies in free space for any other value $\delta_2 \geq \delta_1$. In other words, $V(\delta_1) \subset V(\delta_2)$ when $\delta_2 \geq \delta_1$, and it follows that the immobilizing configuration (x_0, y_0, θ_0) is always in free space for $\delta \geq \delta_0$.

In addition, the intersection of V with a plane $\theta = $ constant is a triangle $T(\theta)$ that may contain an open subset, be reduced to a point, or be empty. In the second case, the three contacts are simultaneously achieved, and (5.3) is satisfied.

It is easy to show that a necessary and sufficient condition for the triangle $T(\theta)$ to contain at least one point is that the point (θ, δ) be *above* the contact curve. This allows us to characterize qualitatively the range of orientations θ for which $T(\theta)$ is not empty: for a given δ, the condition (5.3) is an equation in θ that may have zero, one, or two real solutions, with a double root at the minimum $\delta = \delta_0$ of the curve. In this case, the range of orientations reduces to a single point. For any value $\delta_1 > \delta_0$, there are two distinct roots θ', θ'', and the range of orientations is the arc bounded by these roots and containing θ_0.

In particular, since the volume V is a stack of contiguous triangles $T(\theta)$, it is clear at this point that, for $\delta \geq \delta_0$, V is a non-empty, connected, compact region of $\mathbb{R}^2 \times S^1$. The

analysis confirms that the minimum point (θ_0, δ_0) of the contact curve corresponds to an isolated point of configuration space or equivalently to an immobilizing configuration: indeed, for $\delta = \delta_0$, the triangle $T(\theta_0)$ is reduced to a point, and $T(\theta)$ is empty for any $\theta \neq \theta_0$.

5.2.4 ICS Regions

The discussion so far has characterized the contacts between the discs and the lines supporting the corresponding edges, ignoring the fact that each edge is a compact line segment. For a given value of δ, let us construct a parameterization of the set $E_i(\theta)$ of configurations (x, y) for which disc number i touches the edge e_i. Obviously, $E_i(\theta)$ is itself a line segment supported by the line $L_i(\theta)$.

We first parameterize the corresponding edge e_i by

$$\begin{pmatrix} u_i \\ v_i \end{pmatrix} = d_i \begin{pmatrix} \cos \alpha_i \\ \sin \alpha_i \end{pmatrix} + \eta_i \begin{pmatrix} -\sin \alpha_i \\ \cos \alpha_i \end{pmatrix},$$

with η_i in some interval $[\eta_{i1}, \eta_{i2}]$. The segment $E_i(\theta)$ can now be parameterized by

$$\begin{pmatrix} x - q_i \\ y - r_i \end{pmatrix} = -d_i \begin{pmatrix} c_i \\ s_i \end{pmatrix} - \eta_i \begin{pmatrix} -s_i \\ c_i \end{pmatrix}. \tag{5.5}$$

The constraints $\eta_{i1} \leq \eta \leq \eta_{i2}$ $(i = 1, 2, 3)$ define the regions of configuration space where actual contact will occur. When $E_i(\theta)$ and $E_j(\theta)$ intersect for all $i \neq j$, the three segments completely enclose the triangle $T(\theta)$, and we will say that the corresponding configuration satisfies the *enclosure condition* since there is no escape path for the object in the x, y plane with the corresponding orientation θ. More generally, when all triples of segments in the range of orientations associated with a given δ satisfy the enclosure condition, V itself is an *inescapable configuration space* (ICS) region: in other words, the object is free to move within the region V, but remains imprisoned by the grasp and cannot escape to infinity.

5.2.5 Maximum ICS Regions

We now address the problem of characterizing the maximum value δ^* for which $V(\delta)$ forms an ICS region for any δ in the $[\delta_0, \delta^*]$ interval. We know that at $\delta = \delta_0$ the three segments intersect at the immobilizing configuration, forming an ICS region reduced to a single point. Thus the enclosure condition holds at $\delta = \delta_0$. On the other hand, as $\delta \to +\infty$, the whole configuration space becomes free of obstacles, thus there must exist a critical point for some minimal value of δ greater than δ_0. This guarantees that δ^* has a finite value.

A critical configuration occurs when an endpoint of the segment $E_i(\theta)$ lies on the line $L_j(\theta)$, $j \neq i$. We intersect the lines $L_i(\theta)$ and $L_j(\theta)$ by substituting the parameterization (5.5) in the contact equation (5.2). Writing $\eta_i = \eta_{ik}$ $(k = 1, 2)$ yields

$$\eta_{ik} = -\frac{d_j - d_i \cos(\alpha_i - \alpha_j) + (q_i - q_j)c_j + (r_i - r_j)s_j}{\sin(\alpha_i - \alpha_j)}. \tag{5.6}$$

It follows that critical points lie on one of the six *critical curves* of (θ, δ) space defined by (5.6) for $i, j \in \{1, 2, 3\}$ $(i \neq j)$ and $k = 1, 2$. Note that when $i, j \in \{2, 3\}$, (5.6) is a function of θ only, and the corresponding critical curves are vertical.

We seek the minimum value of $\delta^* > \delta_0$ for which the range of possible object orientations defined by the contact curve includes one of the critical configurations. Let us suppose first that a critical value lies in the interior of the orientation range associated with some $\delta_1 \geq \delta_0$, and denote by $\delta_{\min}$ the minimum value of δ on the critical curve. By definition, we have $\delta_1 \geq \delta_{\min}$. Suppose that $\delta_1 > \delta_{\min}$. Then by continuity, there exists some δ_2 such that $\delta_{\min} < \delta_2 < \delta_1$ and the corresponding range of orientations also contains a critical orientation. The argument holds for any value $\delta > \delta_{\min}$. In other words, either the range of orientations of $\delta_{\min}$ contains a critical orientation, in which case $\delta^* = \delta_{\min}$, or it does not, in which case the critical value associated with δ^* must be one of its range's endpoints. This is checked by intersecting the contact curve and the critical curve. Note that this process must be repeated six times (once per each segment/vertex pair) to select the minimum value of δ^*.
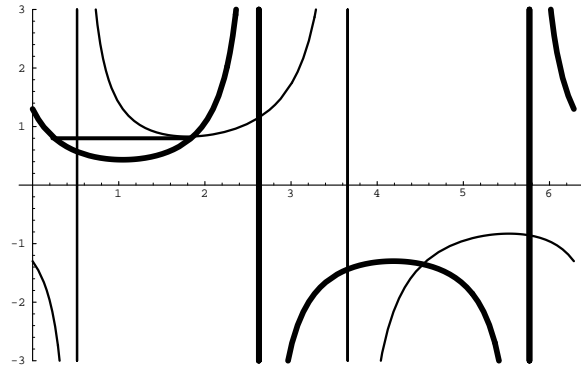
Figure 5.2 The contact and critical curves for a sample object. The critical range of orientations is shown as a horizontal line. See text for details.

Figure 5.2 shows an example, where the contact and critical curves have been constructed for some sample object (the contact curve is drawn with a thicker brush). In this case, the minimum of the critical curve occurs just below the contact curve, and the critical configuration is the intersection of the two curves, lying at the right endpoint of the corresponding range of orientations.

Computing the minimum of the critical curve amounts to solving a trigonometric equation. It is easily shown that intersecting the critical curve and the intersection curve amounts to solving a quadratic equation in $\tan(\theta/2)$ when $i = 2, 3$ and $j = 1$, and a quartic equation in the same variable when $i = 1$, $j = 2, 3$. The intersection can be computed in closed form in both cases.

5.3   2-DOF ICS Regions

We have characterized the range of translations of the robot R_1 along some fixed direction $\boldsymbol{v}$ that ensures that the polygon grasped by the three robots is unable to escape. Naturally, the next step is to characterize the two-degrees-of-freedom (2-dof) motions of R_1 that will achieve the same effect (Figure 5.3).
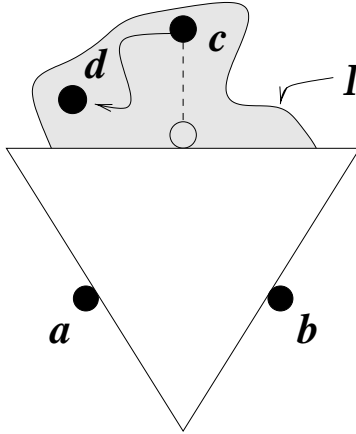
Figure 5.3 Can we construct a two-dimensional region $\mathcal{I}$ where the first robot can roam while still preventing the object to escape?
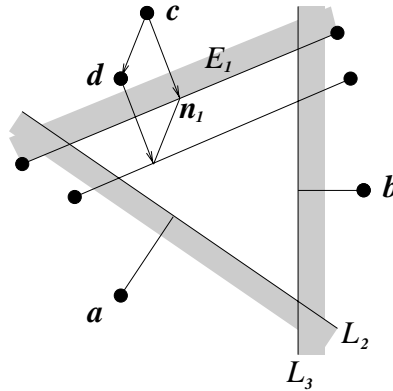
Figure 5.4 The effect of moving R_1 from $\boldsymbol{c}$ to $\boldsymbol{d}$ on the configuration space picture.

Characterizing the set of these motions exactly requires a complex analysis in a generalized five-dimensional (polygon position and orientation (x, y, θ) plus robot position (q_1, r_1)) configuration space. Instead, we address here the simpler problem of using the maximum ICS regions computed in the previous section to construct a conservative approximation $\mathcal{I}$ of this set.

Let us denote by $\boldsymbol{a}$, $\boldsymbol{b}$ and $\boldsymbol{c}$ the positions of the three robots corresponding to some maximum ICS configuration, and let us move the robot R_1 from $\boldsymbol{c}$ to a new position $\boldsymbol{d}$ closer to the associated edge E_1 of the polygon under consideration. As shown by Figures 4.7 and 5.4, this corresponds to translating the line $L_1(\theta)$ parallel to itself, and the corresponding triangle of free configuration space will shrink accordingly.
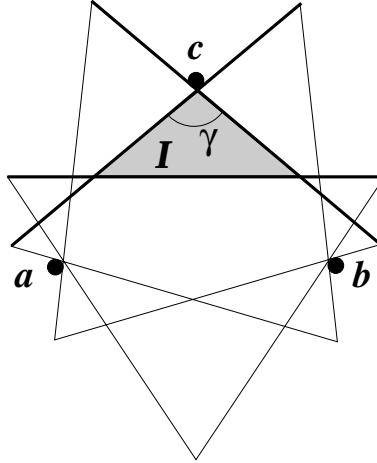
Figure 5.5 Defining a 2-dof ICS region. The edge E_1 is drawn in a thicker pen.

In particular, placing the three robots in $\boldsymbol{a}$, $\boldsymbol{b}$ and $\boldsymbol{d}$ will determine an ICS region *as long as the endpoints of the edge $E_1(\theta)$ do not cross the lines $L_2(\theta)$ and $L_3(\theta)$. The following lemma characterizes a set of points $\boldsymbol{d}$ for which this never happens.*

Lemma 1 *Let $\mathcal{I}$ denote the open triangle bounded by the three lines supporting E_1 when it is immobilized, when it is in its most clockwise orientation, and when it is in its most counterclockwise orientation (Figure 5.5). When the angle γ between the edges of the triangle $\mathcal{I}$ adjacent to $\boldsymbol{c}$ is obtuse, there is no position $\boldsymbol{d}$ of the robot R_1 in $\mathcal{I}$ for which the polygon can escape the robots' grasp.*

Proof: As remarked earlier, it is sufficient to show that, for any point $\boldsymbol{d}$ in $\mathcal{I}$, the endpoints of the line segment $E_1(\theta)$ can never cross the lines $L_2(\theta)$ and $L_3(\theta)$.

Indeed, such a crossing would correspond to an intersection of the contact curve with one of the two critical curves associated with the endpoints of E_1 and the two lines $L_2(\theta)$ and $L_3(\theta)$ in configuration space. As shown in [93], for fixed positions of the robots R_2 and R_3 these critical curves can be described by equations of the form $C_i(\boldsymbol{p}, \theta) = \eta_i$ ($i = 2, 3$), where $\boldsymbol{p}$ denotes the position of R_1, and η_i is a constant.

In addition, it is easy to show that

$$C_i(\boldsymbol{d}, \theta) - C_i(\boldsymbol{c}, \theta) = K[(\boldsymbol{d} - \boldsymbol{c}) \cdot \boldsymbol{n}_1(\theta)],$$
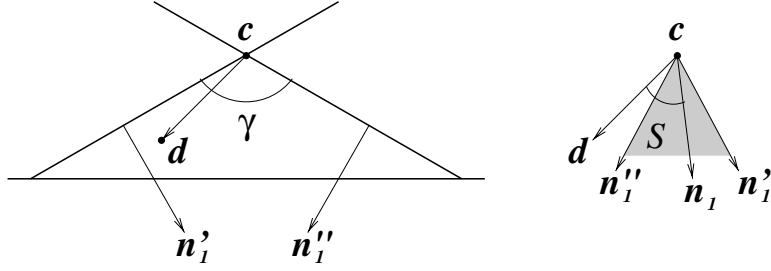
Figure 5.6 When the angle γ is obtuse, the angle between the vector $\boldsymbol{d} - \boldsymbol{c}$ and any normal $\boldsymbol{n}_1$ in the sector S is acute.

where $\boldsymbol{n}_1(\theta)$ denotes the (internal) unit normal to the edge E_1 when the polygon itself is at orientation θ, and K is a positive constant. As shown in the previous section and [93], the critical curve only intersects the contact curve for $\delta > 0$. It follows easily that $C_i(\boldsymbol{c}, \theta) - \eta_i \geq 0$ for $i = 2, 3$.

Let us now denote by $\boldsymbol{n}_1'$ and $\boldsymbol{n}_1''$ the internal normals to the edge E_1 at its extreme counterclockwise and clockwsise orientations when R_1 is at $\boldsymbol{c}$. By definition of the triangle $\mathcal{I}$, we have $(\boldsymbol{d} - \boldsymbol{c}) \cdot \boldsymbol{n}_1' > 0$ and $(\boldsymbol{d} - \boldsymbol{c}) \cdot \boldsymbol{n}_1'' > 0$ for any point $\boldsymbol{d}$ in this triangle.

The possible orientations of the normal $\boldsymbol{n}_1$ to the edge E_1 lie in the sector S bounded (clockwise) by $\boldsymbol{n}_1''$ and (counterclockwise) by $\boldsymbol{n}_1''$ (Figure 5.6). When the angle γ between the edges of $\mathcal{I}$ adjacent to $\boldsymbol{c}$ is obtuse, the angle between the vectors $\boldsymbol{n}_1'$ and $\boldsymbol{n}_1''$ is acute, and it follows that $(\boldsymbol{d} - \boldsymbol{c}) \cdot \boldsymbol{n}_1 > 0$ for any vector $\boldsymbol{n}_1$ in S.

In particular, we have, for any orientation of the object in its maximum ICS region:

$$C_i(\boldsymbol{d}, \theta) - \eta_i > C_i(\boldsymbol{c}, \theta) - \eta_i \geq 0.$$

In particular, the critical curve and the contact curve associated with $\boldsymbol{d}$ do not intersect for any configuration of the polygon in the ICS region associated with the position $\boldsymbol{c}$ of R_1, and the lemma follows immediately. $\square$

It is of course a priori possible that the angle γ be acute. Note, however, that γ tends toward π as δ^* tends toward 0. Therefore, even if the angle γ associated with the maximum value δ^* is acute, we can construct a smaller value of δ^* corresponding to an obtuse angle using a few bisection steps.

94

5.4 Manipulation Planning

In this section, we will assume that an immobilizing grasp has been selected and that the initial object position and orientation are known, and we will show how to actually execute the grasp and then manipulate the polygon, moving the three robots one at a time while guaranteeing that the object will not escape.

First, we follow the strategy proposed in [93] to execute the grasps: if $\boldsymbol{a}$, $\boldsymbol{b}$ and $\boldsymbol{c}$ denote the immobilizing positions of R_1, R_2 and R_3, we move the robots one by one from their home position to $\boldsymbol{a} + \frac{1}{2}\delta^*\boldsymbol{v}$, $\boldsymbol{b} - \frac{1}{2}\delta^*\boldsymbol{v}$ and $\boldsymbol{c} - \frac{1}{2}\delta^*\boldsymbol{v}$. The polygon is now guaranteed to be in the maximum ICS region associated with the robots. We then translate the first robot by $-\delta^*\boldsymbol{v}$.

Although the object may (and indeed will) move when contact occurs, it will end up in the planned immobilized configuration. Note that this approach is robust to uncertainty in the position of the object, but that it requires precise relative motions of the robots.

In the next two sections, we show how to achieve arbitrary translations and rotations of the object once it has been grasped. The overall motion will be decomposed into atomic motions of the three fingers along appropriate trajectories. The object will remain imprisoned in the grasp of the three robots during each motion.

5.4.1 Rotating a Polygon

Once the object has been grasped, we construct the triangle $\mathcal{I}$, knowing that the first robot can follow any trajectory inside $\mathcal{I}$ without letting the polygon escape. In particular, let us consider a circular arc $\boldsymbol{pp'}$ inscribed in the region $\mathcal{I}$ (Figure 5.7). This arc joins the points $\boldsymbol{p}$ and $\boldsymbol{p'}$ in $\mathcal{I}$ with center in $\boldsymbol{a}$ and angle θ.

We can move R_1 to $\boldsymbol{p}$ while staying in the triangle $\mathcal{I}$ since $\mathcal{I}$ is convex. Now consider the following two motions:

1. Move R_1 from $\boldsymbol{p}$ to $\boldsymbol{p'}$ along the arc $\boldsymbol{pp'}$, keeping R_2 and R_3 in their nominal positions $\boldsymbol{a}$ and $\boldsymbol{b}$ (Figure 5.8(a)).
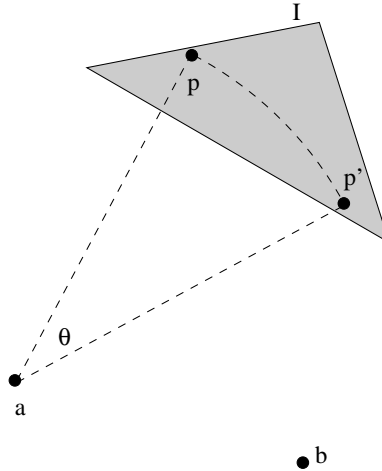
Figure 5.7 A circular arc centered in $\boldsymbol{a}$ and contained in $\mathcal{I}$.

2. Move R_2 from $\boldsymbol{b}$ to a new point $\boldsymbol{b}'$ along a circular arc centered in $\boldsymbol{a}$ and spanning an angle θ, keeping R_1 and R_2 at $\boldsymbol{p}$ and $\boldsymbol{a}$ (Figure 5.8(b)).
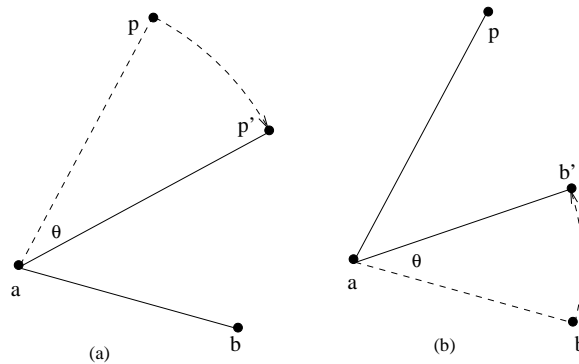
Figure 5.8 Two equivalent rotations.

It is easy to see that the triangles formed by the three robots during both motions only differ by a rotation. By definition of region $\mathcal{I}$, the object cannot escape during motion 1. This property is of course not changed by rotating the triangle formed by the robots, and we can conclude that the object is also imprisoned by their grasp during motion 2.

We can use motion 2 to construct a simple rotation plan. Using the same setup, consider the steps illustrated in Figure 5.4.1.

1. Apply to R_1 a translation from $\boldsymbol{c}$ to $\boldsymbol{p}$ (Figure 5.4.1(b)).
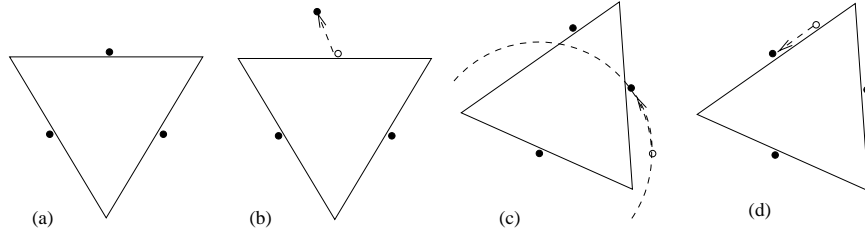
Figure 5.9 Rotation steps.

2. Move R_3 along the circular arc $\boldsymbol{bb}'$ (Figure 5.4.1(c)).

3. Apply to R_1 a second translation back to the immobilizing position (Figure 5.4.1(d)).

We can see that the object is rotated with angle θ counterclockwise from the starting immobilizing configuration. Further, at no point during the entire motion is the object able to escape the robots' grasp. Clockwise rotations are achieved by swapping the roles of the robots R_2 and R_3.

5.4.2   Translating a Polygon

Pure translations are easily decomposed into elementary rotations: let θ' and θ'' be the maximum counterclockwise and clockwise rotation angles associated with the maximum ICS region, and let θ_0 denote the minimum of these two angles. Applying a counterclockwise rotation of angle $\theta \leq \theta_0$ about the second robot followed by a clockwise rotation of angle θ about the third robot will result in a pure translation $\boldsymbol{v}'$ (Figure 5.4.2(left)). Reversing the two rotation steps will result in a pure translation $\boldsymbol{v}''$ (Figure 5.4.2(right)).
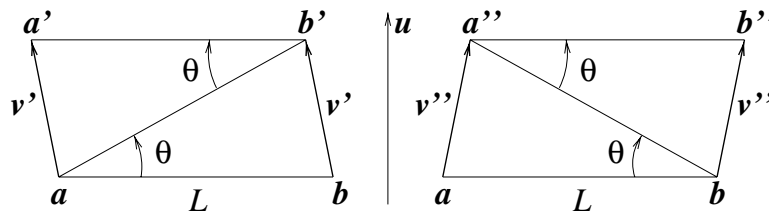
Figure 5.10 A pure translation can be decomposed into two opposite rotation steps.

If L denotes the distance between the original positions $\boldsymbol{a}$ and $\boldsymbol{b}$ of the two robots, and $\boldsymbol{u}$ denotes the counterclockwise normal vector to the line joining $\boldsymbol{a}$ to $\boldsymbol{b}$, it is easy to

show that the translation vectors $\boldsymbol{v}'$ and $\boldsymbol{v}''$ have the same norm $2L\sin\frac{\theta}{2}$, and that the angle between $\boldsymbol{u}$ and these two vectors is $\frac{\theta}{2}$.

In particular any translation of norm smaller than $2L\sin\frac{\theta_0}{2}$ along the vector $\boldsymbol{u}$ can be achieved in four elementary rotation steps.

So far, we have shown how to translate the polygon in a range of directions centered on $\boldsymbol{u}$. We can translate the polygon in arbitrary directions using plans computed for three directions only by switching the roles of the discs and alternating between the three directions. If the chosen directions positively span the plane, it is easy to see that we can arrange a sequence of translations to bring the polygon to any position. One simple choice for these directions is the outward normals at the contacts.

5.5 Implementation and Results

We have implemented the algorithm for planning manipulation sequences described in the previous section. Figure 5.11(top) shows the elementary steps involved in a counterclockwise rotation of an equilateral triangle manipulated by three robots, and Figure 5.11(bottom) shows similar steps for a clockwise rotation.
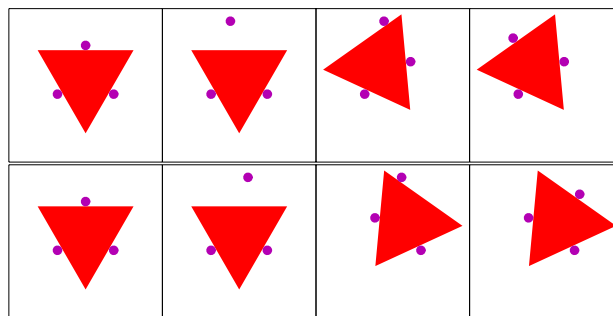

Figure 5.11 Counterclockwise (top) and clockwise (bottom) rotation steps.

More complicated motions can be decomposed into elementary rotation and translation steps. In particular, Figure 5.12 shows intermediate immobilizing configurations in two manipulation sequences that bring the triangle from some initial configuration to a

final one. The triangle is first rotated to the desired orientation, and then translated to the desired position.

(a)   (b)
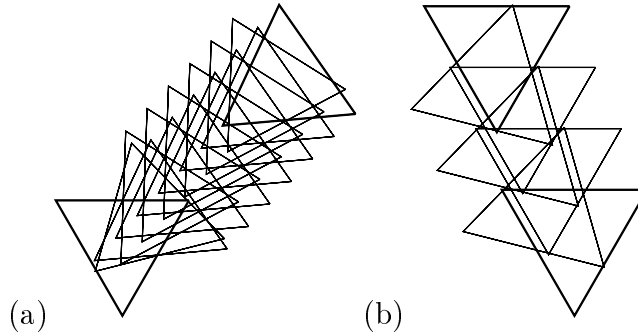
Figure 5.12 Manipulation sequences.

Figure 5.13 shows another example where a simple potential-field method [42] has been used to plan a motion avoiding polygonal obstacles. At each step, virtual attractive and repulsive forces acting on the object are computed to determine the next free-space configuration of the object. To move the object from the current configuration to the next one, a local plan composed of elementary translation and rotation steps is computed. If the local plan is collision free, it is used, otherwise a new candidate configuration is generated and the corresponding local plan is computed. The process is iterated until a collision-free global plan is found.

We have also tested the execution of manipulation plans generated by the algorithm in a real environment. We conduct the experiment with a group of three Scout Nomadic robots. Scout Nomatic robot is a circular-shaped mobile robot with two active wheels. The velocity of each wheel can be independently controled, so the robot can be commanded to trace any circular arc trajectory or to rotate in-place which is important for the execution of the plans. The diameter of the robot is about 62 centimeters. The test object is an equiliteral triangle attached with three passive wheels to reduce the effect of friction with the floor. Each side of the triangle is 125 centemeters long. Figure 5.14 shows a grasping and rotating experiment. The robots move from their home positions (Figure 5.14(a)) to the positions corresponding to the maximum ICS region (Figure 5.14(d). The object is placed in the capture in an arbitrary position (Figure 5.14(e)) and

Figure 5.13 Obstacle avoidance.

a grasp is executed (Figure 5.14(f)). The object is placed in another random position in the capture and the grasp is tested again (Figure 5.14(h)). In both trials, the object successfully reaches the desired position with very small positioning error. In Figure 5.14(i)-(l), the rotation step is executed. Again, the object successfully reaches the target. In Figure 5.15(a)-(p), we show snapshots of the translation which is composed of four rotation steps.

We have also experimented with a longer plan that is generated for obstacle avoidance. Figure 5.16 shows snapshot of the intemediate immobilizing configuration during the execution of the plan. This plan has 85 steps and requires the object to move about 5 meters. The object reaches the target with position error about 3 centimeters. The error is mainly caused by a small jamming towards the end of the execution. Note that it is important to keep fricion at all contact surfaces to be sufficiently low because the execution is performed without any sensor feedback and it is impossible to recover from losing the information about the configuration of the robots. The video clips of all the experiments may be found at `http://www-cvr.ai.uiuc.edu/ponce_grp/research/ics.html`.

(a) (b) (c)

(d) (e) (f)

(g) (h) (i)

(j) (k) (l)

**Figure 5.14** Grasping and rotating experiments.
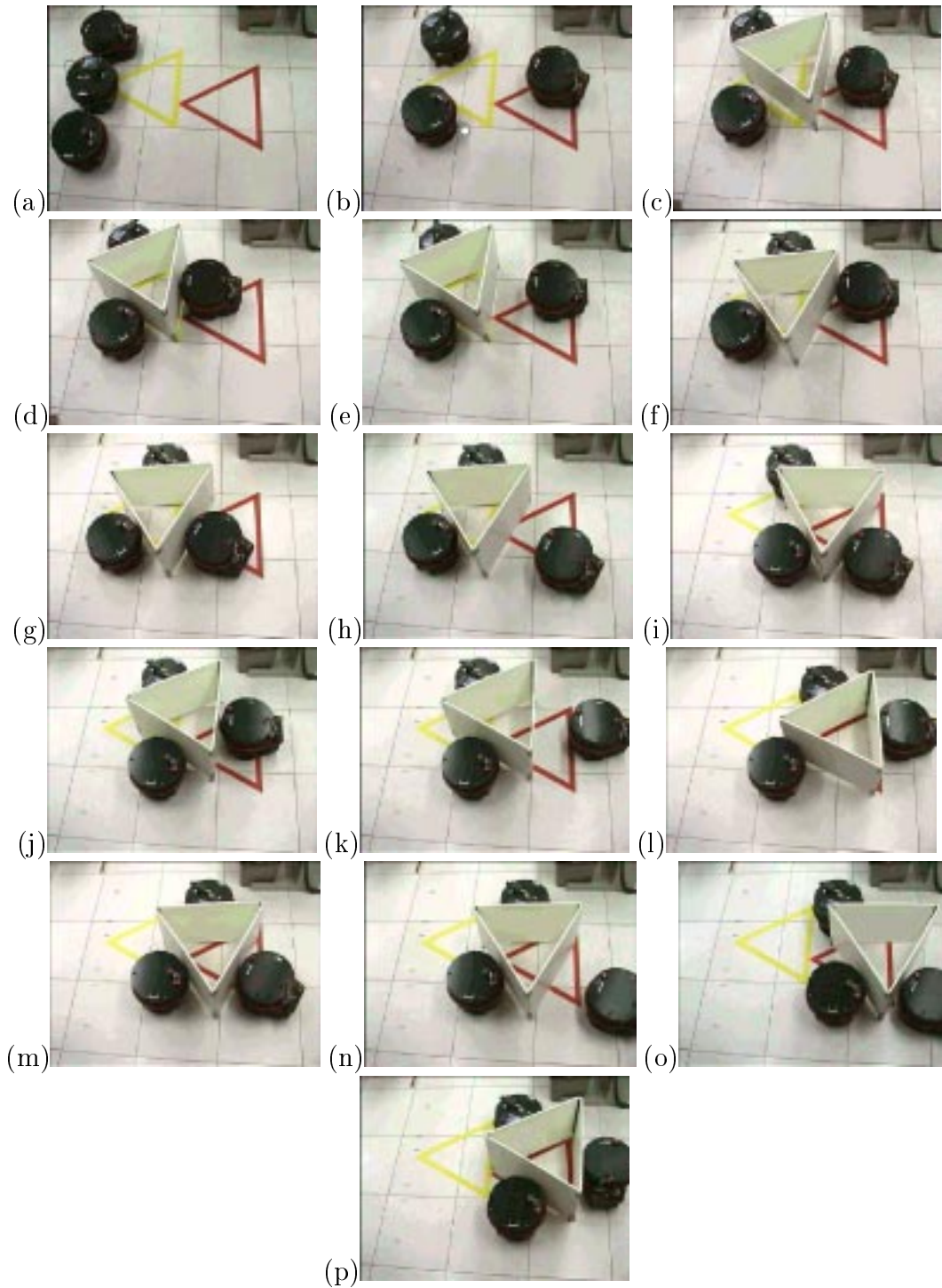
Figure 5.15 Translation experiment.
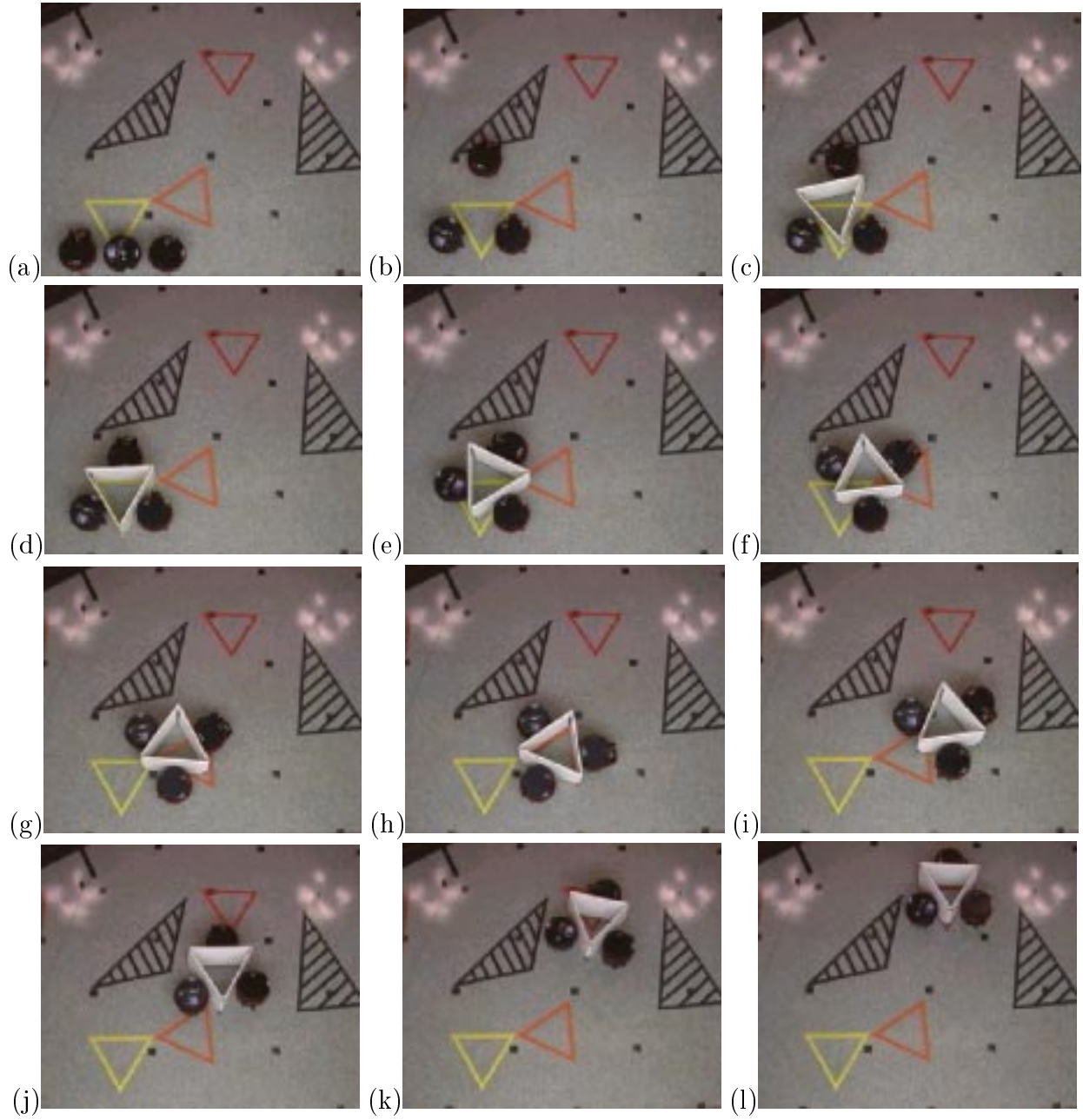
Figure 5.16 An experiment with a longer plan.

5.6   Discussion and Conclusions

We studied the problem of manipulating a planar polygonal object with three disc-shaped robots capable of straight line and circular arc motion in the plane. We have presented an algorithm for grasping the object and bringing it to a desired position and orientations through sequences of atomic robot motions. The presented method is based on the ICS concept (Chapter 4) which is the characterization of the range of possible object motions when two of the robots are fixed and one is allowed to move in the plane with two degrees of freedom. This technique does not assume that contact is maintained during the execution of the grasping/manipulation task, nor does it rely on detailed models of friction or contact dynamics, but it allows the construction of manipulation plans guaranteed to succeed under the weaker assumption that jamming does not occur during the task execution. Besides the manipulation task of our custom-designed reconfigurable gripper, we have shown that the ICS region concept can be applied to a more general manipulation problem.

Exact computation of ICS regions may be complicated for problems with many degrees of freedom. In Section 5.2, a 1-DOF ICS region is exactly derived following the method presented for the reconfigurable gripper in Chapter 4. Although the maximal 1-DOF ICS region can be computed exactly, the range of motion of the robots is severely limited which results in planning complexity [93]. This shortcoming is the motivation to considering problems with higher degree of freedom. We presented in Section 5.3 an extension from 1-DOF to 2-DOF case that provides a sufficient (but not necessary) condition for the 2-DOF ICS region. Although the 2-DOF ICS region is not computed exactly as in the 1-DOF case, an additional degree of freedom significantly improves the range of possible motions of the robots which, in turn, allows simpler planning.

For the planning method with the 2-DOF ICS region presented in this chapter, we allow only one robot to move at a time. It is desirable to have an ICS region with higher degrees of freedom so the circular arc trajectory constraint can be dropped and the three robot can move simultaneously. It is interesting to try to extend the sufficient condition

of the 2-DOF ICS region presented here to handle more degrees of freedom. Such attempt may be very difficult because the condition for the 2-DOF ICS region is closely based on the computation of the 1-DOF ICS region. Instead, we will attack this problem by directly reformulating sufficient conditions for ICS regions with higher degrees of freedom. This approach will be presented in detail in the next chapter.

CHAPTER 6

MOTION PLANNING

6.1   Introduction

This chapter focuses on the problem of using three disc-shaped robots to manipulate a polygonal object in the plane in the presence of obstacles. The proposed approach is based on the concept of 6-DOF ICS region. We characterize the maximal discs (dubbed *maximum independent capture discs*, or *MICaDs* for short) where the robots can move independently while guaranteeing that the object cannot escape their grasp.

We show that, in the absence of obstacles, there is a neighborhood U of any object configuration such that any other configuration in U can be reached using robot motions confined to the associated MICaDs (a property akin to local controllability). This is the basis for an approach to manipulation planning where a nominal path is followed by the three robots by dividing it into maximal segments whose endpoints have overlapping MICaDs.

This approach is extended to manipulation planning in the presence of obstacles by devising an efficient test for collisions between the obstacles and the envelope of all object configurations compatible with a given triple of MICaDs.

The proposed algorithm is guaranteed to generate a plan if there exists a path for the object grown by the diameter of the robots plus some positive number ε. In addition, it does not assume that contact is maintained during the execution of the manipulation task, nor does it rely on detailed (and a priori unverifiable) models of friction or contact

106

dynamics, but it allows the construction of manipulation plans guaranteed to succeed under the weaker assumption that jamming does not occur during the task execution.

6.2   Maximum Independent Capture Discs

We will assume from now on that point robots manipulate a polygonal object (this amounts to shrinking each disc-shaped robot to its center and growing the polygon by the robot radius). We will denote by $\boldsymbol{q}_i = (q_i, r_i)$ $(i = 1, 2, 3)$ the positions of the robots B_1, B_2 and B_3. Also, $\boldsymbol{p} = (x, y, \theta)$ will denote a configuration of the movable polygonal object B, E_1, E_2 and E_3 will denote the three edges under consideration, and $E_i(\theta)$ $(i = 1, 2, 3)$ will denote the set of configurations (x, y) for which the robot B_i touches the edge E_i when the polygon B is at orientation θ.

As mentioned in Section 5.2.4, the robots capture the polygon when the segments $E_i(\theta)$ $(i = 1, 2, 3)$ enclose a triangle for all possible orientations of the polygon (we say that the enclosure condition is satisfied, Fig. 6.1(a)).

(a)   (b)   (c)
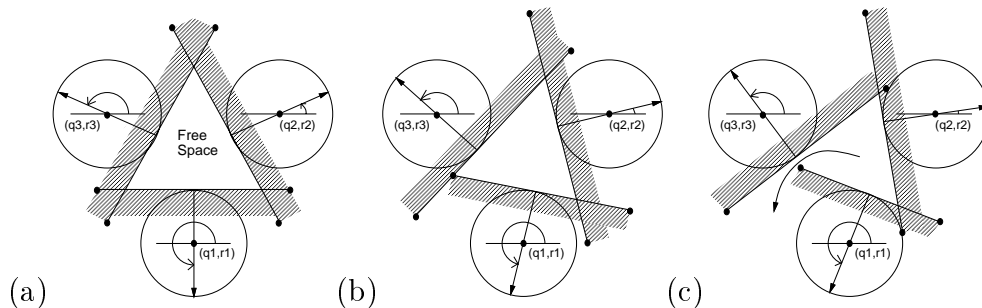
Figure 6.1 Enclosure condition in configuration space: (a) three segments enclosing a triangle; (b) a critical configuration; (c) an opened triangle and an escape path.

Starting from a configuration where the enclosure condition is satisfied, the robots will form an inescapable cage as long as this condition remains satisfied. When it is violated, there must exist some value of the orientation θ at which the segments $E_i(\theta)$ no longer enclose a triangle (Fig. 6.1(c)), allowing the polygon to escape through the opening. Because of the continuity of the motion of the segments $E_i(\theta)$, there must exist a critical orientation $\theta = \theta_c$ for which an endpoint of segment $E_i(\theta_c)$ lies on segment $E_j(\theta_c)$ right

before the condition is violated (Fig. 6.1(b)). If (x_c, y_c) is the position of this endpoint along $E_j(\theta_c)$, we say that (x_c, y_c, θ_c) is a critical configuration of the polygon. We also say that a configuration of the robots is critical when there exists such a critical object configuration. We have just shown that:

Lemma 2 *All paths joining a configuration of the robots that satisfies the enclosure condition to a configuration that violates this condition must contain a critical configuration.*

Let $\boldsymbol{q} = (\boldsymbol{q}_1, \boldsymbol{q}_2, \boldsymbol{q}_3)$ be a configuration of the robots for which the enclosure condition is satisfied. Consider the largest region in the configuration space of the robots that is connected to the configuration $\boldsymbol{q}$ and is free of critical configurations. From Lemma 2, it is easy to see that all configurations in this region must satisfy the enclosure condition since there exists a path free of critical configurations joining $\boldsymbol{q}$ to any configuration in the region. We will not attempt to characterize exactly the maximal region in the joint six-dimensional configuration space of the robots. Instead, we will give simple sufficient conditions for computing disc-shaped regions guaranteed to be free of critical configurations and thus satisfying the enclosure condition.

Definition 3 *We will say that three discs Ω_1, Ω_2 and Ω_3 are* independent capture discs *(or* ICaDs *for short) when, for any configuration $\boldsymbol{q}$ in $\Omega_1 \times \Omega_2 \times \Omega_3$, the robots capture the object.*

The rest of this section presents a method for constructing a triple of maximum-radius independent capture discs. The idea is to start from an immobilizing configuration $\boldsymbol{q}$ of the robots, move these robots away from their initial position until we find a critical configuration, and then characterize the maximum discs enclosed in the space between the two configuration. When the robots and the polygon are at a critical configuration, there exist $i \neq j \in \{1, 2, 3\}$ for which an endpoint of the segment $E_i(\theta)$ lies on the segment $E_j(\theta)$. It is easy to show that this event occurs when the robot B_j touches the edge E_j and the robot B_i is located at the endpoint A_i of the edge E_i that is farthest

from E_j. In such a configuration, the object will either touch two of the robots (Fig. 6.2(a)) or all three of them (Fig. 6.2(b)).
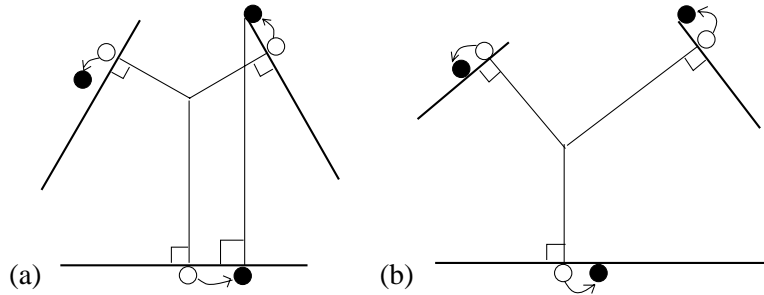

Figure 6.2 The two possible types of critical configurations: (a) double contact; (b) triple contact. In each case, we move from an immobilizing configuration (white discs) to a critical one (black discs).

Let us first focus on the double-contact case. If $d_{i,j}$ denotes the distance between A_i and the edge E_j, it is obvious that there will be no critical configuration when the distance between B_i and B_j is shorter than $d_{i,j}$ (Figure 6.3). More precisely, we have the following result.
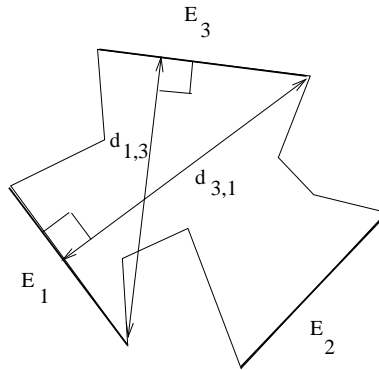

Figure 6.3 Definition of $d_{1,3}$ and $d_{3,1}$.

Lemma 3 *A sufficient condition for the enclosure condition to be satisfied at the configuration $\boldsymbol{q}$ is that:*

$$|\boldsymbol{q}_i - \boldsymbol{q}_j| \leq R_{i,j}, \text{ for } 1 \leq i < j \leq 3, \tag{6.1}$$

where $R_{i,j} = R_{j,i} = \min(d_{i,j}, d_{j,i})$.

This lemma gives us a method for constructing a set of ICaDs (Fig. 6.4): let $\boldsymbol{p}$ denote some object configuration, and consider the discs Ω_i $(i = 1, 2, 3)$ with center $\boldsymbol{u}_i = (u_i, v_i)$ and radius $r_i > 0$ that touch the edge E_i of the object. Let us also define $C_{i,j}$ as the disc centered in $\boldsymbol{u}_i$ with radius $R_{i,j} - r_i$ for $i \neq j \in \{1, 2, 3\}$. The following lemma is an immediate corollary of Lemma 3.
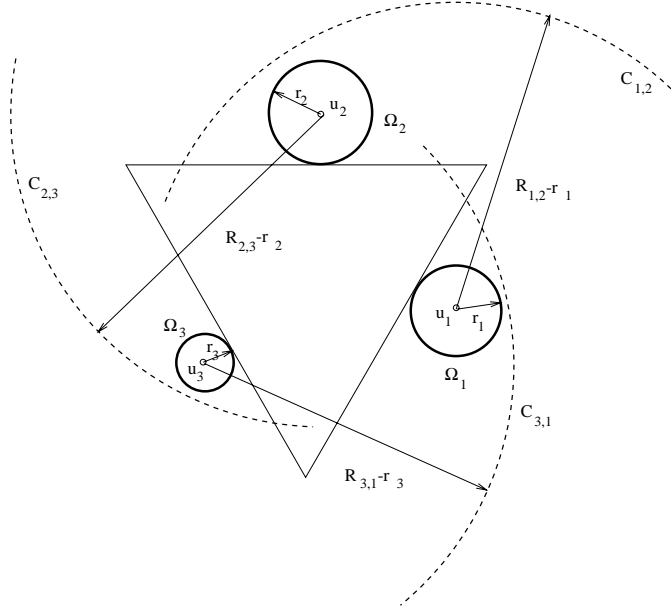

Figure 6.4 Construction of independent capture discs.

Lemma 4 *When the radii r_i $(i = 1, 2, 3)$ are chosen so that $\Omega_1 \subset C_{3,1}$, $\Omega_2 \subset C_{1,2}$ and $\Omega_3 \subset C_{2,3}$, the discs Ω_1, Ω_2 and Ω_3 form independent capture discs.*

Of course, a set of positive radii satisfying the hypotheses of Lemma 4 may not exist. We will come back to this point in a minute. In the mean time, let us assume that there exists a triple r_1, r_2, r_3 satisfying these hypotheses, and let us address the problem of maximizing the smallest one of the radii.

Lemma 5 *The independent capture discs maximizing the smallest of their three radii satisfy the following conditions: (a) Ω_1 is tangent to $C_{3,1}$, Ω_2 is tangent to $C_{1,2}$ and Ω_3 is tangent to $C_{2,3}$; (b) the robot configuration where the discs $\Omega_i, i = 1, 2, 3$ touch the edge E_i must immobilize the object; and (c) the three discs must have the same radius.*
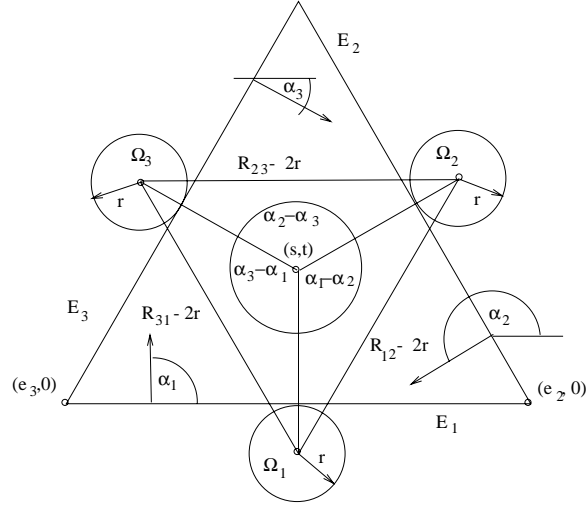
Figure 6.5 Computing r.

Essentially, it can be shown geometrically that there will be room for the smallest one of the discs to grow until the three conditions of the lemma are satisfied, see Appendix A.1 for a detailed proof. In the following, we show how to compute the maximum independent capture discs based on the conditions given in Lemma 5.

Let us denote by r the common radius of the discs and by (s, t) the intersection of the three normals to the object edges at the points where the discs touch them (Figure 6.5). Without loss of generality, we assume that the edge E_1 is on the x-axis. Let $(e_3, 0)^T$ be the intersection point of the line supporting E_3 and the x-axis, and let $(e_2, 0)^T$ be the intersection point of the line supporting E_2 and the x-axis. As before, we denote by α_i, $i = 1, 2, 3$ the offset angles of the edges E_i. Writing that the distance between the centers of Ω_1 and Ω_2 is $R_{1,2} - 2r$ yields:

$$(t + r)^2 + ((s - e_2) \cos \alpha_2 + t \sin \alpha_2 + r)^2 -$$
$$2(t + r)((s - e_2) \cos \alpha_2 + t \sin \alpha_2 + r) \cos(\alpha_2 - \alpha_1) = (R_{1,2} - 2r)^2.$$

Likewise, writing that the distance between the centers of Ω_2 and Ω_3 is $R_{2,3} - 2r$ yields:

$$((s - e_2) \cos \alpha_2 + t \sin \alpha_2 + r)^2 + ((s - e_3) \cos \alpha_3 + t \sin \alpha_3 + r)^2 -$$
$$2((s - e_2) \cos \alpha_2 + t \sin \alpha_2 + r)((s - e_3) \cos \alpha_3 + t \sin \alpha_3 + r) \cos(\alpha_3 - \alpha_2) = (R_{2,3} - 2r)^2,$$

111

and writing that the distance between the centers of Ω_3 and Ω_1 is $R_{3,1} - 2r$ yields:

$$((s - e_3)\cos\alpha_3 + t\sin\alpha_3 + r)^2 + (t + r)^2 -$$
$$2((s - e_3)\cos\alpha_3 + t\sin\alpha_3 + r)(t + r)\cos(\alpha_1 - \alpha_3) = (R_{3,1} - 2r)^2.$$

We have three quadratic equations in three unknowns s, t and r. The maximum capture discs can be found by solving this system of three equations in three unknowns using homotopy continuation [61] and picking the solution that yields the maximum value of r. The centers of the corresponding discs are easily determined by the condition that they must be tangent to the selected object edges.

Now, the system of equations defining the MICaDs may have no real solutions, or no solutions corresponding to physically realizable robot configurations (e.g., the maximum value of r may be negative, or the positions of the MICaD centers may lie outside the actual extent of the corresponding edges). In this case, however, the critical configurations associated with the contact edges must be three-contact configurations (Fig. 6.2(b)), and another set of MICaDs can be found by picking some immobilizing configuration of the three robots, say $\boldsymbol{q}_0 = (\boldsymbol{q}_{10}, \boldsymbol{q}_{20}, \boldsymbol{q}_{30})$, and calculating how far the robots can move away from each other before a critical configuration occurs. More precisely, if $d_{i,j} = |\boldsymbol{q}_{i0} - \boldsymbol{q}_{j0}|$ ($1 \leq i < j \leq 3$), we seek $\delta > 0$ such that

$$|\boldsymbol{q}_i - \boldsymbol{q}_j| = d_{i,j} + \delta, \quad \text{for} \quad 1 \leq i < j \leq 3, \tag{6.2}$$

and, say, $\boldsymbol{q}_1$ coincides with the vertex A_1 of E_1 farthest from the edge E_2 while $\boldsymbol{q}_2$ and $\boldsymbol{q}_3$ lie on the edges E_2 and E_3. This critical configuration is defined by the three equations (6.2) in three unknowns δ, t_2 and t_3, where t_2 and t_3 define the positions of $\boldsymbol{q}_2$ and $\boldsymbol{q}_3$ along the corresponding edges. The solutions can once again easily be found using homotopy continuation, and the solution yielding the minimum positive value of δ is picked. The process is repeated for each pair A_i, E_j and the solution corresponding to the minimum overall δ value is retained.

In this case, the existence of physically-realizable solutions is guaranteed by the fact that $\boldsymbol{q}_0$ is an immobilizing configuration and there must exist some $\delta > 0$ such that a

critical configuration (necessarily associated with three contacts since there is no two-contact solution) occurs when the distance between the three robots is increased by δ. The discs of radius $\delta/4$ touching the edges of the object in $\boldsymbol{q}_{10}, \boldsymbol{q}_{20}, \boldsymbol{q}_{30}$ at its immobilizing configuration are then easily shown to be independent capture discs.

6.3 Motion Planning without Obstacles

Note that the maximum independent capture discs associated with three edges of a polygon are rigidly attached to this polygon. We can therefore consider these discs as a single (if disconnected) rigid object Ω. We attach to this object its own coordinate frame and denote by $\Omega_i(\boldsymbol{p})$ $(i = 1, 2, 3)$ the region of the workspace occupied by the disc Ω_i at configuration $\boldsymbol{p} \in \mathbb{R}^2 \times S^1$. For convenience, we choose the reference frame of Ω such that it coincides with the frame attached to the object and denote by $\boldsymbol{g}_i(\boldsymbol{p})$ $(i = 1, 2, 3)$ the points on the disc boundaries that immobilize the object when it is also at the configuration $\boldsymbol{p}$. Clearly, the three robots form an inescapable cage if there exists a configuration $\boldsymbol{p}$ of the discs Ω such that $\boldsymbol{q}_i \in \Omega_i(\boldsymbol{p})$ for $i = 1, 2, 3$. Also, when $\boldsymbol{q}_i = \boldsymbol{g}_i(\boldsymbol{p})$ for $i = 1, 2, 3$ the robots will immobilize the object at its configuration $\boldsymbol{p}$.

Lemma 6 *Given some object configuration $\boldsymbol{p}$ and assuming that the radius r of the capture discs is positive, there always exists a neighborhood U of $\boldsymbol{p}$ for which $\Omega_i(\boldsymbol{p}) \cap \Omega_i(\boldsymbol{p}') \neq \emptyset$ for $i = 1, 2, 3$ and any configuration $\boldsymbol{p}'$ in U.*

This result follows directly from the fact that the mapping $\boldsymbol{u}_i : \mathbb{R}^2 \times \mathcal{S}^1 \to \mathbb{R}^2$ that associates with a configuration $\boldsymbol{p}$ of the object the center of the corresponding disc $\Omega_i(\boldsymbol{p})$ is continuous. Thus the preimage of the open ball centered in $\boldsymbol{u}_i(\boldsymbol{p})$ with radius $2r$ is also an open set $U_i(\boldsymbol{p})$, not empty since it contains $\boldsymbol{p}$. The set $U = \cap_{i=1}^{3} U_i(\boldsymbol{p})$ is also open and nonempty, and it defines a neighborhood of $\boldsymbol{p}$ where $\Omega_i(\boldsymbol{p}) \cap \Omega_i(\boldsymbol{p}') \neq \emptyset$ for $i = 1, 2, 3$ and any $\boldsymbol{p}' \in U$.

Lemma 7 *Given an object configuration $\boldsymbol{p}$ and any other configuration $\boldsymbol{p}'$ in the neighborhood U defined in Lemma 6, and some configuration $\boldsymbol{q}$ in $\Omega_1(\boldsymbol{p}) \times \Omega_2(\boldsymbol{p}) \times \Omega_3(\boldsymbol{p})$,*

113

there exists a trajectory of the three robots starting in $\boldsymbol{q}$ that will bring the object to the configuration $\boldsymbol{p}'$.

The proof of this corollary is constructive: if $\boldsymbol{q} = (\boldsymbol{q}_1, \boldsymbol{q}_2, \boldsymbol{q}_3)$, move each robot from $\boldsymbol{q}_i$ to some point in $\Omega_i(\boldsymbol{p}) \cap \Omega_i(\boldsymbol{p}')$ for $i = 1, 2, 3$, then move the robots again to the immobilizing configuration $\boldsymbol{q}' = (\boldsymbol{q}_1', \boldsymbol{q}_2', \boldsymbol{q}_3')$ associated with $\Omega_1(\boldsymbol{p}') \times \Omega_2(\boldsymbol{p}') \times \Omega_1(\boldsymbol{p}')$. Of course, one should make sure that the robots never leave the corresponding discs, but this is easy since the discs are convex so the motions can be limited to translations. Note that Lemma 7 states a property akin to *local controllability* in manipulation planning [49]. Since, in the absence of obstacles, the configuration space space of the object is connected and the configuration $\boldsymbol{p}$ can be arbitrarily chosen, we can iteratively apply this procedure to bring the object from any initial configuration to any final one.

Let us now address the problem of commanding the robots so that the manipulated object follows some pre-specified path $\mathcal{P}$ parameterized by $\boldsymbol{p} : [0, 1] \to \mathbb{R}^2 \times S^1$. To reduce the possibility of jamming due to friction, we will not attempt to immobilize the object except at its goal configuration. The three robots can be thought of as a moving cage along the path. To simplify the notation, we will use $\Omega_i(t)$ for $\Omega_i(\boldsymbol{p}(t))$ and $E_i(t)$ for the location of the edge E_i associated with the object configuration $\boldsymbol{p}(t)$. Suppose that the robots B_i are at $\boldsymbol{q}_i \in \Omega_i(t)$ for $i = 1, 2, 3$ and thus capture the object. To progress by δ along the path, we command each robot to move from $\boldsymbol{q}_i$ to the point $\boldsymbol{q}_i^*(t, \delta)$ in $\Omega_i(t) \cap \Omega_i(t + \delta)$ that is closest to the line $E_i(t + \delta)$. From Lemma 6, there always exists some $\delta > 0$ for which $\Omega_i(t) \cap \Omega_i(t + \delta)$ is not empty (we will see in a minute how to compute the maximum possible value for δ). Note that the three robots can move simultaneously without any need for synchronization.

It should be noted that other destinations in the intersection of the capture discs could be chosen as well, but we prefer the proposed choice because it tends to allow smaller space for the object to move in while being captured. Besides, it is easy to compute the point in the intersection of the two discs that is closest to a given line outside the intersection (since $E_i(t+\delta)$ touches $\Omega_i(t+\delta)$, it is outside the intersection as well). Figure 6.6 shows the only two possibilities: the closest point can either be at the intersection

of the two circular boundaries of the discs (Fig. 6.6(a)) or at the point on a circular boundary whose tangent is parallel to the line (Fig. 6.6(b)).
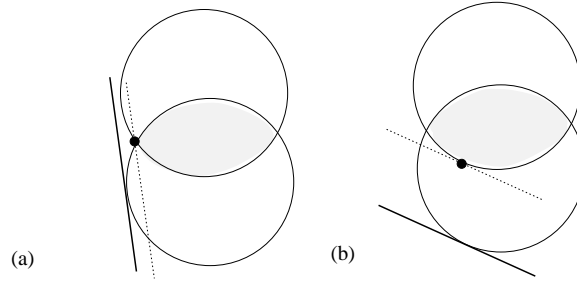

Figure 6.6 The point in the intersection of two circles that is closest to a given line.

To move the object along the chosen path, we first command the robots B_i to move to $\Omega_i(0)$ for $i = 1, 2, 3$, so that they can capture the object at the initial configuration $\boldsymbol{p}(0)$. The step described above is then repeated until the robots B_i are in $\Omega_i(1)$ and the object can be immobilized and brought to the goal configuration $\boldsymbol{p}(1)$. To find an efficient plan, we must determine the maximum value of δ for each step in the sequence. More precisely, for a given value t, we want to find the largest δ_{max} for which $\Omega_i(t) \cap \Omega_i(t+\delta) \neq \emptyset$ for $i = 1, 2, 3$ when $0 < \delta \leq \delta_{max}$. Because of the continuity of the path $\mathcal{P}$, if $\Omega_i(t) \cap \Omega_i(t+\delta') = \emptyset$ for some $\delta' > 0$, there must exist $\delta_i^* \in [0, \delta']$ for which the boundaries of the discs $\Omega_i(t)$ and $\Omega_i(t + \delta_i^*)$ touch each other before the two discs no longer intersect. Clearly, the maximum distance we can travel along the path cannot be greater than δ_i^*. Fortunately, it is not difficult to characterize the set of object configurations of the object such that one of the independent capture discs touches a fixed disc with the same radius.

Consider Fig. 6.7, which shows a triangle and the associated MICaDs, one of which touches the disc $\mathcal{C}$ centered in $\boldsymbol{c}$ with radius r. We denote by ϕ the orientation of the line joining the disc centers, and by $\mathcal{A}_i(\phi)$ the MICaD under consideration, with center $\boldsymbol{a}_i(\phi)$ and radius r. Since the capture discs and the object are rigidly attached, the position of the object's reference point can be written as $\boldsymbol{x}(\theta, \phi) = \boldsymbol{a}(\phi) + \boldsymbol{k}(\theta)$, where θ is the object orientation, $\boldsymbol{k}(\theta) = k(\cos\theta, \sin\theta)$, and k is an appropriate constant.

It is easy to show that when we keep θ constant and rotate $\mathcal{A}_i(\phi)$ about $\mathcal{C}$ while maintaining contact between the two discs, $\boldsymbol{x}(\theta, \phi)$ traces a circle $\mathcal{E}(\theta)$ with center $\boldsymbol{e}(\theta) =$
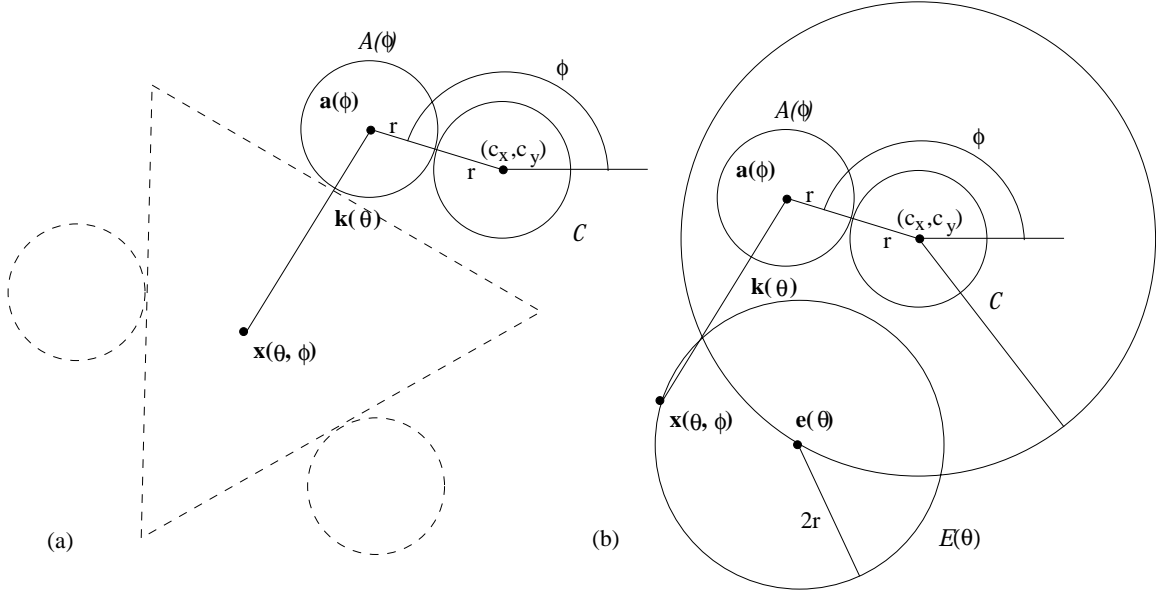
Figure 6.7 Object configurations such that one of the MICaDs touches a fixed circle: (a) general setup; (b) close-up of relevant features.

$\boldsymbol{c} + \boldsymbol{k}(\theta)$ and radius $2r$. Points on this circle correspond to object configurations where the MICaD $\mathcal{A}_i(\phi)$ touches $\mathcal{C}$ at some orientation ϕ while the object is at orientation θ. If we allow the orientation of the object to change, the center of the circle $\mathcal{E}(\theta)$ will trace another circle whose center is at $\boldsymbol{c}$ and radius is k. Therefore, the set of the configurations of the object for which the capture disc is tangent to the disc $\mathcal{C}$ forms a helicoidal surface $\mathcal{I}_i$ in the object configuration space (Figure 6.8). To compute δ_i^*, we take $\mathcal{C} = \Omega_i(t)$ and compute the intersections between $\mathcal{P}$ and the surface $\mathcal{I}_i$ using a one-dimensional numerical search method. The arc joining $\boldsymbol{p}(t)$ to the first intersection $\boldsymbol{p}(t^*)$ determines $\delta_i^* = t^* - t$. To compute δ_{max}, we repeat this process for $i = 1, 2, 3$, and return the smallest of the three δ_i^* values.

6.4   Motion Planning with Obstacles

We can adapt as follows our approach to the case where obstacles are present: first, find a path $\mathcal{P}$ for the object grown by the diameter of the robots, using some exact obstacle-avoidance algorithm for polygons (e.g., [4]); second, use the strategy outlined in
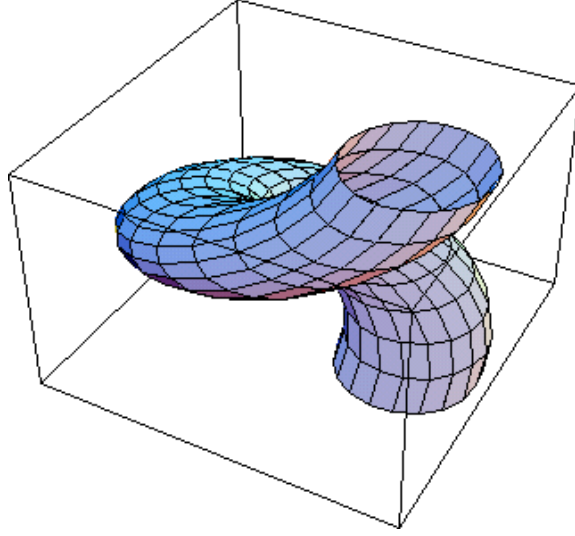
Figure 6.8 A helicoid.

the previous section to follow that path in steps that are as large as possible yet small enough to avoid collisions. More precisely, if δ^* denotes the distance to be traveled along $\mathcal{P}$ at each step and $\boldsymbol{q}_i$ denotes the current configuration of the robot B_i $(i = 1, 2, 3)$, we have the following algorithm whose output is a polygonal path P for the robots:

```
1   for i ← 1 to 3 do qᵢ = qᵢ(0);
2   P ← {(q₁, q₂, q₃)}; t ← 0;
3   repeat
4       δ_max ← MAX_DELTA(t);
5       use bisection to seek maximum δ* ∈ [0, δ_max]
6       for which CLEAR(q₁, q₂, q₃, t, δ*) returns TRUE;
7       for i ← 1 to 3 do qᵢ ← qᵢ*(t, δ*);
8       P ← P ∪ {(q₁, q₂, q₃)}; t ← t + δ*;
9   until t = 1;
10  P ← P ∪ {(g₁(1), g₂(1), g₃(1))};
11  return P.
```

Here, the function MAX_DELTA(t) implements the calculation of the maximum step size in the absence of obstacles, as described in the previous section. The function

$\texttt{CLEAR}(\boldsymbol{q}_1, \boldsymbol{q}_2, \boldsymbol{q}_3, t, \delta^*)$ returns $\texttt{TRUE}$ if it is not possible for the object to collide with the obstacles when the robots B_i move from $\boldsymbol{q}_i$ to $\boldsymbol{q}_i^*(t, \delta^*)$ for $i = 1, 2, 3$ and $\texttt{FALSE}$ otherwise. The rest of this section shows how to efficiently implement this boolean function. At each step in the plan, the three robots move simultaneously and independently from each other along line segments. Thus, implementing $\texttt{CLEAR}$ requires the ability to test whether the object may collide with the obstacles for any position of each robot along the corresponding line segment. The following lemma simplifies the calculations.

Lemma 8 *If ICS($\boldsymbol{q}_1, \boldsymbol{q}_2, \boldsymbol{q}_3$) denotes the set of free configurations of the object associated with the robot configurations $\boldsymbol{q}_i$ $(i = 1, 2, 3)$, then*

$$\bigcup_{\substack{\boldsymbol{q}_i \in \overline{\boldsymbol{q}_i' \boldsymbol{q}_i''} \\ i = 1, 2, 3}} ICS(\boldsymbol{q}_1, \boldsymbol{q}_2, \boldsymbol{q}_3) = \bigcup_{\substack{\boldsymbol{q}_i \in \{\boldsymbol{q}_i', \boldsymbol{q}_i''\} \\ i = 1, 2, 3}} ICS(\boldsymbol{q}_1, \boldsymbol{q}_2, \boldsymbol{q}_3)$$

for any two configurations $\boldsymbol{q}' = (\boldsymbol{q}_1', \boldsymbol{q}_2', \boldsymbol{q}_3')$ and $\boldsymbol{q}'' = (\boldsymbol{q}_1'', \boldsymbol{q}_2'', \boldsymbol{q}_3'')$ in the same triple of MICaDs.

The proof of this lemma is elementary and is given in Appendix A.2. Its implications are clear: despite the fact that each robot can be anywhere on a line segment in the associated MICaD, Lemma 8 shows that testing whether the object can collide with the obstacles reduces to performing the collision test at the eight configurations where each robot is fixed at either end of the associated line segment.

Given one of these configurations, we want to test for possible collisions of the captured object with an obstacle. Directly testing the intersection of the ICS with a configuration space obstacle is complicated and computationally expensive. Instead, we reformulate our problem in the workspace of the robots: if we define the *envelope* of an object as the region of the plane that it sweeps as its configuration varies within the ICS, testing for potential collisions reduces to testing whether the object envelope intersects these obstacles. Since we deal with polygonal obstacles, this only requires knowing how to test the intersection between the envelope and a line segment.

When the object is in the ICS associated with three robots and the corresponding edges, it can only touch the robots along these edges. The boundary of the envelope of

an object corresponds to its configurations for which two of the edges are in contact with the corresponding robots, and it is therefore composed of three parts associated with these double contacts (Fig. 6.9). When a line segment intersects the envelope, it must intersects at least one of these parts.


(a)

(b)

(c)
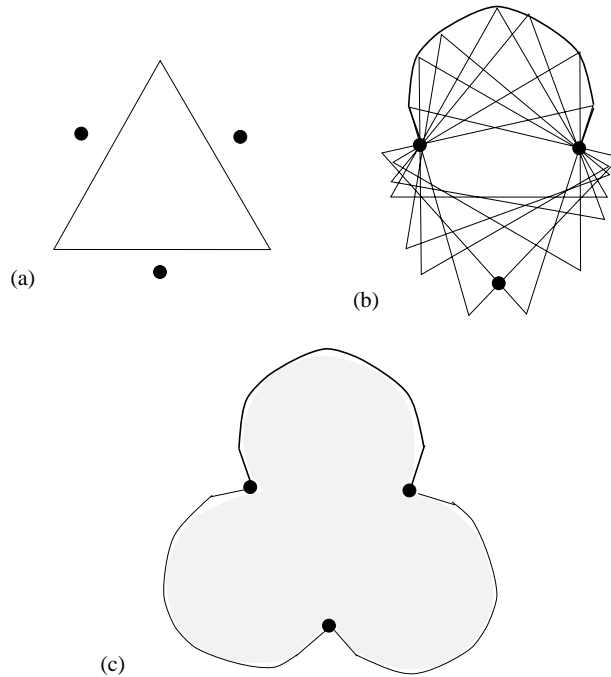
Figure 6.9 The envelope of a triangle: (a) the triangle and the three robots capturing it; (b) snapshots of the object rotating while maintaining contact with the two top robots; (c) the corresponding envelope.

Let us first focus on testing the intersection of a line segment with the part of the envelope boundary associated with the *infinite* line supporting one the object edges. More concretely, let us consider the object configurations for which the robots B_1 and B_2 touch the edges E_1 and E_2. Let L_a be the line supporting some other edge E_a of the polygon (Figure 6.10). We have the following lemma.

Lemma 9 *As the object rotates while maintaining contact with B_1 and B_2, L_a rotates as well and remains tangent to a fixed circle C_a.*

The proof of this lemma is relatively straightforward and is given in Appendix A.3. The object configurations that maintain contact with the robots B_1 and B_2 have a single
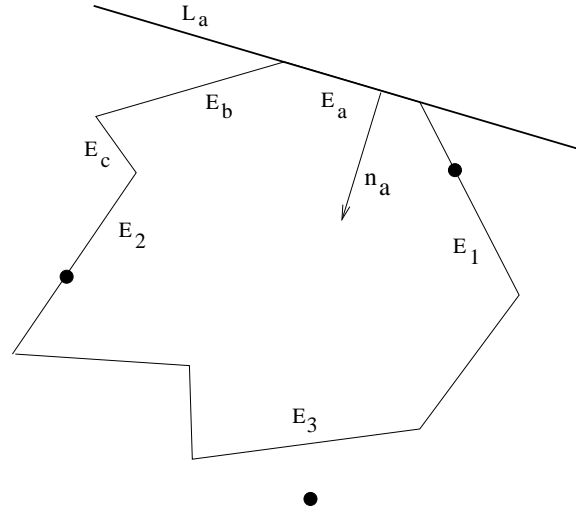
Figure 6.10 Sample object with the line under consideration.

degree of freedom and they can be parameterized by the object orientation θ. But since the object cannot escape, θ must be in some range $[\theta_L, \theta_H]$ where θ_L and θ_H correspond to two configurations for which the object touches the three edges. Figure 6.11(a) shows the region S_a swept by L_a as the object rotates in the range $[\theta_L, \theta_H]$.
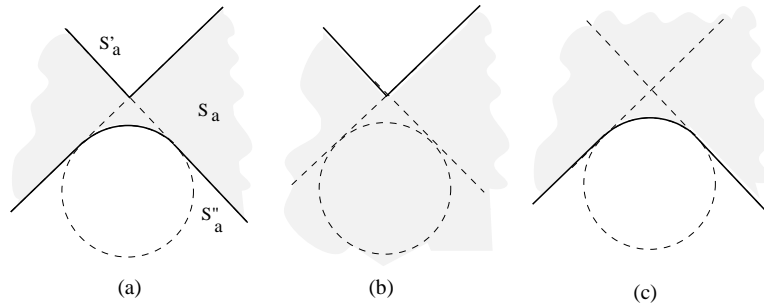

Figure 6.11 Regions swept by (a) the line L_a, (b)-(c) the half spaces bounded by L_a

Let us pretend for a moment that L_a is the only edge of the object. The line L_a cuts the plane into two halves. The envelope of the object is the region swept by the object-sided half containing the internal normal $\boldsymbol{n}_a$ of L_a. In the case shown in Figure 6.10, $\boldsymbol{n}_a$ always points to the half plane that contains the circle C_a. This means that S'_a is the only boundary of the envelope of the object (of course, if $\boldsymbol{n}_a$ pointed in the opposite direction, S''_a would be the boundary instead). In general, there are two types of the boundaries:

- T1: composed of two line segments (for example, S'_a in Figure 6.11(a)), and

- T2: composed of two line segments and a circular arc (for example, S''_a in Figure 6.11(a)).

Note that the two line segments in both types are part of the line L_a of the object at θ_L and line L_a of the object at θ_H (see the dashed lines in Figure 6.11(b)-(c)).

In general, to classify what type of boundary will result, we compute the circle C_a. If the internal normal of the line points to the half plane containing the circle then we have a boundary of type T1, otherwise we have a boundary of type T2. It is easy to see that when a line intersects the envelop, it must either (1) intersect the line L_a of the object at orientation θ_L, (2) intersect the line L_a of the object at orientation θ_H, or (3) intersect the circular arc part of the boundary of the envelope (for type T2 only).

Of course, the edges bounding the object only have a finite extent. To take this into account, we now consider the edge E_a itself instead of its supporting line L_a. The region swept by this edge as the object rotates under the double-contact constraint is a subset of the region S_a swept by the line L_a. It is bounded by the curves traces by the endpoints of the edge E_a as it rotates around the circle C_a. In Appendix B, we will show that computing the intersection of the curve traced by an object vertex and a given line segment reduces to solving a trigonometric equation in the object orientation θ (which can be done in closed form), then testing whether this orientation is in the range $[\theta_L, \theta_H]$, and finally checking whether the corresponding intersection point is within the extent of the line segment.

We are now ready to define the routine for testing whether the envelop intersects with a line segment. The routine is described in the following pseudocode. The input of the routine includes a given line segment, and the positions of the three robots. We denote by $\mathcal{E}$ the input line segment and by e' and e'' its endpoints.

1   Compute the most clockwise and counterclockwise orientations θ_L and θ_H;

2   test the intersection of $\mathcal{E}$ and the object at orientations θ_L and θ_H;

3   `for` double contacts with E_i and E_j `do`

4   **for** every vertex v between E_i and E_j **do**

5   test the intersection of $\mathcal{E}$ and the curve traced by the vertex v;

6   **for** every edge E between E_i and E_j **do**

7   **if** E yields type T2 boundary

              then compute the circular part boundary and test the intersection with $\mathcal{E}$;

8   compute the intersection of endpoints of $\mathcal{E}$ and E, and

           report intersection with orientation $\theta \in [\theta_L, \theta_H]$.

Note that, by all vertices between E_i and E_j, we mean all the endpoints of the edges between E_i and E_j. For example, in Figure 6.10, the edges between E_1 and E_2 include edges E_a, E_b and E_c and hence the vertices belonging to these edges are the vertices between E_1 and E_2.

Computing the orientations θ_L and θ_H in line 1 amounts to solving a univariate quadratic equation obtained from the system of equation defining three simultaneous contacts. In line 2, parts of the boundary of type T1 and T2 that are line segments are tested. This is done for all three choices of double contacts because at both extreme orientations (θ_L and θ_H), the three designated edges are simultaneously in contact with the robots. The **for** loop in line 3 has to repeat for the three choices of double contacts. Note that when the intersection is detected, the routine returns **TRUE** and terminate, otherwise it returns **FALSE** before it stops. Computing intersection in line 8 amounts to solving system defining three simultaneous contacts which are two contacts between the fixed robots B_i, B_j and E_i, E_j, and between an endpoint of $\mathcal{E}$ and E.

We have shown how to test the intersection between the envelope and an obstacle edge. This process takes time linear in the size of the polygon, and it must be repeated for every obstacle edge (or until some intersection is found). This simple approach can be improved by limiting collision checking to obstacles in the vicinity of the envelope: we compute bounding rectangles for the envelope and each obstacle, and efficiently test the intersection between these rectangle. It is easy to find the smallest *isothetic* rectangle (i.e., with sides parallel to the coordinate axes) bounding a polygonal obstacle. To find an

isothetic bounding rectangle for the envelope, we first compute the radius of the smallest circle that contains the object (Fig. 6.12(a)): this is known as the *smallest enclosing circle* problem in computational geometry, and the radius can be found in in time linear in the size of the polygon by a randomized algorithm [104]. We place three circles with this radius in the workspace so that each one passes through a pair of the robots and its center is outside the triangle formed by the three robots (Fig. 6.12(b)). The bounding rectangle is computed as the smallest isothetic rectangle that contains the three circles. It is easy to show that the envelope is contained in this rectangle.


(a)　　　　　　　　　　　　　　　　　　(b)
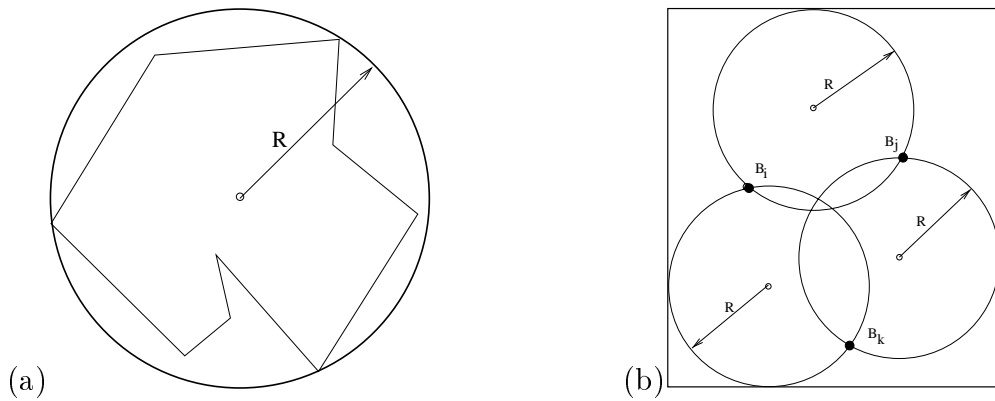
Figure 6.12 Constructing a box bounding the envelope: (a) the smallest circle containing the object, and (b) a simple bounding box of the envelope.

We want to find all the obstacle rectangles that intersect the envelope rectangle. As shown in [99, 100], this *orthogonal intersection searching* can be solved with query time $O(A + \log P)$ and preprocessing time $O(P \log P)$, where A is the number of obstacle bounding rectangles intersecting the reference rectangle, and P is the total number of rectangles.

It is easy to show that the motion planning algorithm presented in this paper is guaranteed to generate a plan avoiding obstacles when there exists such a path for the object grown by the diameter of the robots plus some arbitrarily small positive number ε: this is a direct consequence of the controllability condition of Lemma 7, the clearance ε ensuring that there is an open free neighborhood in configuration space of any point along the path.

6.5   Discussion and Conclusions

We have introduced in this chapter the concept of maximum independent capture discs (MICaDs), where the three robots can move independently while guaranteeing that an object cannot escape their grasp. We have given a simple method for constructing the MICaDs associated with a polygonal object, and shown they could be used as a basis for motion planning in the presence of obstacles. We are currently implementing the proposed approach and plan to conduct experiments using the Nomadic Scout robots available in our laboratory.

So far, we have only implemented the construction of MICaDs associated with double contacts, and Fig. 6.13 shows a couple of examples. The three-contact case and the motion planning algorithm have not been implemented yet. Note that the discs may be quite small depending on the choice of edges and object geometry (Fig. 6.13(c)), which suggests taking the whole object boundary into account instead of three edges at a time during the construction of capture regions.
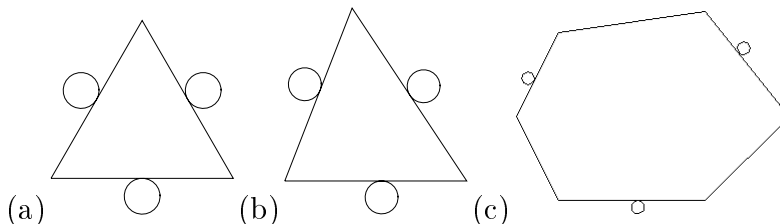

Figure 6.13 Examples of MICaDs. Each example took less than 1 second to compute on a SUN SparcStation 10.

Friction may of course cause the robots to jam during the execution of the motion plan. We have tried to minimize the risk of jamming by avoiding to completely grasp the object until the end of the manipulation task: indeed, grasping requires establishing three simultaneous contacts, with a much higher chance for jamming than when a single contact or a pair of contacts occur. Nonetheless, friction should be dealt with explicitly, and therefore we investigate the effect of friction in the next chapter.

124

CHAPTER 7

FRICTION

7.1 Introduction

Friction is ussually considered desirable for grasping: it is known to lower the number of fingers required to achieve force closure [59, 52], and it also helps the object to stick better to the fingers allowing higher tolerance for errors in the positioning [63, 70]. Most approaches to grasping are static and mainly focus on the computation of the grasp position [63, 64, 73, 72, 15]. It is usually assumed that the object to be grasped is located at the desirable configuration and it does not move during the grasp execution. In practice, this assumption is of course not always satisfied: when all the contacts are not made at exactly the same time, the contact occuring first may cause the object to move. If the object does not move too far, it can still be succesfully grasped with the help of friction, but likely to be at a wrong position.

The problems of capturing the object to be grasped and making an approach for the grasp are commonly overlooked in grasp planning (not always, see [68]) but they are sometimes addressed in the context of object manipulation. Some manipulation methods assume that the contact is never broken (by limiting the operating velocity to simplify dynamics, for example), so the capturing problem can be avoided [1, 49, 55]. An assumption of frictionless contacts is also usually made to guarantee that the object can be grasped at the desired configuration [31, 32, 33, 96, 94, 92]. Although it may not be difficult to arrange for these assumptions to be satisfied in particular settings, a
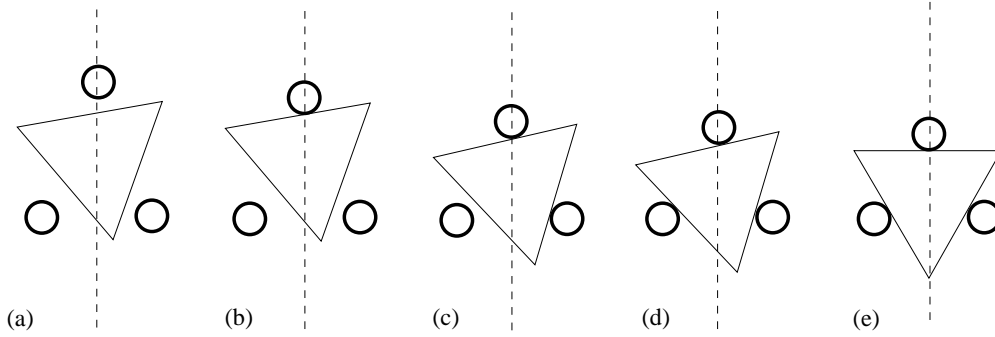
Figure 7.1 Grasping the object within the capture.

true solution requires a better understanding of what actually happens in a more general environment. We have already presented an approach to capturing based on inescapable configuration space regions in Chapter 4, 5 and 6. In this chapter, we investigate the effect of friction.

More precisely, we will consider the problem of grasping a polygonal object that is already captured by the robots. The setup is similar to the one presented in Chapter 5 (Figure 7.1). The object sits on a horizontal plane and cannot escape from the capture of three disc-shaped robots. We assume that the two robots at the bottom of the figure are fixed and the top robot can move only along the dashed line trajectory. Figure 7.1(a)-(e) shows snapshots of the top robot appraching the object. The object is pushed as the contact with the top robot is made (the object may also bounce within the capture). At some point, it will have three simultaneous contacts with the robots. At this point, as the top robot attempts to push further, the possible scenarios are [1]:

(a) The top robot continues pushing as the object rotates.

(b) The top robot cannot push any further and the object is at an immobilizing configuration.

(c) The top robot cannot push further but the object is not at an immobilizing configuration.

---

[1]This assumes of course that the two bottom robots are heavy enough, with enough friction with the ground, that they will not move.

126

If an equilibrium is not achieved, the object can still be moved by the net force. With three simultaneous contacts and the pushing robot moving along a straight line, the motion of the object has one degree of freedom (Figure 7.1(d)). From case (a), if the robot keeps pushing, at some point it will stop because: (1) the object reaches the immobilizing configuration (case (b), Figure 7.1(e)), or (2) because of friction, an equilibrium is achieved before the object is pushed to the immobilizing configuration (case (c), Figure 7.1(d)). With frictionless contacts, the desirable outcome (b) is guaranteed. In this chapter, we study the conditions under which jamming occurs due to friction (case (c)).

7.2 Related Work

Dry friction is a natural phenomenon that happens in everyday life. Its behavior has been modeled by the well-known Coulomb laws [9]: (1) the friction force is independent of the area of the sliding surface; (2) it is proportional to the load; (3) the kinetic friction, i.e., the force required to keep a body sliding at a constant velocity, does not depend on the velocity and it is smaller than or equal to the static friction, i.e., the force required to start sliding. Although Coulomb's model of friction is simple, the process of two solid bodies sliding along each other is very complex and involves interactions from microscopic to macroscopic scales. Therefore, without surprise, deviations from Coulomb's laws can be found in experiments. Typical deviations include: (1) static friction is not constant but increases with sticking time [77, 36], and (2) when the sliding velocity is large, kinetic friction increases virtually linearly with the velocity [36].

Although Coulomb's law is far from perfect, it is simple and seems to work sufficiently well in most cases. This is why it is, by far, the most popular friction model that has been applied in robotics. As mentioned in the previous section, friction is usually considered desirable for grasping. Most grasping fingers are usually covered with rubber or other elastic material to increase contact friction. Assuming Coulomb friction, Ngugen [63] proposed a geometric method for computing maximal independent two-finger grasps of

polygon, i.e., segments of the polygonal boundary where the two fingers can be positioned independently while maintaining force closure, requiring as little positional accuracy from the robot as possible. This approach has been generalized to handle various number of fingers and different object geometries in [15, 68, 72, 74]. Jamming has rarely been mentioned in the context of grasping because the main goal of most grasping tasks is only to securely hold the object in the hand; accurately positioning the object is not the main focus. If the object needs to be placed in a specific configuration, the current configuration of the object in the grasp will normally be provided (by a vision-based object recognition system, for example) to the robot so it can adjust its configuration appropriately for the execution of the positioning task.

In keeping with the idea of Reduced Intricacy Sensing and Control (RISC) robotic of Canny and Goldberg [13] manipulation of workpieces without or with minimal sensory data has gained attention in the robotics community [33, 78, 1]. This manipulation scheme usually relies on simple and robust devices [32]. To develop reliable manipulation algorithms, it is clear that jamming should be well understood. However, progress in this area has been slow. The most extensively studied jamming situation is for the problem of inserting a peg into a hole. Simunovic [90] introduced the terms "wedged" and "jammed" in the context of inserting a planar peg into a hole after he noticed that wedging might occur at shallow insertion depths as the possible contact forces including friction could cover the entire wrench space. In [106], Whitney proposed quasi-static condtions to avoid wedging and jamming for the peg-in-hole problem. He and Nevin [105] later developed the remote-center compliance (RCC) wrist which is a passive mechanism allowing the forces that arise due to small positioning errors to cause the peg to self-align with the hole.

Donald and Pai [22] analyzed jamming for systems with more general geometries. They developed a simulation-based technique to predict jamming during assembly of two-dimensional workpieces. A similar technique for three-dimensional workpieces was developed by Dupont [24]. Recently, Trinkle et al.[97] proposed an analytical condition

to test for the impossibility of jamming in three-dimensional, quasistatic multi-rigid-body system.

7.3   Jamming

In the previous chapters, we preprocessed the objects of interest by shrinking the robots to their centers and growing the object by the radius of the robots. In this chapter, we are interested in both the configuration of the object and the robots *and* in the actual contact points where forces are applied. Therefore, it is important not to confuse the shrunk robots and the actual contact points.

We will assume from now on Coulomb friction, i.e., that the magnitude of the frictional force cannot be greater than $N \tan \alpha_f$ (Figure 7.2) where N is the normal force and α_f is the half friction cone angle (when there is no sliding, the tangential force exerted at the contact is compensated by a frictional force). Note that α_f is a constant depending on the material of the contact surfaces.
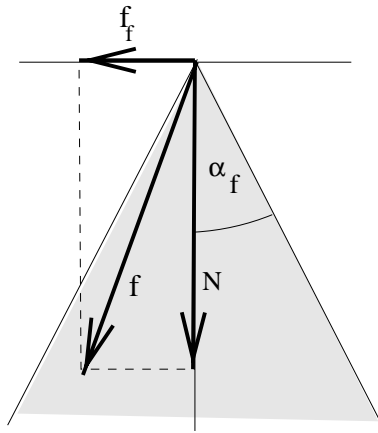

Figure 7.2 Coulomb friction.

As mentioned before, jamming occurs when all the forces at the contacts including friction achieve an equilibrium. Jamming occuring when there are one or two contacts between the robots and the object can usually be dealt with by exerting larger force at the contacts. In this chapter, we focus in the case of three contacts for which the chance
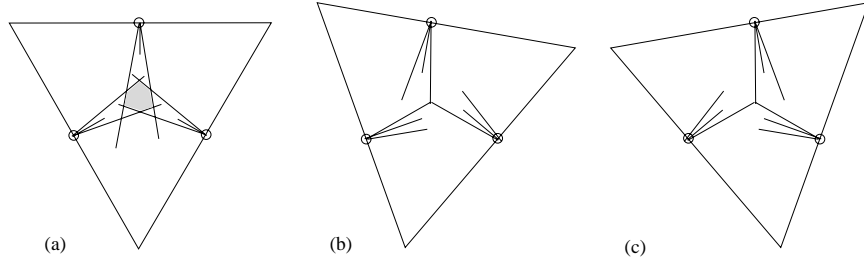
Figure 7.3 Friction cones at (a) the immobilizing configuration, and (b),(c) the two critical orientations.

of jamming is much higher. When the pushing robot moves along a line segment, the object configuration with three simultaneous contacts has one degree of freedom that can be parameterized by the orientation of the object. In this section, we characterize the range of orientations where jamming may occur. In other words, we compute the range of the object orientations for which an equilibrium can be achieved.

There are two sources of friction: (1) friction between the robots and the object, and (2) friction between the object and its supporting plane. Let us begin by assuming that there is no friction between the object and its supporting plane.

Consider Figure 7.3. Since we assume that there is no friction between the object and its supporting plane, there are only three forces to consider. These are the forces applied at the contacts between the robots and the object. These forces must lie within the friction cones at the contacts. Clearly, an equilibrium can be achieved only when the three forces intersect. This implies that an equilbrium can be achieved only when the three friction cones intersect (Figure 7.3(a)).

Computing the range of orientations $[\theta', \theta'']$ for which an equilibrium can be achieved therefore amounts to computing the range of orientations for which the three friction cones can intersect. It is easy to see that the most clockwise (resp. counterclockwise) orientation of this range corresponds to the orientation at which the counterclockwise (resp. clockwise) edges of the three cones intersect (Figure 7.3(b)-(c)).

In the following, we describe how to compute the critical orientations θ' and θ''. To simplify the contact analysis, we assume for the time being that the robots have zero radius (the general case will be discussed in Section 7.3.2). Most of the notation is

the same as in Chapter 5. That is, we denote by θ the orientation of the object, by α_i, $i = 1, 2, 3$ the offset angle of the internal normal of edge E_i, and by $\boldsymbol{q}_i = (q_i, r_i)^T$, $i = 2, 3$ the location of the fixed robots. The location of the movable robot is given by $(q_1 + \delta \cos \alpha, r_1 + \delta \sin \alpha)^T$ where α denotes the orientation of the line trajectory and δ denotes the coordinate of the robot along this trajectory line. Without loss of generality, we arrange the set up such that the immobilizing configuration occurs at $\theta = 0$ and $\delta = 0$.

The most counterclockwise orientation at which an equilibrium can be achieved corresponds to the orientation for which the clockwise edges of the three friction cones at the contacts intersect (see Figure 7.4).
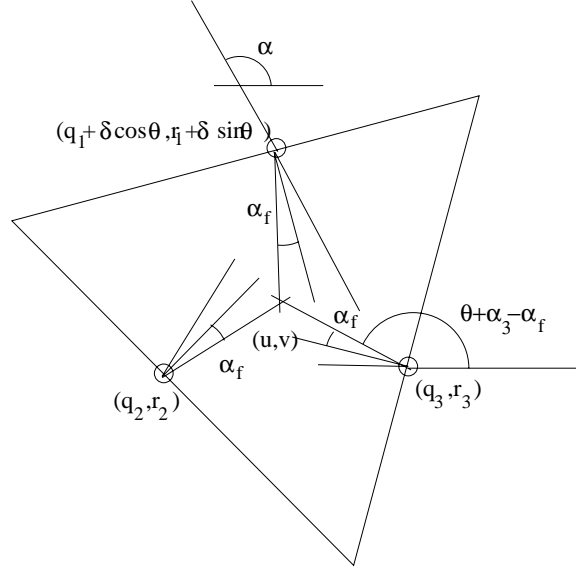

Figure 7.4 Friction cones at a critical orientation.

Writing that these three edges intersect at $(u, v)^T$ yields:

$$\begin{cases} (u - (q_1 + \delta \cos \alpha))c_1 + (v - (r_1 + \delta \sin \alpha))s_1 = 0, \\ (u - q_2)c_2 + (v - r_2)s_2 = 0, \\ (u - q_3)c_3 + (v - r_3)s_3 = 0, \end{cases} \tag{7.1}$$

where $c_i = \cos(\theta + \alpha_i + \pi/2 + \alpha_f)$ and $s_i = \sin(\theta + \alpha_i + \pi/2 + \alpha_f)$, $i = 1, 2, 3$.

After eliminating u and v, we have:

$$\delta \sin(\theta + \gamma_1) + A \sin(\theta + \gamma_2) = 0$$

where γ_1, γ_2 and A are appropriate constants.

From Chapter 5, the relationship between δ and θ can be written as:

$$\delta \sin(\theta + \gamma_3) + B \sin(\theta + \gamma_4) + C \;=\; 0$$

where γ_3, γ_4, B and C are appropriate constants.

Using both equations above, we can easily eliminate δ to obtain a trigonometric equation in θ which can be solved in closed form. Note that the clockwise critical orientation can be computed similarly by formulating the equations corresponding to the intersection of the counterclockwise edges of the friction cones (intead of the clockwise edges shown above).

This calculation yields the range $[\theta', \theta'']$ for which an equilibrium can be achieved. Jamming is possible when the orientation of the object is within this interval, so it is desirable that its size be small. Can we adjust anything to make jamming range smaller? In the following section, we show the case where a special orientation of the trajectory line cause θ' to be $-\alpha_f$ and θ'' to be α_f. We will examine how the range of jamming orientations is affected by the orientation α of the trajectory line.

7.3.1 Influence of Line orientation on Jamming

First, we will examine the special case where internal normal of edge E_1 at the immobilizing configuration ($\alpha = \alpha_1 + \pi$). We are going to show that $\theta' = -\alpha_f$ and $\theta'' = \alpha_f$ in this case.

Figure 7.5 illustrates the situation. At the immobilizing configuration, the axes of the three friction cones intersect at P (Figure 7.5(a)). Note that the trajectory line coincides with the axis of the friction cone at the contact between the pushing robot and the object. Consider the object as it rotates counterclockwise by an angle α_f. Accordingly, the axes of the friction cones at the two fixed robots (bottom one) rotate counterclockwise by an angle α_f. Their clockwise edges also rotate counterclockwise by an angle α_f and intersect at P. It is easy to see that, regardless of the position of the pushing robot on the trajectory line, the clockwise edge of the friction cone at the pushing robot now becomes
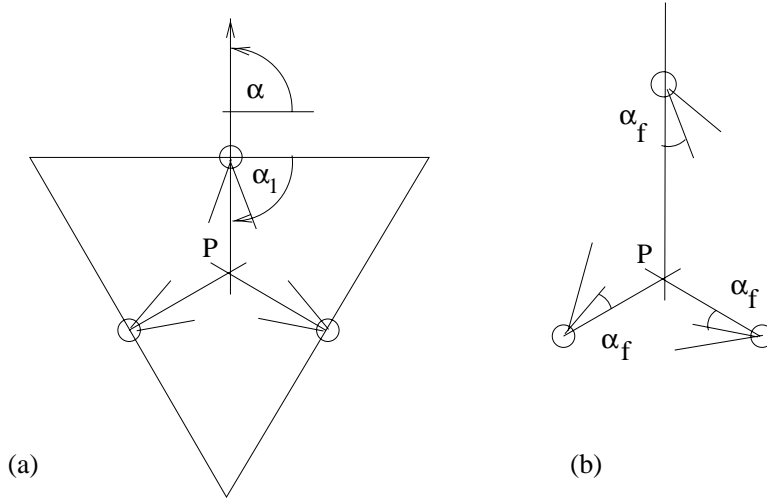
Figure 7.5 A special case.

coincident with the trajectory line which also intersects P (Figure 7.5(b), a similar result can be shown for the clockwise rotation). Thus $\theta'' = -\theta' = \alpha_f$.

What will happen if the direction of the line trajectory is set differently? Consider the case where $\alpha = \alpha_1 + \phi$, $\pi/2 < \phi < \pi$. At the immobilizing configuration, we assume that the clockwise edges of the friction cones at the two fixed robots intersect at Q_1 (Figure 7.6(a)). As the object rotates counterclockwise by angle α_f (rotates from $\theta = 0$ to $\theta = \alpha_f$), these two edges also rotates counterclockwise by angle α_f and intersect and P (Figure 7.6(b)). Consider the clockwise edge of the friction cone at the pushing robot. As the object rotates counterclockwise by angle α_f (the robot moves accordingly from A to B), this edge moves from L_1 to L_1' and sweeps the shaded region. Clearly, this edge passes P before $\theta = \alpha_f$, and the part of the curve (including P) traced by the intersection of the two clockwise edges of the friction cones of the fixed robots is contained in the region R_1. Therefore, the clockwise edges of the three friction cones must intersect at some $\theta < \alpha_f$.

Now consider the clockwise rotation. When $\theta = 0$, the counterclockwise edges of the friction cones at the two fixed robots intersect at Q_2 (Figure 7.6(a)) and when $\theta = -\alpha_f$, these edges intersect at P (Figure 7.6(c)). Let us denote by Z_2 the curve of the intersection of these edges as θ goes from 0 to $-\alpha_f$. As the object rotates clockwise from
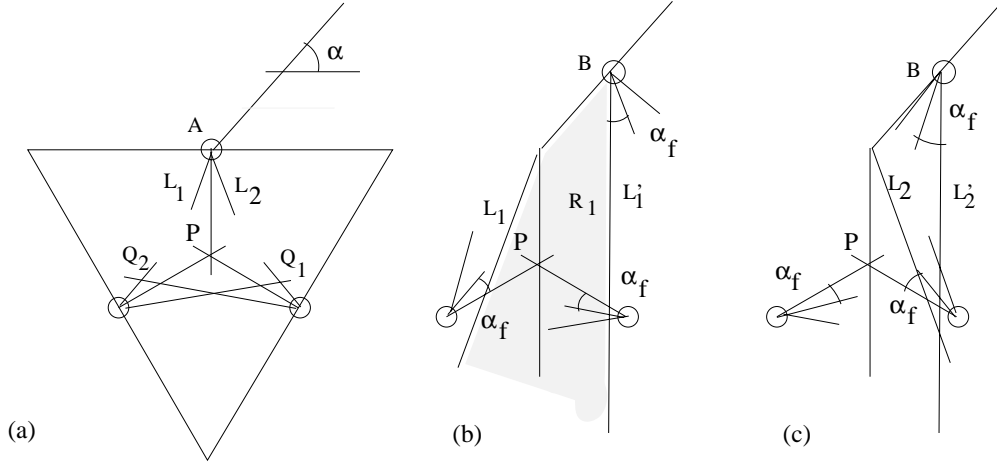
Figure 7.6 Jamming range when angle $\alpha \neq \pi/2$.

$\theta = 0$ to $\theta = -\alpha_f$, the counterclockwise edge of the friction cone at the pushing robot moves from L_2 to L_2' (Figure 7.6(c)). It is easy to see that the region swept by this edge does not contain the curve Z_2. This means that the counterclockwise edges of the three friction cones do not intersect during $-\alpha_f < \theta < 0$. In other words, the object need to rotates further than α_f for the counterclockwise edges to intersect and jamming to become impossible.

In summary, for this setting of the direction of the trajectory line, the range of the object orientations for which an equilibrium can be achieved is $\theta' < \theta < \theta''$ where $\theta' < -\alpha_f$ and $\theta'' < \alpha_f$. That is, the range of counterclockwise jamming orientations is smaller than the range of clockwise jamming orientations. Note that if the trajectory line slants in the other direction, we can imagine a mirrored copy of Figure 7.6(c) which we will obtain the range of jamming orientations to be $\theta' < \theta < \theta''$ where $\theta' > -\alpha_f$ and $\theta'' > \alpha_f$.

7.3.2   Influence of Robot Radius on Jamming

We now consider the robots with radii greater than zero. In Figure 7.7, we have three robots with radius $r > 0$. We show the friction cone at the contact between the object and the bottom left robot. Clearly, as the object rotates, the edges of the friction cones

134
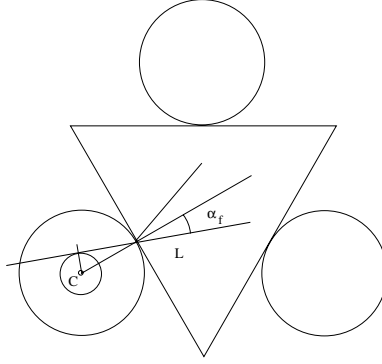
Figure 7.7 Grasping using robots with non-zero radius.

also rotate. Unlike the zero-radius case, however, these edges do not pass through the center of the robot. Being aware of this fact, we formulate equations similar to (7.1) to express that the three edges intersect, and compute the critical orientations defining the jamming range. In particular, we will have:

$$\delta \sin(\theta + \gamma_1) + A \sin(\theta + \gamma_2) + B = 0,$$

where γ_1, γ_2, A and B are appropriate constants. Note that there is one more constant than the previous formulation. As before, the relationship between δ and θ of the object having three simultaneous contacts (Section 5.2.1) can be used to eliminate δ. The resulting equation is, again, a univariate equation of degree four.

Let us look closely at one contact. In Figure 7.8, we superimpose figures to show a contact with robots of radius zero, r_1, and r_2, where $0 < r_1 < r_2$. At the immobilizing configuration, the three robots share the same contact point, and the edges of the friction cones coincide. We denote by L the line where the clockwise edges coincide (Figure 7.8(a)). As the object rotates counterclockwise by some angle, the clockwise edges rotate accordingly by the same angle (Figure 7.8(b)). The clockwise edge of the friction cone of the robot with radius r_2 (resp. r_1 and zero) rotates from L to L_2 (resp. L_1 and L_0). We can see that the clockwise edge of the robot with greater radius sweeps a larger region than the edge of the friction cone of the robot with a smaller radius. This is also true for the robots making contacts with the other two edges of the object. Remember that we have to compute the intersection of the edges of the three friction cones at the three

135
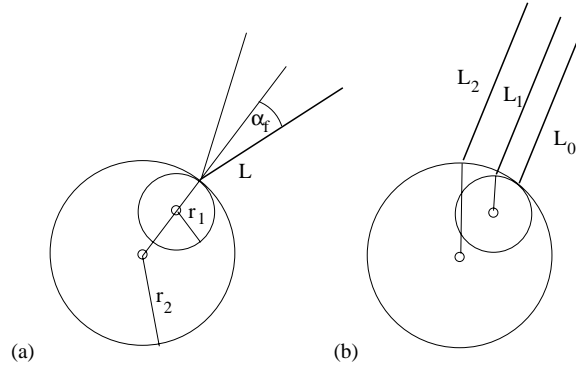
Figure 7.8 The friction cones associated with different robots' radii.

contacts to obtain the jamming range. For three robots with larger radius, the three edges intersect when the object rotates by a smaller angle than it would for the robots with smaller radius. We can therefore conclude that the larger radius yields a smaller range of jamming orientations.

So far, we can see that the amount of force applied by the pushing robot is not involved in the computation of the critical orientations. That is, for the case where friction only comes from the contacts between the object and the robots, the magnitude of this force has no influence on the range of jamming orientations. No matter how hard the robot pushes, the object could still be stuck.

7.3.3 Accounting for Friction between the Object and its Supporting Plane

We are now ready to take into account friction between the object and its supporting plane. By Coulomb's laws, the maximum magnitude of frictional force at any point in the contact region is proportional to the normal pressure at the point. By considering the entire contact region and assuming that the coefficient of friction is uniform over the region, we can consider the total frictional force as a single force applied at the centroid of the pressure distribution (in the opposite direction to the net horizontal force). Let us assume further that the pressure distribution does not change during the grasp. As a result, the centroid of the pressure distribution is fixed with the object and we have

$|\boldsymbol{f}_f| \leq \mu_f N$ where $\boldsymbol{f}_f$ is the frictional force between the object and its supporting plane, μ_f is the coefficient of friction and N is the magnitude of the net normal load. We denote by $\boldsymbol{q}_f$ the centroid of the pressure distribution and by $W = \mu_f N$ the maximum magnitude of $\boldsymbol{f}_f$.

In the following, we list the conditions for equilibrium. Note that we need to consider only horizontal forces because we assume that the object does not have any vertical motion, which means that the net normal load and the reaction force from the ground cancel each other.

Let us denote by $\boldsymbol{f}_i, i = 1, 2, 3$ the forces at the contact $\boldsymbol{q}_i$. When the object is in equilibrium, all forces must cancel:

$$\boldsymbol{f}_1 + \boldsymbol{f}_2 + \boldsymbol{f}_3 + \boldsymbol{f}_f \ = \ 0,$$

and net moment is zero (calculated around $\boldsymbol{q}_f$ here):

$$\sum_{i=1}^{i=3}((\boldsymbol{q}_i - \boldsymbol{q}_f) \times \boldsymbol{f}_i) \ = \ 0.$$

The following constraints must also be satisfied. The forces at the contacts must lie in their friction cones:

$$\boldsymbol{f}_i \in \mathcal{C}_i, \ \ i = 1, 2, 3,$$

where $\mathcal{C}_i$ is a cone at the origin with half angle α_f and the internal normal of the edge E_i as the main axis.

The magnitude of the friction $\boldsymbol{f}_f$ cannot exceed W:

$$\boldsymbol{f}_f \in \mathcal{S}_W,$$

where $\mathcal{S}_W$ is a disk at the origin with radius W.

When the orientation θ is given (Figure 7.9), the contact points $\boldsymbol{q}_i, (i = 1, 2, 3)$, the axis of friction cone $C_i, (i = 1, 2, 3)$ and the center of friction $\boldsymbol{q}_f$ can be calculated. As a result, the equilibrium constraints can be written as a set of linear equations in $\boldsymbol{f}_i, (i = 1, 2, 3)$ and $\boldsymbol{f}_f$. The fact that the contact forces must lie in the corresponding friction cones can also be written as linear inequalities in $\boldsymbol{f}_i$. For the constraint on the
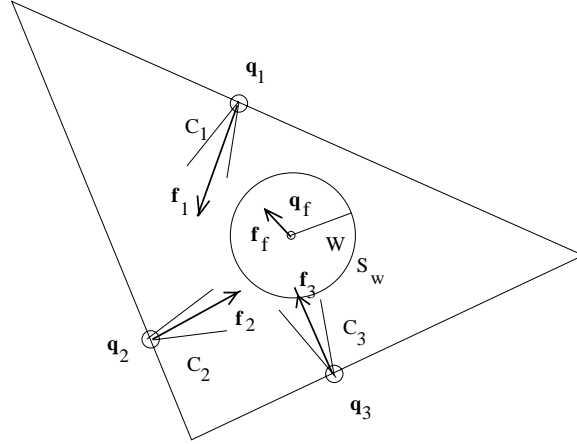
Figure 7.9 Force diagram when friction between the object and its supporting surface is considered.

magnitude of the friction force $\boldsymbol{f}_f$, we approximate the circle $\mathcal{S}_W$ with the smallest n-gon that encloses the circle and rewrite the constraint as a set of linear inequalities in $\boldsymbol{f}_f$.

We also want the magnitude of the normal component of the force at the contact with the pushing robot to be set to a constant F to eliminate the trivial case of equilibrium when all forces are zero and to reflect the amount of pushing force over which we have some control. This condition can be written as:

$$
\boldsymbol{f}_1 \cdot \left(\begin{array}{c} \cos(\theta + \alpha_1) \\ \sin(\theta + \alpha_1) \end{array} \right) = F,
$$

which is linear in $\boldsymbol{f}_1$ when θ is given.

As a result, for a given orientation θ, we can use linear programming to determine whether equilibrium can be achieved. We can then use bisection to seek the range of jamming orientations by using linear programming to test for the existence of equilibrium configurations at each bisection step. For the initial smallest range, we can use the jamming range of orientations obtained for the same setting but with no friction between the object and its supporting surface (set $W = 0$) in which we know how to compute. For the largest possible range, we can use the range of orientations the object can rotate at the maximum ICS (Chapter 5) because the object orientation cannot be outside this range if it has to be in the capture of the robots.

The magnitude of the friction force $\boldsymbol{f}_f$ cannot exceed W. The constant W is proportional to the normal load (which is assumed to be constant) and is independent from the force exerted by the pushing robot: intuitively that the effect of $\boldsymbol{f}_f$ on the range of jamming orientations will decrease as the ratio $\frac{F}{W}$ increases. This is confirmed by the simulation result in the Section 7.4.

7.4   Simulation Experiments

In this section, we present some simulation results that illustrate the observations presented in the previous sections. The sample object is an equilateral triangle with unit edges. The direction of the trajectory line is the angle α. The object is immobilized when the orientation $\theta = 0$ and the robots are at the midpoint of the edges. We compute the range of jamming orientations which is composed of two parts: (1) counterclockwise jamming orientations ($\theta > 0$), and (2) clockwise jamming orientations ($\theta < 0$). The implementation follow the formulation described in the previous sections. The programs were written in C++ programming language and run on a 450-MHz personal computer. For all examples given here, the running times are less than one second. In the first two examples, we assume no friction between the supporting surface and the object.
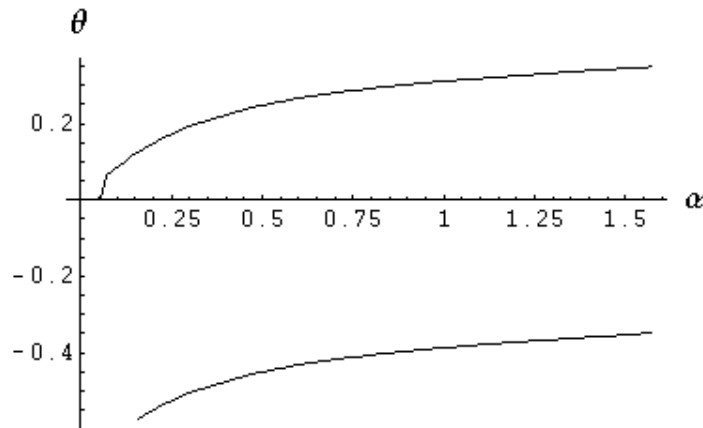

Figure 7.10 The jamming range of orientations as a function of the direction of the trajectory line.

We show in Figure 7.10 the range of jamming orientations as a function of the orientation of the trajectory line. We can see that when the direction α is $\pi/2$, the range is well balanced (the range of counterclockwise jamming orientations is as large as the range of clockwise jamming orientation). As we decrease α, the trajectory line slants to the right side and the range of counterclockwise jamming orientations becomes smaller while the range of clockwise jamming orientations becomes larger. The opposite happens when we increase α. Again, this result confirms the observation mentioned in Section 7.3.1. Note that for this result, the program was written to compute the orientations θ' and θ'' at a given α by solving the quartic equation described at the beginning of Section 7.3.
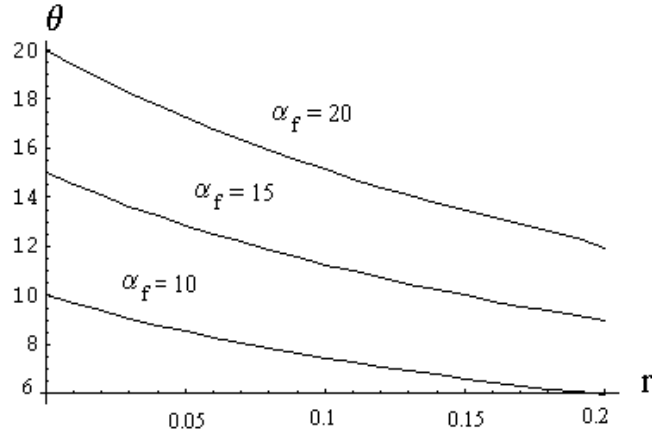

Figure 7.11 The counterclockwise jamming range of orientations as a function of the radius of the robots.

Figure 7.11 shows the range of jamming orientions (in degrees) as a function of the radius of the robots relative to the size of the triangle at various half-cone angles. The trajectory line is set at $\alpha = \pi/2$ so the range is well balanced. Therefore, in Figure 7.11, we show only the counterclockwise jamming range of orientations as we vary the radius of the robots from 0 to 0.2 unit. The range becomes smaller as the radius gets larger as explained in Section 7.3.2. For this result, a program was written to compute the orientations θ' and θ'' at a given radius r by solving the quartic equation given in Section7.3.2.
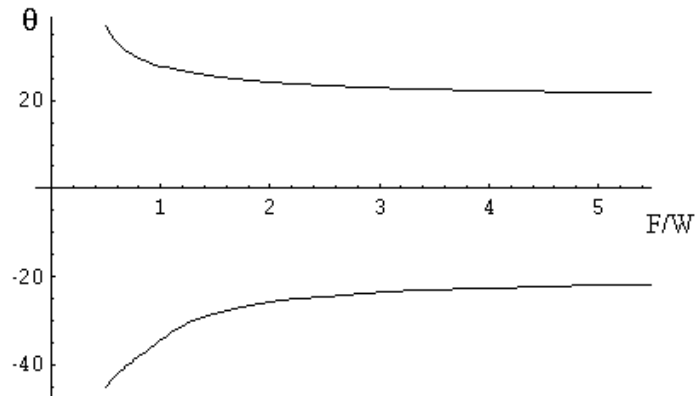
Figure 7.12 The jamming range of orientations (in degrees) as a function of the ratio F/W.

Finally, we plot in Figure 7.12 the range of jamming orientations (in degree) as a function of the ratio F/W. The half cone angle α_f is set to 20 degrees. We can see that the effect of the friction force $\boldsymbol{f}_f$ on the range of jamming orientations decreases as the ratio F/W increases. The range converges to the case of no friction $\boldsymbol{f}_f$ as F/W increases. The program generating this result was written following the description given in 7.3.3.

7.5   Discussion and Conclusions

We have studied jamming in grasping. One of the main objectives of this chapter is to develop a more reliable method for grasping under friction. We have learned how the range of jamming orientations is affected by friction and other factors including the trajectory direction, the radius of the robots, and the magnitude of the pushing force relative to the friction with the ground.

The effect of friction between the object and the supporting surface is reduced as we increase the magnitude of the pushing force. To avoid damaging the object and to guarantee that the other two robots are not pushed away, the magnitude of the pushing force can be increased only upto some limit. As mentioned in the previous section, increasing the pushing force cannot improve any jamming effect of the friction between the object and the robots. It is therefore preferable that the friction between the robots

141
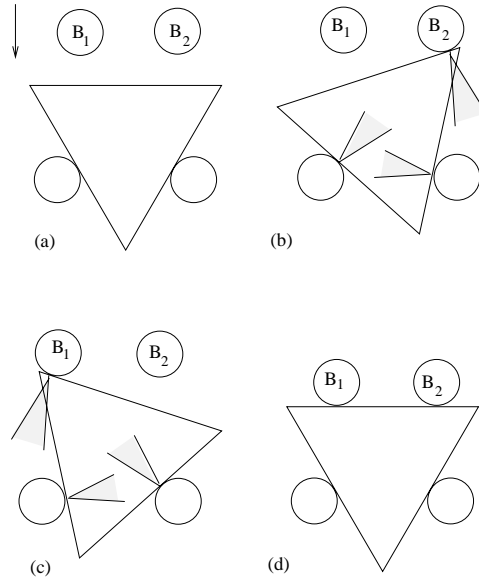
Figure 7.13 Grasping with four robots.

and the object is low and the object is so light that the friction between the object and the ground surface can easily be overriden by the pushing force. A larger robot radius can also help reducing the range of jamming orientations but, on-line adjustment of the radius is of course usually impossible.

It is clear that the chance of jamming during the range of orientations near the immobilizing configuration is very high. The manipulation plan not attempting to immobilize the object is therefore reduce the chance that the object be in this range of orientations, and reduce the risk of jamming. It is very interesting to consider adding another pushing robot. Used in conjunction with a simple strategy outlined below. This may significantly reduce the range of jamming orientations or even avoid jamming altogether. Consider Figure 7.13. Here we have two pushing robots B_1 and B_2. The goal is to grasp the object by placing each robots near the end points of the grasped edge (Figure 7.13(d)). The first step is to move both pushing robots into the inescapable region associated with the two fixed robots so the object cannot escape. Then, we move the robots to the locations for which the robots can grasp the object if they are translated along the direction of the arrow (Figure 7.13(a)). To grasp the object, we translate both robots simultaneously along the arrowed direction. In this example, we can see that at any point during the

142

translation, when three simultaneous contacts with the object are possible, the three friction cones at the contacts do not intersect (Figure 7.13(b)-(c)). The only possibility for jamming to occur is therefore due to the friction between the object and its supporting surface which we can usually counter by pushing harder. The key idea is that, at any point, the object can be in contact with at most three robots and the placement of the robots are arranged such that the friction cones at the contacts do not intersect. An obvious application of this idea would be in the design of a manipulation planner that can generate plans guaranteed to be jam-free even with friction.

CHAPTER 8

CONCLUSION

We have addressed the problem of immobilizing and manipulating parts with devices that have a mixture of discrete and continuous degrees of freedom. We have devised efficient algorithms for planning immobilizing fixtures, grasps, in-hand manipulation sequences and obstacle avoidance manipulation plans for parts with known geometry.

We believe that the key contribution of the thesis is the introduction of the concept of inescapable configuration space region as a framework for manipulation planning. Within this framework, the main contributions of the thesis are:

1. *A fixture planning algorithm for three-dimensional parts.* This is, to the best of our knowledge, the first algorithm ever proposed for fixturing true three-dimensional objects with arbitrary pose (see [11, 101] for related work using prismatic objects and three-dimensional objects with pre-specified pose).

2. *The design and construction of a novel reconfigurable gripper.* This gripper has the potential for achieving a level of dexterity comparable to dextrous robotic hands [40, 87] at a fraction of the cost. (This part of our work was done in collaboration with Dr. Narayan Srinivasa.)

3. *An efficient algorithm for planning immobilizing grasps with the reconfigurable gripper.* This is a variant of the fixture planning algorithm, but it exploits the special geometry of the gripper for additional efficiency. We have implemented this algorithm and tested it with the prototype of the gripper.

144

4. *The exact characterization of inescapable configuration space regions for the gripper.* ICS regions generalize the notion of immobilizing grasps: the object is not immobilized but is constrained to lie within a compact region of the free configuration space (see [80] for related work in the two-dimensional, two-finger case). The ICS region associated with a given gripper configuration is characterized through a detailed analysis of contact constraints in configuration space.

5. *An efficient algorithm for in-hand manipulation planning.* Unlike previous approaches to the same problem (see [1, 26, 33, 49, 55] for example), this approach does not make strong assumptions about contact dynamics and does not attempt to predict the exact motion of the part. Instead, atomic part motions are effected by progressively reducing the set of admissible configurations to a single point, and complex in-hand manipulation sequences are planned by efficiently constructing and searching the adjacency graph formed by overlapping ICS regions. This algorithm has been implemented and tested with the prototype of the gripper.

6. *An efficient algorithm for manipulating polygonal objects with three disc-shaped robots.* The algorithm is developed based on the concept of ICS and capable of generating plans to bring the object to a desired configuration. The algorithm has been fully implemented and tested using Scout Nomadic robots.

7. *A novel robot motion planning for three disc-shaped robot to manipulate polygonal objects among polygonal obstacles.* The planning algorithm is based on the concept of independent inescapable region and is capable of generating plans allowing three robots to move simulataneously while guaranteeing that the object cannot escape and cannot collide with any obstacle.

8. *A characterization of jamming configurations under Coulomb friction.* This characterization provides detailed analysis about how jamming occurs during a grasping task. The results may be helpful to grasp and manipulation planning that tries to reduce the risk of jamming.

145

Minor contributions include the proof that second-order immobilizing grasps and fixtures of polyhedra effected with spherical locators are stable. This complements previous work by Nguyen [64], Howard and Kumar [38], and Rimon and Burdick [83].

Beyond the research described in this thesis, there are some related research issues that are worth mentioning.

Fixture Planning. There are obviously polyhedral objects which cannot be fixtured with our device (a trivial example is an object whose diameter is smaller than the inter-locator distance). It would be interesting to characterize precisely the class of fixturable objects (see [107] for a discussion of the two-dimensional case). Another interesting avenue of research would be to extend the proposed algorithm to parts bounded by algebraic patches (see [103, Chapter 6] for the two-dimensional case). The overall approach proposed in this thesis extends to this case in a straightforward way, but working out the details of how to enumerate locator configurations and dealing with the very high degree of the equations involved should prove quite challenging.

Manipulation Planning with the Reconfigurable Gripper. Our manipulation planning approach requires computing all possible grasping configurations as a preprocessing step. Usually, only few of them are needed to construct a manipulation sequence. Also, this is obviously expensive particularly for polyhedral objects with many faces. It would be interesting to to find another approach that does not require the preprocessing stage. This may be possible by merging the preprocessing and the planning steps together with an additional heuristic function that guides generating only the configurations likely to be included in the plan. With much fewer configurations to consider, the amount of time spent in the graph construction step should be significantly reduced.

Manipulation Planning with Mobile Robots. There are numerous interesting ways to extend the material presented in Chapter 5 and 6. One of them is to consider adding a fourth robot. The addition has potential to considerably increase robustness and dexterity to the system. Besides grasping with four robots that may significantly reduce the vulnerability to jamming (Section 7.5), capturing and manipulating several objects simultaneously is possible. Capturing two objects with four robots clearly can be per-

formed by placing the robots in such a way that allows each object to be caged by the other object and two of the robots. With four robots, *finger gaiting* could be considered. This would allow the robots to switch the triple of the edges of the object they are designated to without allowing the object to escape. Maneuvering through some obstacles may be more difficult with some triples than the others. The ability to switch triples to accomodate obstacle avoidance should result in more efficient plans. Another interesting issue is to consider the whole boundary of the manipulated object. Because the ICS region is defined for a chosen triple of edges, the quality of plans generated by the current approach depends on how well the triple is chosen. Taking the whole object boundary into account in generating a capturing region would obviously eliminate this concern and, because the interaction between neighboring edges, has potential in producing larger capturing regions.

APPENDIX A

Proofs of Lemmas of Chapter 6

A.1   Proof of Lemma 5

Lemma 5 *The independent capture discs maximizing the smallest of their three radii satisfy the following conditions: (a) Ω_1 is tangent to $C_{3,1}$, Ω_2 is tangent to $C_{1,2}$ and Ω_3 is tangent to $C_{2,3}$; (b) the robot configuration where the discs $\Omega_i, i = 1, 2, 3$ touch the edge E_i must immobilize the object; and (c) the three discs must have the same radius.*

Proof:

1. Ω_1 *is tangent to* $C_{3,1}$, Ω_2 *is tangent to* $C_{1,2}$ *and* Ω_3 *is tangent to* $C_{2,3}$. It is easy to see in Figure 6.4 that when this condition is not satisfied, there is space for the smallest disk to grow. Figure A.1 shows an example after the radius r_3 has been increased until this condition is satisfied.

2. *The robot configuration where the disks* $\Omega_i, i = 1, 2, 3$ *touch the edge* E_i *must immobilize the object.* Even when the first condition is satisfied, it is still possible for the radii to increase. Figure A.1 illustrates this: the first condition is satisfied but the three normals at the contact between the independent disks and the object do not intersect. This implies that the object is not immobilized by the disks, therefore the object can move to a configuration where it does not touch the disks (Figure A.2), providing space for the disks to get larger.
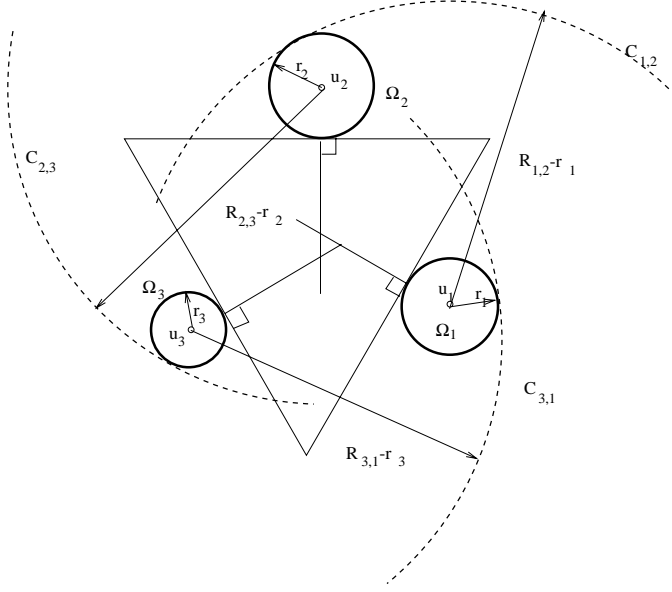
Figure A.1 Independent inescapable disks with condition 1 satisfied.

3. $r_1 = r_2 = r_3$. Let us consider Figure A.3. We denote by $L_{i,j}$ the line segment joining two points in the disk Ω_i and the disk Ω_j that are farthest from each others. Clearly, $L_{i,j}$ passes through the centers of both disks. For the first condition to be satisfied, the length of $L_{i,j}$ must be maintained constant at $R_{i,j}$. In Figure A.3(a), we assume that the first two conditions are satisfied and r_2 is the smallest radius. To increase the radius r_2, we change the intersection point between $L_{1,2}$ and $L_{2,3}$ (which is the location of the center of Ω_2). For the disks not to intersect with the object and to maintain the constant length of each $L_{i,j}$, as r_2 increases, the object must move toward Ω_1 and Ω_3 and the radii r_1 and r_3 must decrease (Figure A.3(b)). Since this process can always be applied as long as the radius of the smallest disk is strictly smaller than the other ones, this radius is maximized when all three radii are equal. $\square$

149
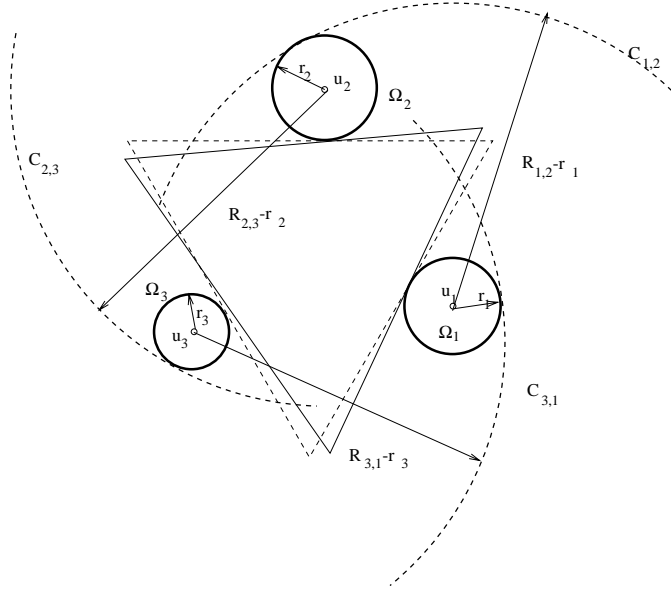
**Figure A.2** When the disks do not immobilize the object, there is some space for the smallest disk to grow.
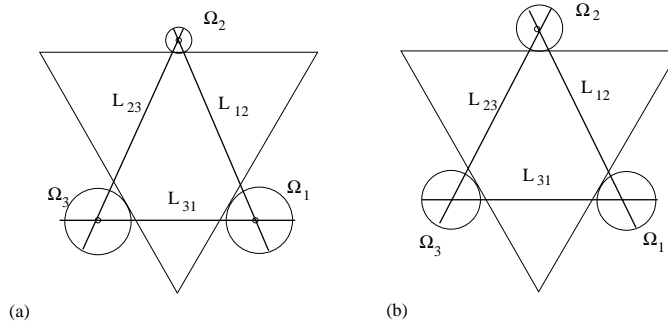
Figure A.3 Growing the smallest disk.

A.2   Proof of Lemma 8

Lemma 8 *If ICS(q_1, q_2, q_3) denotes the set of free configurations of the object associated with the robot configurations q_i ($i = 1, 2, 3$), then*

$$\bigcup_{\substack{q_i \in \overline{q'_i q''_i} \\ i = 1, 2, 3}} ICS(q_1, q_2, q_3) = \bigcup_{\substack{q_i \in \{q'_i, q''_i\} \\ i = 1, 2, 3}} ICS(q_1, q_2, q_3)$$

for any two configurations $q' = (q'_1, q'_2, q'_3)$ and $q'' = (q''_1, q''_2, q''_3)$ in the same triple of MICaDs.

Proof: The set $ICS(\boldsymbol{q}_1, \boldsymbol{q}_2, \boldsymbol{q}_3)$ is a volume bounded by three ruled surfaces, each of which corresponds to the set of configurations for which the robot B_i at $\boldsymbol{q}_i$ is in contact with edge E_i of the object.

When B_i is at the point $\boldsymbol{q}'_i$, the corresponding ruled surface is:

$$V'_i = (x - q'_i)\cos(\theta + \alpha_i) + (y - r'_i)\sin(\theta + \alpha_i) + d_i \ \geq \ 0.$$

Likewise, when B_i is at the point $\boldsymbol{q}''_i$, the corresponding rule surface is:

$$V''_i = (x - q''_i)\cos(\theta + \alpha_i) + (y - r''_i)\sin(\theta + \alpha_i) + d_i \ \geq \ 0.$$

For $\eta_i + \mu_i = 1, \ \ \eta_i, \mu_i \geq 0$, we have:

$$V(\eta_i, \mu_i) = \eta_i V'_i + \mu_i V''_i =$$

$$(x - (\eta_i q'_i + \mu_i q''_i))\cos(\theta + \alpha_i) + (y - (\eta_i r'_i + \mu_i r''_i))\sin(\theta + \alpha_i) + d_i \ = \ 0.$$

The equation $V(\eta_i, \mu_i) = 0$ defines the ruled surface associated with having robot B_i at $\eta_i \boldsymbol{q}'_i + \mu_i \boldsymbol{q}''_i$ (which is a point on the line segment $\overline{\boldsymbol{q}'_i \boldsymbol{q}''_i}$). Clearly, this rule surface is always between the ruled surfaces $V'_i = 0$ and $V''_i = 0$. Therefore, we can write:

$$\mathcal{V}_i(\eta_i, \mu_i) \ \subset \ \mathcal{V}'_i \cup \mathcal{V}''_i,$$

where we denote by $\mathcal{V}_i(\eta_i, \mu_i)$ the volume $V_i(\eta_i, \mu_i) \geq 0$, by $\mathcal{V}'_i$ the volume $V'_i \geq 0$, and by $\mathcal{V}''_i$ the volume $V''_i \geq 0$.

Using the above statement and considering $i = 1, 2, 3$, we can write:

$$\mathcal{V}_1(\eta_1, \mu_1) \cap \mathcal{V}_2(\eta_2, \mu_2) \cap \mathcal{V}_3(\eta_3, \mu_3) \ \subset \ (\mathcal{V}'_1 \cup \mathcal{V}''_1) \cap (\mathcal{V}'_2 \cup \mathcal{V}''_2) \cap (\mathcal{V}'_3 \cup \mathcal{V}''_3).$$

The left hand side of the statement above is $\text{ICS}(\boldsymbol{q}_1, \boldsymbol{q}_2, \boldsymbol{q}_3)$ where $\boldsymbol{q}_i$ can be anywhere on the line segment $\overline{\boldsymbol{q}'_i \boldsymbol{q}''_i}$ (depending on η_i and μ_i). That the above statement is true independent of the values of η_i and μ_i implies:

$$\bigcup_{\substack{\eta_i + \mu_i = 1 \\ \eta_i, \mu_i \geq 0 \\ i = 1, 2, 3}} \mathcal{V}_1(\eta_1, \mu_1) \cup \mathcal{V}_2(\eta_2, \mu_2) \cup \mathcal{V}_3(\eta_3, \mu_3) \ \subset \ (\mathcal{V}'_1 \cup \mathcal{V}''_1) \cap (\mathcal{V}'_2 \cup \mathcal{V}''_2) \cap (\mathcal{V}'_3 \cup \mathcal{V}''_3). \quad \text{(A.1)}$$

Using basic set algebra, the right hand side of the statement above can be expanded as:

$$(\mathcal{V}_1' \cap \mathcal{V}_2' \cap \mathcal{V}_3') \cup (\mathcal{V}_1' \cap \mathcal{V}_2' \cap \mathcal{V}_3'') \cup (\mathcal{V}_1' \cap \mathcal{V}_2'' \cap \mathcal{V}_3') \cup (\mathcal{V}_1' \cap \mathcal{V}_2'' \cap \mathcal{V}_3'')\cup$$

$$(\mathcal{V}_1'' \cap \mathcal{V}_2' \cap \mathcal{V}_3') \cup (\mathcal{V}_1'' \cap \mathcal{V}_2' \cap \mathcal{V}_3'') \cup (\mathcal{V}_1'' \cap \mathcal{V}_2'' \cap \mathcal{V}_3') \cup (\mathcal{V}_1'' \cap \mathcal{V}_2'' \cap \mathcal{V}_3'').$$

The above expression is the union of eight sets. Each set is the ICS for the configuration having the robot B_i located at either end of the line segment $\overline{\boldsymbol{q}_i' \boldsymbol{q}_i''}$. For example, the second term, $\mathcal{V}_1' \cap \mathcal{V}_2' \cap \mathcal{V}_3''$ is $\text{ICS}(\boldsymbol{q}_1 = \boldsymbol{q}_1', \boldsymbol{q}_2 = \boldsymbol{q}_2', \boldsymbol{q}_3 = \boldsymbol{q}_3'')$.

Because the term $\mathcal{V}_i'$ can be written as $\mathcal{V}_i(\eta_i = 1, \mu_i = 0)$ and the term $\mathcal{V}_i''$ can be written as $\mathcal{V}_i(\eta_i = 0, \mu_i = 1)$ the reverse of the statement (A.1) is true as well. $\square$

A.3 Proof of Lemma 9

Lemma 9 *As the object rotates while maintaining contact with B_1 and B_2, L_a rotates as well and remains tangent to a fixed circle C_a.*

Proof: Let us consider Figure A.4. The three lines L_1, L_2 and L_a belong to the same object, the points $\boldsymbol{q}_1 = (q_1, r_1)^T$ and $\boldsymbol{q}_2 = (q_2, r_2)^T$ are fixed and the normals at $\boldsymbol{q}_1$, $\boldsymbol{q}_2$ and $\boldsymbol{q}_a = (q_a, r_a)^T$ intersect at $(s, t)^T$ where $\boldsymbol{q}_a$ is a point on L_a. We want to show here that when the object rotates while maintaining simultaneous contacts between $\boldsymbol{q}_1$ and L_1 and between $\boldsymbol{q}_2$ and L_2, the point $\boldsymbol{q}_a$ will trace a circle C_a and the line L_a is always tangent to this circle.

Let us denote by θ the orientation of the object and by α_1, α_2 and α_a the constant offet angles of the internal normals of the three edges. The first three equations define L_1, L_2 and L_a which are the lines supporting the three edges under consideration (E_1, E_2 and E_a).

$$\begin{cases} (x - q_1)\cos(\theta + \alpha_1) + (y - r_1)\sin(\theta + \alpha_1) = 0 \\ (x - q_2)\cos(\theta + \alpha_2) + (y - r_2)\sin(\theta + \alpha_2) = 0 \\ (q_a - x)\cos(\theta + \alpha_a) + (r_3 - y)\sin(\theta + \alpha_a) - d = 0. \end{cases} \tag{A.2}$$
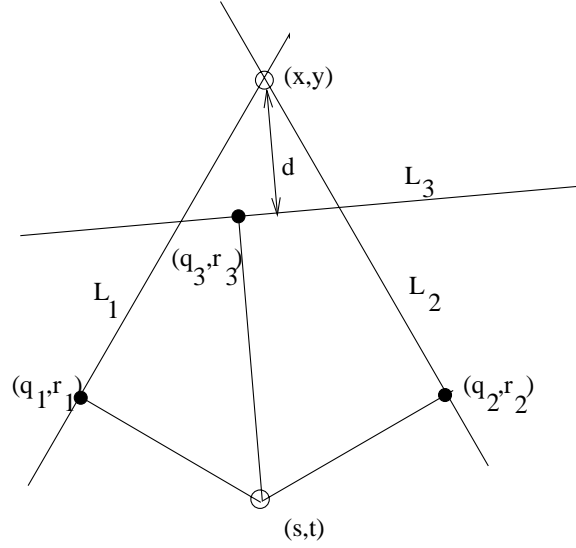
Figure A.4 The line L_3 as the object rotates.

The next three equations express the fact that the three internal normals at the contacts intersect at the point (s, t) (immobilizing the object).

$$\begin{cases} (s - q_1)\cos(\theta + \alpha_1 + \pi/2) + (t - r_1)\sin(\theta + \alpha_1 + \pi/2) = 0 \\ (s - q_2)\cos(\theta + \alpha_2 + \pi/2) + (t - r_2)\sin(\theta + \alpha_2 + \pi/2) = 0 \\ (s - q_a)\cos(\theta + \alpha_a + \pi/2) + (t - r_a)\sin(\theta + \alpha_a + \pi/2) = 0. \end{cases} \quad \text{(A.3)}$$

Eliminating x and y from (A.2) yields:

$$(r_a - r_2)\cos(\alpha_1 - \alpha_2 - \alpha_a - \theta) + (r_2 - r_1)\cos(\alpha_1 + \alpha_2 - \alpha_a + \theta) - 2d\sin(\alpha_1 - \alpha_2) +$$
$$(r_1 - r_a)\cos(\alpha_1 - \alpha_2 + \alpha_a + \theta) - (q_2 - q_a)\sin(\alpha_1 - \alpha_2 - \alpha_a - \theta) +$$
$$(q_1 - q_2)\sin(\alpha_1 + \alpha_2 - \alpha_a + \theta) - (q_1 - q_a)\sin(\alpha_1 - \alpha_2 + \alpha_a + \theta) = 0.$$
$$\text{(A.4)}$$

Likewise, eliminating s and t from (A.3) yields:

$$(q_a - q_2)\cos(\alpha_1 - \alpha_2 - \alpha_a - \theta) + (q_2 - q_1)\cos(\alpha_1 + \alpha_2 - \alpha_a + \theta) +$$
$$(q_1 - q_a)\cos(\alpha_1 - \alpha_2 + \alpha_a + \theta) + (r_2 - r_a)\sin(\alpha_1 - \alpha_2 - \alpha_a - \theta) -$$
$$(r_1 - r_2)\sin(\alpha_1 + \alpha_2 - \alpha_a + \theta) + (r_1 - r_a)\sin(\alpha_1 - \alpha_2 + \alpha_a + \theta) = 0.$$
$$\text{(A.5)}$$

Applying some algebraic manipulation to eliminate θ yields:

$$\{2q_a\sin(\alpha_1-\alpha_2)+(r_1-r_2)\cos(\alpha_1-\alpha_2)+(r_2-r_1)\cos(\alpha_1+\alpha_2-2\alpha_a)-$$
$$(q_1+q_2)\sin(\alpha_1-\alpha_2)+(q_1-q_2)\sin(\alpha_1+\alpha_2-2\alpha_a)\}^2+$$
$$\{2r_3\sin(\alpha_1-\alpha_2)-(q_1-q_2)\cos(\alpha_1-\alpha_2)-(q_2-q_1)\cos(\alpha_1+\alpha_2-2\alpha_a)+ \qquad\text{(A.6)}$$
$$(r_1+r_2)\sin(\alpha_1-\alpha_2)+(r_1-r_2)\sin(\alpha_1+\alpha_2-2\alpha_a)\}^2=$$
$$4d^2\sin^2(\alpha_1-\alpha_2).$$

It is easy to see that (A.6) defines a circle with the constant radius d in the (q_a,r_a) plane. Let us call this circle C_a and denote by $\boldsymbol{c}=(c_x,c_y)^T$ the center of this circle. From (A.6), c_x and c_y can be written as a function of θ. By eliminating r_a from (A.4) using (A.5) we can write q_a as a function of θ. Likewise, by eliminating q_a from (A.4) using (A.5), we can also write r_a as a function of θ. We obtain

$$\boldsymbol{q}_3=(q_a,r_a)=\frac{1}{2\sin(\alpha_1-\alpha_2)}\begin{pmatrix}(r_2-r_1)\cos(\alpha_1-\alpha_2)-(r_2-r_1)\cos(\alpha_1+\alpha_2-2\alpha_a)+\\(q_1+q_2)\sin(\alpha_1-\alpha_2)+(q_2-q_1)\sin(\alpha_1+\alpha_2-2\alpha_a)+\\d\sin(\alpha_1-\alpha_2-\alpha_a-\theta)+d\sin(\alpha_1-\alpha_2+\alpha_a+\theta)\\\\(q_1-q_2)\cos(\alpha_1-\alpha_2)+(q_2-q_1)\cos(\alpha_1+\alpha_2-2\alpha_a)+\\d\cos(\alpha_1-\alpha_2-\alpha_a-\theta)-d\cos(\alpha_1-\alpha_2+\alpha_a+\theta)+\\(r_1+r_2)\sin(\alpha_1-\alpha_2)-r_1\sin(\alpha_1+\alpha_2-2\alpha_a)+\\r_2\sin(\alpha_1-\alpha_2-2\alpha_a)\end{pmatrix}.$$
$$\text{(A.7)}$$

The unit tangent of the line L_a is $\boldsymbol{n}_a=(\cos(\theta+\alpha_a+\pi/2),\sin(\theta+\alpha_a+\pi/2))^T$, and it follows immediately that

$$(\boldsymbol{q}_a-\boldsymbol{c})\cdot\boldsymbol{n}_a=0.$$

That is, we have shown that the line L_a is always tangent to the circle C_a as the object changes its orientation during the double-contact constrained motion. *Box*

APPENDIX B

Intersection between a Curve Traced by a Vertex and a Line Segment

In Figure B.1, the object in Figure 6.10 is drawn as a dotted polygon. Let the given line be defined by:

$$u \cos \alpha + v \sin \alpha + d = 0, \tag{B.1}$$

where α and d are some constants. Consider the curve $U = \{(u(\theta), v(\theta))^T, \ \theta_L \leq \theta \leq \theta_H\}$
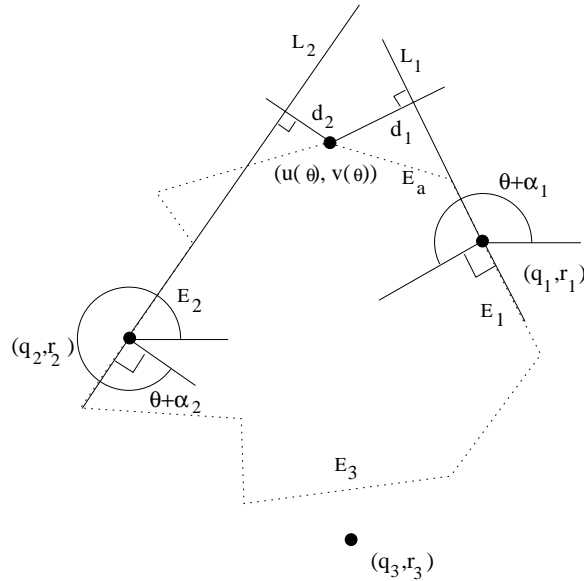

Figure B.1 Parameterizing the endpoint $(u(\theta), v(\theta))^T$.

where $(u(\theta), v(\theta))^T$ is an endpoint of the edge E_a when the object is at orientation θ.

Writing that the distance from $(u(\theta), v(\theta))^T$ to line L_1 (the line supporting E_1) is constant d_1 yields:

$$\left(\begin{array}{c} u(\theta) - q_1 \\ v(\theta) - r_1 \end{array} \right) \cdot \left(\begin{array}{c} \cos(\theta + \alpha_1) \\ \sin(\theta + \alpha_1) \end{array} \right) = (u(\theta) - q_1)\cos(\theta + \alpha_1) + (v(\theta) - r_1)\sin(\theta + \alpha_1) = d_1.$$

(B.2)

Likewise, writing that the distance from $(u(\theta), v(\theta))^T$ to line L_2 (the line supporting E_2) is d_2 yields:

$$(u(\theta) - q_2)\cos(\theta + \alpha_2) + (v(\theta) - r_2)\sin(\theta + \alpha_2) = d_2. \qquad \text{(B.3)}$$

We want to compute the intersection of curve U and line L. Suppose that the intersection occurs at $(u, v)^T$. We can then set $u(\theta) = u$ and $v(\theta) = v$ in (B.2) and (B.3), and use the resulting equations to eliminate u and v in (B.1). We obtain after some simplification:

$$(r_1 - r_2)\cos(\alpha - \alpha_1 - \alpha_2 - 2\theta) \; + \; (q_1 - q_2)\sin(\alpha - \alpha_1 - \alpha_2 - 2\theta) -$$

$$2d_2 \sin(\alpha - \alpha_1 - \theta) \; + \; 2d_1 \sin(\alpha - \alpha_2 - \theta) \; + \; K \quad = \quad 0, \qquad \text{(B.4)}$$

where

$$K \quad = \quad r_2 \cos(\alpha - \alpha_1 + \alpha_2) \; - \; r_1 \cos(\alpha + \alpha_1 - \alpha_2) +$$

$$2d \sin(\alpha_1 - \alpha_2) \; + \; q_1 \sin(\alpha + \alpha_1 - \alpha_2) \; - \; q_2 \sin(\alpha - \alpha_1 + \alpha_2)$$

Finding the roots of this equation amounts to solving a trigonometric eqation in θ which can be done in closed form. The intersection points of U and L are the points $(u, v)^T$ at the root orientations θ that are within the range $[\theta_L, \theta_H]$. To compute the intersection of a line segment supported by the given line L, an extra step is needed for testing whether any of the obtained intersection points is contained in the line segment.

REFERENCES

[1] S. Akella and M.T. Mason. Parts orienting by push-aligning. In *IEEE Int. Conf. on Robotics and Automation*, pages 414–420, Nagoya, Japan, May 1995.

[2] D.S. Arnon, G. Collins, and S. McCallum. Cylindrical algebraic decomposition I and II. *SIAM J. Comput.*, 13(4):865–889, November 1984.

[3] H. Asada and A. By. Kinematics of workpart fixturing. In *Proc. IEEE Int. Conf. on Robotics and Automation*, pages 337–345, St Louis, MI, 1985.

[4] Francis Avnaim, Jean D. Boissonnat, and Bernard Faverjon. A practical exact motion planning algorithm for polygonal objects amidst polygonal obstacles. Technical Report 890, INRIA, 1988.

[5] R.S. Ball. *A treatise on the theory of screws*. Cambridge University Press, 1900.

[6] J. Bausch and K. Youcef-Toumi. Kinematics methods for automated fixture reconfiguration planning. In *Proc. IEEE Int. Conf. on Robotics and Automation*, pages 1396–1401, Cincinatti, OH, 1990.

[7] A. Blake. Computational modelling of hand-eye coordination. *Phil. Trans. R. Soc. Lond. B*, 337:351–360, 1992.

[8] O. Bottema and B. Roth. *Theoretical Kinematics*. North Holland Publishing Co., 1979.

[9] F. P. Bowden and D. Tabor. *Friction and lubrication*. Oxford University Press, 1954.

[10] R.C. Brost and K. Goldberg. A complete algorithm for synthesizing modular fixtures for polygonal parts. In *IEEE Int. Conf. on Robotics and Automation*, pages 535–542, San Diego, CA, May 1994.

[11] R.C. Brost and R.R. Peters. Automatic design of 3D fixtures and assembly pallets. In *IEEE Int. Conf. on Robotics and Automation*, pages 495–502, Minneapolis, MN, April 1996.

[12] J.F. Canny. Collision detection for moving polyhedra. *IEEE Trans. Patt. Anal. Mach. Intell.*, 8(2):200–209, 1986.

[13] J.F. Canny and K.Y. Goldberg. "RISC" for industrial robotics: recent results and open problems. In *IEEE Int. Conf. on Robotics and Automation*, pages 1951–1958, San Diego, CA, 1994.

[14] B.M. Chazelle. Filtering search: a new approach to query answering. In *IEEE Symposium on Foundatons of Computer Science*, pages 122–132, Tucson, AZ, November 1983.

[15] I.M. Chen and J.W. Burdick. Finding antipodal point grasps on irregularly shaped objects. In *IEEE Int. Conf. on Robotics and Automation*, pages 2278–2283, Nice, France, June 1992.

[16] Y.C. Chou, V. Chandru, and M. Barash. A mathematical approach to automatic configuration of machining fixtures: analysis and synthesis. *ASME Journal of Engineering for Industry*, 111:299–306, 1989.

[17] G.E. Collins. *Quantifier Elimination for Real Closed Fields by Cylindrical Algebraic Decomposition*, volume 33 of *Lecture Notes in Computer Science*. Springer-Verlag, New York, 1975.

[18] J. Czyzowicz, I. Stojmenovic, and J. Urrutia. Immobilizing a polytope. volume 519 of *Lecture Notes in Computer Sciences*, pages 214–227. Springer-Verlag, 1991.

[19] M. Daimon and T. Yoshida. Study for designing fixtures considering dynamics of thin-walled-plate and box-like workpieces. *Annals of the CIRP*, 34(1):319–322, 1985.

[20] C. Davidson and A. Blake. Caging planar objects with a three-finger one-parameter gripper. In *IEEE Int. Conf. on Robotics and Automation*, pages 2722–2727, Leuven, Belgium, 1998.

[21] M.P. do Carmo. *Differential Geometry of Curves and Surfaces*. Prentice-Hall, Englewood Cliffs, NJ, 1976.

[22] B. R. Donald and D. K. Pai. On the motion of compliantly-connected rigid bodies in contact part 2: a system for analyzing designs for assembly. In *IEEE Int. Conf. on Robotics and Automation*, May 1990.

[23] J. Donoghue, W.S. Howard, and V. Kumar. Stable workpiece fixturing. In 23rd *biennial ASME mechanics conference*, Minneapolis, Sept. 1994.

[24] P. E. Dupont and S. P. Yamajako. Jamming and wedging in constrained rigid-body dynamics. In *IEEE Int. Conf. on Robotics and Automation*, May 1994.

[25] P.J. Englert. *Principles for Part Setup and Workholding in Automated Manufacturing*. PhD thesis, Dept. of Mechanical Engineering and Robotics Institute, Carnegie-Mellon University, Pittsburgh, PA, 1987.

[26] M.A. Erdmann and M.T. Mason. An exploration of sensorless manipulation. *IEEE Journal of Robotics and Automation*, 4:369–379, 1988.

[27] C. Ferrari and J.F. Canny. Planning optimal grasps. In *IEEE Int. Conf. on Robotics and Automation*, pages 2290–2295, Nice, France, June 1992.

[28] P.M. Ferreira and C.R. Liu. Generation of workpiece orientation for machining using a rule-based system. *Journal of Robotics and Computer-Integrated Manufacturing*, 1988.

[29] J.B.J. Fourier. Reported in: Analyse des travaux de l'académie royale des sciences pendant l'année 1824. In *Partie mathématique, Histoire de l'Académie Royale des Sciences de l'Institut de France*, volume 7, xlvii-lv. 1827. Partial English translation in: D.A. Kohler, Translation of a Report by Fourier on his work on Linear Inequalities, *Opsearch* 10 (1973) 38-42.

[30] M.V. Gandhi and B.S. Thompson. Automated design of modular fixtures for flexible manufacturing systems. *Journal of Manufacturing Systems*, 5(4):243–252, 1986.

[31] K. Goldberg and M.T. Mason. Bayesian grasping. In *IEEE Int. Conf. on Robotics and Automation*, pages 1264–1269, May 1990.

[32] K.Y. Goldberg. A kinematically-yielding gripper. In 22nd *Int. Symp. on Industrial Automation*, 1992. See U.S. Patent 5,098,145.

[33] K.Y. Goldberg. Orienting polygonal parts without sensors. *Algorithmica*, 10(2):201–225, 1993.

[34] C.C. Hayes and P.K. Wright. Automatic process planning: using feature interactions to guide search. *Journal of Manufacturing Systems*, 8(1):1–16, 1989.

[35] F.B. Hazen and P. Wright. Workholding automation: innovations in analysis. *Manufacturing Reviews*, 3(4):224–237, 1990.

[36] F. Helot, t. Baumberger, B. Perrin, B. Caroli, and C. Caroli. *Phys. Rev. E*, 49, 1994.

[37] T. Hishi. Research for high-productivity machining in japan. In *Int. Conf. on High Productivity Machining, Materials and Processing*, pages 15–26, 1985.

[38] W.S. Howard and V. Kumar. Stability of planar grasps. In *Proc. IEEE Int. Conf. on Robotics and Automation*, pages 2822–2827, San Diego, CA, May 1994.

[39] K.H. Hunt. *Kinematic Geometry of Mechanisms*. Clarendon, Oxford, 1978.

[40] S.C. Jacobsen, J.E. Wood, D.F. Knutti, and K.B. Biggers. The Utah-MIT Dextrous Hand: Work in progress. *International Journal of Robotics Research*, 3(4):21–50, 1984.

[41] Z. Ji. *Dexterous hands: optimizing grasp by design and planning*. PhD thesis, Stanford University, Dept. of Mechanical Engineering, 1987.

[42] O. Khatib. Real-time obstacle avoidance for manipulators and mobile robots. *International Journal of Robotics Research*, 5(1):90–98, 1986.

[43] K. Lakshminarayana. Mechanics of form closure. Technical Report 78-DET-32, ASME, 1978.

[44] C. Lassez and J-L. Lassez. Quantifier elimination for conjunctions of linear constraints via a convex hull algorithm. In B. Donald, D. Kapur, and J. Mundy, editors, *Symbolic and Numerical Computation for Artificial Intelligence*, pages 103–122. Academic Press, 1992.

[45] J-L. Lassez. Querying constraints. In *ACM conference on Principles of Database Systems*, Nashville, 1990.

[46] J.-C. Latombe. *Robot Motion Planning*. Kluwer Academic Publishers, 1991.

[47] S.H. Lee and M.R. Cutkosky. Fixture planning with friction. *Trans. of the ASME*, 112:320–327, August 1991.

[48] T. Lozano-pérez. The design of a mechanical assembly system. MIT AI Memo 397, MIT Artificial Intelligence Lab, December 1976.

[49] K.M. Lynch and M.T. Mason. Stable pushing: mechanics, controllability, and planning. In K.Y. Goldberg, D. Halperin, J.-C. Latombe, and R. Wilson, editors, *Algorithmic Foundations of Robotics*, pages 239–262. A.K. Peters, 1995.

[50] D. Manocha. *Algebraic and Numeric Techniques for Modeling and Robotics*. PhD thesis, Computer Science Division, Univ. of California at Berkeley, 1992.

[51] D. Manocha. Computing selected solutions of polynomial equations. In *Int. Symp. on Symbolic and Algebraic Computation*, pages 1–8, Oxford, England, 1994.

[52] X. Markenscoff, L. Ni, and C.H. Papadimitriou. The geometry of grasping. *International Journal of Robotics Research*, 9(1):61–74, February 1990.

[53] X. Markenscoff and C.H. Papadimitriou. Optimum grip of a polygon. *International Journal of Robotics Research*, 8(2):17–29, April 1989.

[54] A. Markus, Z. Markusz, J. Farka, and J. Filemon. Fixture design using prolog: an expert system. *Robotics and Computer Integrated Manufacturing*, 1(2):167–172, 1984.

[55] M.T. Mason. Mechanics and planning of manipulator pushing operations. *International Journal of Robotics Research*, 5(3):53–71, 1986.

[56] J.M. McCarthy. *An Introduction to Theoretical Kinematics*. MIT Press, 1990.

[57] B. Mirtich and J.F. Canny. Optimum force-closure grasps. Technical Report ESRC 93-11/RAMP 93-5, Robotics, Automation, and Manufacturing Program, University of California at Berkeley, July 1993.

[58] B. Mishra. Worksholding – analysis and planning. In *IEEE/RSJ Int. Workshop on Intelligent Robots and Systems*, pages 53–56, Osaka, Japan, 1991.

[59] B. Mishra, J.T. Schwartz, and M. Sharir. On the existence and synthesis of multi-finger positive grips. *Algorithmica, Special Issue: Robotics*, 2(4):541–558, November 1987.

[60] B. Mishra and N. Silver. Some discussion of static gripping and its stability. *IEEE Systems, Man, and Cybernetics*, 19(4):783–796, 1989.

[61] A.P. Morgan. *Solving Polynomial Systems using Continuation for Engineering and Scientific Problems*. Prentice Hall, Englewood Cliffs, NJ, 1987.

[62] R.M. Murray, Z. Li, and S.S. Sastry. *A mathematical introduction to robotic manipulation*. CRC Press, 1994.

[63] V-D. Nguyen. Constructing force-closure grasps. *International Journal of Robotics Research*, 7(3):3–16, June 1988.

[64] V-D. Nguyen. Constructing stable grasps. *International Journal of Robotics Research*, 8(1):27–37, February 1989.

[65] M.S. Ohwovoriole. *An extension of screw theory and its application to the automation of industrial assemblies*. PhD thesis, Stanford University, Stanford, CA, 1980.

[66] M.S. Ohwovoriole. An extension of screw theory. *Journal of Mechanical Design*, 103:725–735, 1981.

[67] M.A. Peshkin and A.C. Sanderson. Planning robotic manipulation strategies for workpieces that slide. *IEEE Journal of Robotics and Automation*, 4(5), 1988.

[68] N.S. Pollard and T. Lozano-Pérez. Grasp stability and feasibility for an arm with an articulated hand. In *IEEE Int. Conf. on Robotics and Automation*, pages 1581–1585, Cincinatti, OH, 1990.

[69] J. Ponce. On planning immobilizing fixtures for three-dimensional polyhedral objects. In *IEEE Int. Conf. on Robotics and Automation*, pages 509–514, Minneapolis, MN, April 1996.

[70] J. Ponce and B. Faverjon. On computing three-finger force-closure grasps of polygonal objects. In *International Conference on Advanced Robotics*, pages 1018–1023, Pisa, Italy, June 1991.

[71] J. Ponce and B. Faverjon. On computing three-finger force-closure grasps of polygonal objects. *IEEE Transactions on Robotics and Automation*, 11(6):868–881, December 1995.

[72] J. Ponce, D. Stam, and B. Faverjon. On computing force-closure grasps of curved two-dimensional objects. *International Journal of Robotics Research*, 12(3):263–273, June 1993.

[73] J. Ponce, A. Sudsang, S. Sullivan, B. Faverjon, J.-D. Boissonnat, and J.-P. Merlet. Algorithms for computing multi-finger force-closure grasps of polyhedral objects. In *Workshop on Algorithmic Foundations of Robotics*, San Francisco, CA, 1994. Preprints.

[74] J. Ponce, S. Sullivan, A. Sudsang, J-D. Boissonnat, and J-P. Merlet. On computing four-finger equilibrium and force-closure grasps of polyhedral objects. Technical Report Beckman Institute Tech. Report UIUC-BI-AI-RCV-95-04, Beckman Institute, University of Illinois, February 1995.

[75] J. Ponce, S. Sullivan, A. Sudsang, J-D. Boissonnat, and J-P. Merlet. On computing four-finger equilibrium and force-closure grasps of polyhedral objects. *International Journal of Robotics Research*, 16(1):11–35, February 1997.

[76] F.P. Preparata and M.I. Shamos. *Computational Geometry - An Introduction*. Springer-Verlag, 1985.

[77] E. RabinowiczF. *Friction and wear of materials*. Wiley and Sons, 1965.

[78] A.S. Rao and K.Y. Goldberg. Manipulating algebraic parts in the plane. Technical Report RUU-CS-93-43, Dept. of Computer Science, Utrecht University, 1993.

[79] F. Reulaux. *The kinematics of machinery*. MacMillan, NY, 1876. Reprint, Dover, NY, 1963.

[80] E. Rimon and A. Blake. Caging 2D bodies by one-parameter two-fingered gripping systems. In *IEEE Int. Conf. on Robotics and Automation*, pages 1458–1464, Minneapolis, MN, April 1996.

[81] E. Rimon and J. W. Burdick. Towards planning with force constraints: On the mobility of bodies in contact. In *Proc. IEEE Int. Conf. on Robotics and Automation*, pages 994–1000, Atlanta, GA, May 1993.

[82] E. Rimon and J. W. Burdick. Mobility of bodies in contact: A new 2nd order mobility index for multiple-finger grasps. In *Proc. IEEE Int. Conf. on Robotics and Automation*, pages 2329–2335, San Diego, CA, May 1994.

[83] E. Rimon and J. W. Burdick. Mobility of bodies in contact: How forces are generated by curvature effects. In *Proc. IEEE Int. Conf. on Robotics and Automation*, pages 2336–2341, San Diego, CA, May 1994.

[84] E. Rimon and J. W. Burdick. Mobility of bodies in contact-I: A new 2nd order mobility index for multi-finger grasps. *IEEE Transactions on Robotics and Automation*, 1995. Submitted. A preliminary version appeared in *IEEE Int. Conf. on Robotics and Automation*, pages 2329-2335, San Diego, CA, 1994.

[85] E. Rimon and J. W. Burdick. Mobility of bodies in contact-II: How forces are generated by curvature effects? *IEEE Transactions on Robotics and Automation*, 1995. Submitted. A preliminary version appeared in *IEEE Int. Conf. on Robotics and Automation*, pages 2336-2341, San Diego, CA, 1994.

[86] B. Roth. Screws, motors, and wrenches that cannot be bought in a hardware store. In *Int. Symp. on Robotics Research*, pages 679–693. MIT Press, 1984.

[87] J.K. Salisbury. *Kinematic and force analysis of articulated hands*. PhD thesis, Stanford University, Stanford, CA, 1982.

[88] J. Schwartz and M. Sharir. On the piano movers' problem: II. General techniques for computing topological properties of real algebraic manifolds. In J. Schwartz, M. Sharir, and J. Hopcroft, editors, *Planning, Geometry and Complexity of Robot Motion*, pages 51–96. Ablex Publishing Corp., Norwood, NJ, 1987.

[89] B. Shirinizadeh. Issues in the design of reconfigurable fixture modules for robotics. *Journal of Manufacturing Systems*, 12(1):1–14, 1993.

[90] S. Simunovic. Force information in assembly. In *5th International Conference on Intelligent Robots and Systems, year=1975, pages=415-431.*

[91] P. Somov. Über Gebiete von Schraubengeschwindigkeiten eines starren Korpers bie verschiedener Zahl von Stutzflachen. *Zeitricht für Mathematik und Physik*, 45:245–306, 1900.

[92] A. Sudsang and J. Ponce. In-hand manipulation: geometry and algorithms. In *IEEE/RSJ International Conference on Intelligent Robots and Systems*, pages 98–105, Grenoble, France, September 1997.

[93] A. Sudsang and J. Ponce. On grasping and manipulating polygonal objects with disc-shaped robots in the plane. In *IEEE Int. Conf. on Robotics and Automation*, Leuven, Belgium, 1998.

[94] A. Sudsang, J. Ponce, and N. Srinivasa. Algorithms for constructing immobilizing fixtures and grasps of three-dimensional objects. In J.-P. Laumont and M. Overmars, editors, *Algorithmic Foundations of Robotics II*, pages 363–380. AK Peters, Ltd., 1997.

[95] A. Sudsang, J. Ponce, and N. Srinivasa. Grasping and in-hand manipulation: Geometry and algorithms. *Algorithmica, Special Issue: Robotics*, 1998.

[96] A. Sudsang, N. Srinivasa, and J. Ponce. On planning immobilizing grasps for a reconfigurable gripper. In *IEEE/RSJ International Conference on Intelligent Robots and Systems*, pages 106–113, Grenoble, France, September 1997.

[97] J. C. Trinkle, S. L. Yeap, and L. Han. When quasistatic jamming is impossible. In *IEEE Int. Conf. on Robotics and Automation*, May 1996.

[98] J.C. Trinkle. On the stability and instantaneous velocity of grasped frictionless objects. *IEEE Transactions on Robotics and Automation*, 8(5):560–572, October 1992.

[99] V. Vaishnavi and D. Wood. Data structures for the rectangle containment and enclosure problems. *Computer Graphics and Image Processing*, 13:372–384, 1980.

[100] V. Vaishnavi and D. Wood. Rectilinear line segment intersection, layered segment trees, and dynamization. *J. Algorithms*, 3:160–176, 1982.

[101] R. Wagner, Y. Zhuang, and K. Goldberg. Fixturing faceted parts with seven modular struts. In *IEEE Int. Symp. on Assembly and Task Planning*, pages 133–139, Pittsburgh, PA, August 1995.

[102] A. Wallack and J.F. Canny. Planning for modular and hybrid fixtures. In *IEEE Int. Conf. on Robotics and Automation*, pages 520–527, San Diego, CA, 1994.

[103] A.S. Wallack. *Algorithms and Techniques for Manufacturing*. PhD thesis, Computer Science Division, Univ. of California at Berkeley, 1995.

[104] Emo Welzl. Smallest enclosing disks (balls and ellipsoids). In H. Maurer, editor, *New Results and New Trends in Computer Science*, volume 555 of *Lecture Notes Comput. Sci.*, pages 359–370. 1991.

[105] D. E. Whitney and J. L. Nevins. What is the romote center compliance (rcc) and what can it do? In *9th International Symposium on Industrial Robots*, March 1979.

[106] D.E. Whitney. Quasi-static assembly of compliantly supported rigid parts. *J. Dyn. Sys., Meas. Contr.*, 104:65–77, 1982.

[107] Y. Zhuang, K. Goldberg, and Y.C. Wong. On the existence of modular fixtures. In *IEEE Int. Conf. on Robotics and Automation*, pages 543–549, San Diego, CA, May 1994.

VITA

Attawith Sudsang was born in Thailand, in 1971. He received a B.Eng. degree with highest honors in Computer Engineering from Chulalongkorn University, Bangkok, Thailand. He received an M.S. degree in Computer Science in 1994, and a Ph.D. degree in Computer Science in 1999, both from the University of Illinois at Urbana-Champaign.